

PARAMETRIC SYNTHESIS OF AUTOPILOT FOR BANK-TO-TURN MISSILE

2018

A Thesis Submitted

*in Partial Fulfilment of the Requirements
for the Degree of*

DOCTOR OF PHILOSOPHY

By

Shiv Narayan

to the

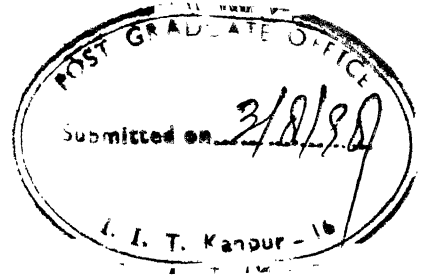
**DEPARTMENT OF ELECTRICAL ENGINEERING
INDIAN INSTITUTE OF TECHNOLOGY, KANPUR, INDIA
JULY, 1998**

**dedicated
to
my parents**

14 JUN 2000^{EE}
CENTRAL LIBRARY
I. I. T., KANPUR
A 131063

TH
EE/1998/P
N164P

A-31063



Certificate

It is certified that the work contained in the thesis entitled **PARAMETRIC SYNTHESIS OF AUTOPILOT FOR BANK-TO-TURN MISSILE**, by Shiv Narayan has been carried out under my supervision and that this work has not been submitted elsewhere for a degree.

(Dr. K. E. Holé)

Professor

Department of Electrical Engineering

Indian Institute of Technology

Kanpur-208016, India

Date : July, 1998

Synopsis

Name of student : Shiv Narayan

Roll No. 9110470

Degree for which submitted : Ph D

Department: Electrical Engineering

Thesis Title : PARAMETRIC SYNTHESIS OF AUTOPILOT FOR BANK-TO-TURN MISSILE

Name of thesis supervisor : Dr K. E. Hole

Month and year of thesis submission : July 1998.

Two basic methods of controlling a missile to achieve the commanded acceleration are skid-to-turn (STT) and bank-to-turn (BTT) . In STT, the body acceleration is attained by permitting the missile to develop both an angle of attack and a sideslip angle . In contrast , a BTT missile should not have, ideally, any sideslip . To achieve the desired orientation, it is rolled (banked) such that the plane of maximum aerodynamic normal force is first oriented in the desired direction and then the force is controlled by adjusting the angle of attack.

The function of an autopilot is to cause the missile to achieve the commanded acceleration as closely as possible , while maintaining closed loop stability and certain constraints on other operating variables. A BTT missile is asymmetric in configuration, having very strong roll-yaw coupling. Due to the asymmetric airframe, the missile has tendency for sideslip. If sideslip is allowed to develop, it would give rise, in conjunction with angle of attack , to large roll rates. Therefore, for a BTT missile, the most significant constraint is on allowable sideslip.

Because of the large roll rates due to sideslip, the roll-yaw channels are strongly coupled and can be considered as a single system. The linearized pitch dynamics, on the other hand, can be treated separately from roll-yaw dynamics. Thus, on the whole, the autopilot design for a BTT missile consists, essentially, of the design of two autopilots : one for the pitch acceleration command tracking, known as longitudinal autopilot, and another for commanding the roll rate about the velocity vector of the missile, known as the lateral autopilot.

There are basically two schemes of designing a linear time invariant (LTI) controller : the first one based on analytical methods and , the second one based on parameter optimization methods. The most common examples of analytical methods are linear quadratic Gaussian (LQG) based designs and H_∞ optimal controller designs. These analytical methods minimize a simple objective function for finding a controller. The weight matrices are specified in the objective function. The major disadvantage of these methods is that the design specifications need to be translated into objective function and the weight matrices . In complex systems, this is a difficult problem .

On the other hand, in the parameter optimization methods one starts with the controller structures . The next step is to form an objective function that represents design specifications. An objective function can be formed by weighted sum or maximum of various performance indices . Certain explicit constraints may also be added and the design is posed as nonlinear optimization problem which can be solved using optimization methods. The main advantages of parameter optimization are :

(i) A much greater range of objective functions and constraints can be allowed than those in analytical methods.

(ii) If the designer is certain that some controller of the selected architecture will do the job, the parameters of the controller can be obtained using parameter optimization .

(iii) If a controller has been designed using analytical methods, it can be improved using parameter optimization methods.

(iv) The designer has the freedom as regards the structure of the controller.

However, the parameter optimization methods pose the problem that they do not guarantee global solution. Moreover, they require initial guess to start the optimization process. These drawbacks can be overcome by using recent technique of Simulated Annealing (SA), which provides global optimal solution. As regards the choice of the controller structure, the controller parametrizations based on the factorization approaches due to Youla et al and Desoer et al can be used.

A fast maneuvering, high performance BTT missile has to function in an uncertain and changing environment. This demands certain level of time domain and frequency domain responses from the missile system. The parametric methods of controller design provide a good framework for meeting the demanding requirements on the time domain and frequency domain performances. The time domain and frequency domain performance functions can be defined based on the design requirements and the design problem can be posed as an optimization problem that can be solved using optimization methods. Most of the autopilot designs for BTT missiles reported in the literature are based on the analytical methods. The autopilot design in this framework has not been reported.

Therefore, the motivations behind the work reported in this thesis are :

(i) To explore the possibility of parametric synthesis of longitudinal (pitch) autopilot and develop design algorithm using nonlinear optimization methods.

(ii) To explore the possibility of parametric synthesis of longitudinal autopilot in two degrees of freedom (TDOF) configuration and develop the design algorithm using Simulated Annealing (SA) technique.

(iii) To explore the possibility of parametric synthesis of lateral (roll-yaw) autopilot and develop the design algorithm using SA technique.

(iv) To investigate the robustness of the designed autopilot.

A brief description of the work reported in this thesis is given below :

The first chapter introduces the control problem for BTT missile, the autopilot design requirements, and presents a brief literature survey on the subject. The motivations behind the research work carried out in this thesis are given along with the brief description of the subsequent chapters.

In the second chapter, the longitudinal autopilot has been designed based on the pole-zero assignment using nonlinear optimization methods. The control law is based on the Youla factorization in the ring of polynomials. The design problem has been posed as nonlinear optimization problem which has been solved using the direct search methods of Simplex search, Powell's conjugate direction and Pattern search.

In the third chapter, the longitudinal autopilot has been designed in TDOF configuration. The time domain and frequency domain performances have been achieved independently through the choice of two free parameters. These two free parameters are selected using closed loop model matching concept and frequency domain loop shaping /using constrained optimization with SA technique , for achieving the time domain and frequency domain performances, respectively.

In the fourth chapter, the lateral (roll-yaw) autopilot has been designed for stability axis roll rate command tracking using constrained optimization with Simulated Annealing. The control law, which is based on Youla parametrization, facilitates input-output decoupling of roll and yaw channels. As a result of which body axis roll rate and yaw rate capabilities are achieved independently.

In the fifth chapter, the robustness analysis has been carried out for neglected and mismodeled actuator dynamics and neglected sensor dynamics.

In the sixth chapter, the thesis is concluded and the main findings and contributions are highlighted.

Acknowledgement

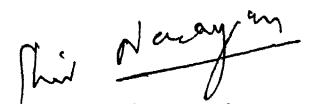
It is with a deep sense of gratitude that I express my indebtedness to Dr. K. E. Hole for his excellent supervision, guidance and encouragement during the thesis work.

I am extremely grateful to Prof. V. P. Sinha for his sincere advice and encouragement throughout the course of thesis work. I sincerely thank Dr. S. C. Srivastava for extending his lab facilities during the course of thesis work.

I take this opportunity to thank my research fellows for stimulating discussions. I also thank Mr. YDS Arya who helped me in better utilization of computer facilities.

I thank authorities at HBTI, Kanpur, where presently I am working, for allowing me to devote some time for the research obligations necessary to complete the Ph.D programme.

Finally, words are insufficient to express my gratitude towards my wife Shiromani and sons Neerav and Nishant who encouraged me to continue my work inspite of hardships to them.


(Shiv Narayan)

Contents

	Page
Synopsis	iv
Acknowledgement	viii
List of Figures	xii
List of Tables	xv
1 Introduction	1
1.1 General	1
1.2 Literature Survey	5
1.3 Motivation	8
1.4 Thesis Organisation	11
2 Pitch Autopilot Synthesis Based on Pole-zero Assignment with Nonlinear Optimization	13
2.1 Introduction	13
2.2 Missile Pitch Dynamics	15
2.3 Pole-Zero Assignment Control Law	16
2.4 Minimization of Control Input	18
2.5 Design Algorithm	19
2.6 Design Example	22
2.7 Results and Discussion	29
2.8 Conclusions	32
3 A Two Degrees of Freedom Parametric Longitudinal Autopilot Synthesis using Model Matching and Constrained Optimization with Simulated Annealing	33
3.1 Introduction	33
3.2 Parametrization of Stabilizing Controllers with TDof	35

3.2.1	Notations	35
3.2.2	TDOF Configuration	36
3.2.3	The Class of Stabilizing Controllers	38
3.3	Design for Pitch Acceleration Command Tracking - Using Closed Loop Model Matching Concept	39
3.3.1	General	39
3.3.2	Problem Formulation	40
3.3.3	Algorithm	44
3.4	Design for Shaping Frequency Domain Responses	46
3.4.1	General	47
3.4.2	Frequency Domain Performance Specifications	54
3.4.3	Objective Function	54
3.4.4	Simulated Annealing Technique	54
3.5	Example	55
3.5.1	Design for Acceleration Command Tracking	55
3.5.2	Design for Frequency Response Shaping	60
3.5.3	Results and Discussion	63
3.6	Conclusions	65
4	Synthesis of Decoupled Roll-Yaw (Lateral) Autopilot Using Constrained Optimization with Simulated Annealing	66
4.1	Introduction	66
4.2	Roll-Yaw Missile Dynamics and Closed Loop Design Goals	68
4.3	Control Law Based on Decoupling and Pole-Zero Assignment	68
4.4	Performance Specifications	73
4.4.1	Time Domain Performance Specifications	73
4.4.2	Frequency Domain Performance Specifications	75
4.5	Formulation of the Design Problem	78
4.5.1	Objective Function	78

4.5.2 Simulated Annealing Technique	78
4.6 Design Methodology	78
4.7 Design Algorithm	79
4.8 Design Examples	81
4.8.1 Example 1	81
4.8.2 Example 2	92
4.8.3 Results and Discussion	104
4.9 Conclusions	105
5 Robustness Analysis	107
5.1 Introduction	107
5.2 Robustness Theory for Singular Value Based Analysis	107
5.3 Autopilot Robustness Analysis	109
5.3.1 Actuator Uncertainty Analysis	110
5.3.1.1 Neglected Actuator Dynamics	110
5.3.1.2 Mismodeled Actuator Dynamics	113
5.3.2 Sensor Uncertainty Analysis	118
5.3.3 Results and Discussion	112
5.4 Conclusions	123
6 Conclusions	125
6.1 General	125
6.2 Review of the Work Done	125
6.3 Suggestions for Further Work	128
Bibliography	130
Appendix 1 Missile Dynamics	139
Appendix 2 Parametrization of Stabilizing Controllers with TDOF Configuration	142
Appendix 3 Fundamental Relations of Sensitivity and Complementary Sensitivity Functions	145

List of Figures

1.1	A BTT missile configuration	2
1.2	Air to Air missile block diagram	3
2.1	Longitudinal autopilot	15
2.2	Unity feedback system	16
2.3	Unit step response	29
2.4	Nyquist plot	30
2.5	Actuator deflection	31
3.1	Feedback control system with TDOF	36
3.2	Servo system with TDOF	37
3.3	Standard feedback configuration	37
3.4	Diagram showing M-circle constraint with respect to point $(-1 + j0)$ and Nyquist plot of the loop gain	48
3.5	The perturbed plant for the loop margin constraint	49
3.6	System with a time varying nonlinearity	49
3.7	An example of a sector $[a,b]$ nonlinearity $f(x,t_0)$	51
3.8	Typical gain characteristics of sensitivity and complementary sensitivity functions	52
3.9	Unit step responses	59
3.10	Elevator fin deflection	59
3.11	Nyquist plot	64
3.12	Bode magnitude plot with the loop broken at the input of the plant	64
3.13	Gain characteristics of complementary sensitivity and sensitivity functions at the plant input	65
4.1	Multivariable feedback control system	69

4.2	Unit step response for the body axis roll rate and yaw rate	88
4.3	Aileron and rudder deflections	88
4.4	Sideslip	89
4.5	Bode magnitude plot for the roll and yaw rate channels	89
4.6	Sensitivity and complementary sensitivity functions for the roll channel at the output	90
4.7	Sensitivity and complementary sensitivity functions for the yaw channel at the output	90
4.8	Unit step response for the stability axis roll rate	91
4.9	Stability axis roll rate response	98
4.10	Yaw rate response	98
4.11	Aileron and rudder deflections	99
4.12	Step response for the stability axis roll rate	99
4.13	Sideslip response	100
4.14	Sideslip due to stability axis roll rate	100
4.15	Sideslip	101
4.16(a)	Magnitude plots for the stability axis roll rate and yaw rate channels	101
4.16(b)	Phase plots for the stability axis roll rate channel and yaw rate channel	102
4.17	Sensitivity and complementary sensitivity functions for the roll rate channel at the plant output	102
4.18	Sensitivity and complementary sensitivity functions for the yaw channel at the plant output	103
5.1	Feedback control system	110
5.2	Pitch robustness to neglected actuator dynamics in Chapter 2	112
5.3	Pitch robustness to neglected actuator dynamics in Chapter 3	
5.4(a)	Roll-yaw robustness to neglected actuator dynamics in	

Chapter 4 (Example 1)	114
5.4(b) Roll-yaw robustness to neglected actuator dynamics in Chapter 4 (Example 2)	114
5.5 Pitch robustness to mismodeled actuator dynamics in Chapter 2	116
5.6 Pitch robustness to mismodeled actuator dynamics in Chapter 3	116
5.7(a) Roll-yaw robustness to mismodeled actuator dynamics in Chapter 4 (Example 1)	117
5.7(b) Roll-yaw robustness to mismodeled actuator dynamics in Chapter 4 (Example 2)	117
5.8 Pitch robustness to neglected sensor dynamics in Chapter 2	120
5.9 Pitch robustness to neglected sensor dynamics in Chapter 3	120
5.10 Roll-yaw robustness to neglected sensor dynamics in Chapter 4 (Example 1)	121
5.11 Roll-yaw robustness to neglected sensor dynamics in Chapter 4 (Example 2)	121
A4.1 The SA minimization algorithm	149

List of Tables

2.1	Variation of solution vector $\bar{X} = \{p_1, p_2, p_3, p_4\}$ with respect to starting solution and penalty factor (λ)	27
2.2	Autopilot design results	30
3.1	Comparative view of the time response specifications with various values of k	60
4.1	Time domain and frequency domain performances for the body axis roll rate and yaw rate (Example 1)	91
4.2	Time domain and frequency domain performances for the body axis roll rate and yaw rate (Example 2)	104
4.3	Tradeoff among rise time, overshoot and bandwidth	104
5.1	Robustness Results	123

α = Angle of Attack
 β = Sideslip Angle

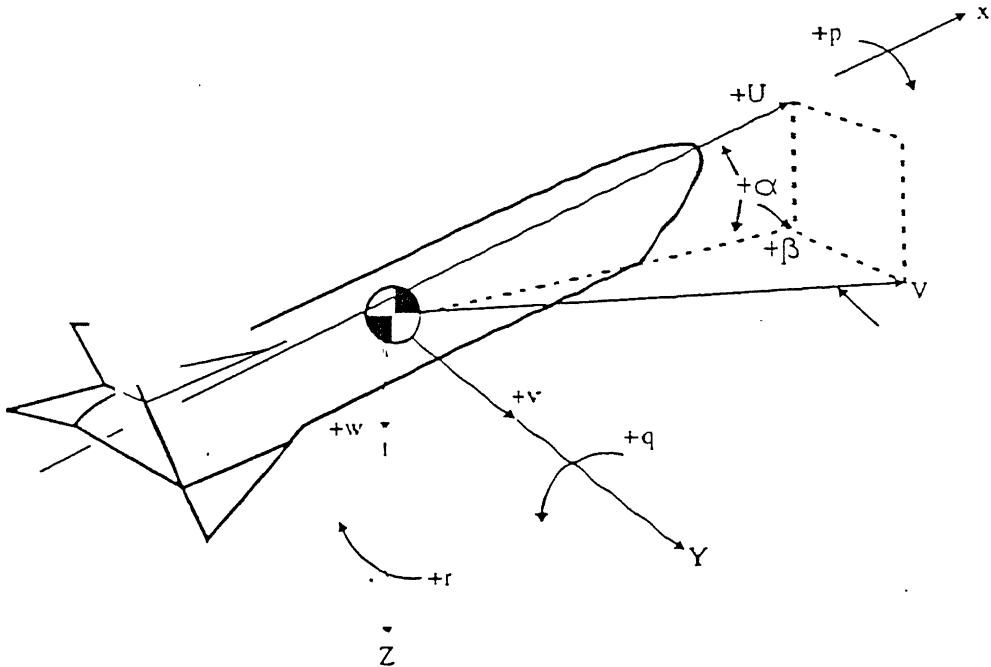


Figure 1.1 : Asymmetric BTT Missile Configuration

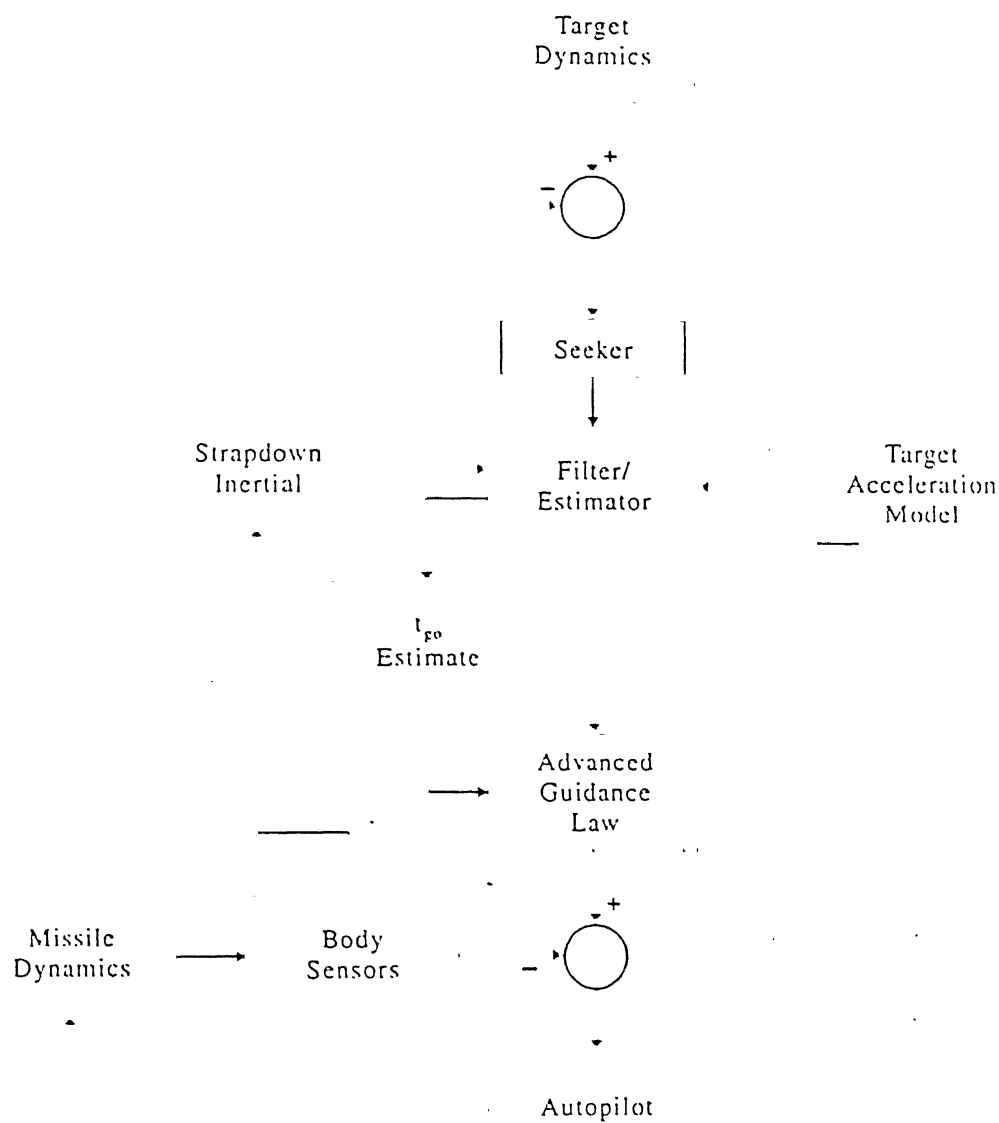


Figure 1.2 : Air to Air Missile Block Diagram

"skidding" motion to the missile; hence the name "skid-to-turn". In contrast, a BTT should not have, ideally any sideslip. To achieve the desired orientation, it is rolled (banked) so that the plane of maximum aerodynamic normal force is oriented in the desired direction and the force is controlled by adjusting the angle of attack.

According to control of missile motion in pitch, yaw and roll plane, the autopilots are classified as longitudinal, lateral and roll autopilots respectively.

The actual missile dynamics is nonlinear in nature and involves coupling among the pitch, yaw and roll axes. Moreover, the missile has to function in changing environments which gives rise to uncertainties in aerodynamic characteristics, mass and balance, wind, flexible body mode dynamics, actuator and sensor nonlinearities and noise.

Because of the above characteristics of the missile plant, the possible approaches for the design of autopilot for the missile could be:

(i) to design an autopilot for combined three axes nonlinear system to track acceleration commands in all the three channels (pitch, yaw and roll) and, simultaneously, ensuring stability of the overall system.

(ii) to linearize the missile dynamics at an operating point and design linear time invariant (LTI) autopilot to track the commanded accelerations.

When the design is based on linear time invariant (LTI) model, the dynamic interactions among pitch, yaw and roll axes could be ignored and the robust controller be designed to achieve the stability and performance requirements. In this approach coupling is taken as disturbance acting on the system and robust controller is designed for each channel to take care of the plant uncertainties and parameter variations.

Another approach could be to take linearized plant as multi input and multi output (MIMO) system and design a linear time invariant controller for this plant for commands tracking, maintaining stability of the overall closed loop system.

In an asymmetric bank-to-turn (BTT) missile configuration, as shown in Fig.1.1 [7], very strong roll-yaw coupling is present. In its operation the BTT missile is first banked so as to have plane of the maximum aerodynamic normal force in the direction of target and, then, develops an angle of attack to achieve desired acceleration. The

function of the autopilot is to cause the missile to achieve the commanded acceleration as closely as possible, while maintaining closed loop system stability and certain constraints on the other operating variables, and control signals. Due to asymmetric airframe, the missile has tendency for sideslip. If sideslip is allowed to develop, in conjunction with angle of attack it would give rise to large roll rates. Therefore, for a BTT missile, the most significant constraint is on the allowable sideslip.

For the reason of large roll rates due to sideslip, the linearized pitch dynamics are separated from linear coupled roll-yaw dynamics. Therefore, the autopilot design for a kind of BTT missile shown in Fig 1.1, consists of the design of two autopilots: one for the pitch acceleration command tracking, known as longitudinal autopilot, and another for commanding the roll rate about the velocity vector of the missile, known as lateral autopilot.

1.2 Literature Survey

The autopilots for the missiles have been designed using classical, modern control, and adaptive control techniques.

The vast majority of autopilots have been designed using classical approach [3,4]. In classical methods, the design is based on a linear missile model. The linear missile model is obtained by linearizing the dynamics of the missile at an operating point, and, the model thus obtained is assumed valid in the neighbourhood of the operating point. The design is performed by ignoring the dynamic interactions among the pitch, yaw and roll axes. This permits individual channel designs for each pitch, yaw and roll axes.

Although, the classical designs are based on single input single output (SISO) control theory, their performance can be enhanced through multivariable analysis. Wise [4] used multivariable singular value techniques to maximize performance and stability robustness of an existing roll-yaw autopilot designed with classical method. Nesline et al [5] designed robust missile autopilot using combined optimal/classical approach. Modern control theory has been used in conjunction with classical control theory to achieve a robust design which deals with the uncertainties of the high frequency effects while giving optimal performance in the low frequency range.

William et al [6] designed an autopilot using modern state space approach. The design is based on a tenth order model of the missile dynamics which is decoupled into separate roll and pitch/yaw sub-systems by treating roll rate as an exogenous input to the pitch/yaw equations. The models are linearized over specified operating region and gains are scheduled on dynamic pressure and roll rate. Unmeasured states are estimated using a constant gain, reduced order Kalman filter, and the separation principle is invoked to compute controller gains. The desired roll channel time response is obtained using a pole placement controller design procedure. Robust pitch/yaw channel gains are determined using LQG theory with loop transfer recovery (LQG/LTR). Integral control action is obtained by treating the commanded accelerations from the guidance system as state variables.

Other design methodologies using modern control theory are given in [7-15]. Wise [7] eliminated the steady state command errors, which are inherent in LQR error state equation formulations by incorporating integral control into LQG/LTR design. A trade off is established between stability robustness recovery (LTR) and sensor noise amplification, which limits the amount of recovery possible.

Lin and Lee [10] used GSLQ (Generalized Singular Linear Quadratic) control to BTT autopilot design. Control constraints were imposed by pole placement techniques. Good stability margins were obtained at each of the output, and excellent command tracking was achieved in the presence of sinusoidal disturbances and roll, pitch and yaw couplings.

Reichert [11] designed dynamically scheduling multiple linear time invariant (LTI) controllers, using H_∞/μ synthesis for systems with widely varying plant dynamics. Wise et al [12] and, Wise and Nguyen [13] designed autopilots using H_∞ and projective controls, respectively, for normal acceleration command tracking. Projective controls is used to retain the eigen-structure of an H_∞ optimal state feedback controller using a low order output feedback compensator, and retains the performance robustness and disturbance attenuation properties of the state feedback design.

Sobel and Cloutier [14] applied eigen-structure assignment to the design of an autopilot for the extended medium range air to air technology (EMRAAT) missile. Eigen-structure assignment is a state variable multi input multi output (MIMO) design

method that allows placement of the system eigen-vectors as well as their corresponding eigen-values. In this design the eigen-structure assignment feedback gains are computed by choosing desired eigen-vectors based on mode decoupling and using the orthogonal projection solution to compute achievable eigen-vectors.

Shamma and Cloutier [15] applied gain scheduling technique for a missile for longitudinal autopilot. This design methodology does not involve linearization about an operating point. Rather, the missile dynamics are brought to a quasilinear-parameter varying (LPV) form via a state transformation. Once in quasi-LPV form a robust controller using μ -synthesis is designed to achieve the angle of attack control via fin deflections. The final design is an inner/outer loop structure, with the angle of attack control being the outer loop. The effect of the inner loop is to linearize the missile dynamics in an approximate and band limited manner thereby leading to a simplified outer loop design with guaranteed inner loop robustness properties.

Benshabat and Chait [16] applied quantitative feedback theory (QFT) to a class of missiles that exhibit unstable and non-minimum phase behaviour over a large flight envelope. This technique overcame the problems related with gain scheduling. The advantages in using QFT are that (1) it is possible to investigate the feasibility of fixed controllers for the whole flight envelope, and, (2) it reveals tradeoffs between the size of flight envelope, controller complexity and closed loop specifications.

Lin et al [17] designed a robust autopilot for the HAVE DASH II missile system. The controllers are solved using the generalized Hamiltonian approach which unifies a class of robust control designs in the same framework. Among the autopilot designs are the linear quadratic Gaussian (LQG) autopilot, generalized singular linear quadratic (GSLQ) autopilot, and H_∞ autopilot. All the designs are formulated in the canonical form and solved based on the generalized Hamiltonian formulation. Krause and Stein [18] proposed a general adaptive control structure within which an autopilot design was accomplished with tuned system performance and robustness guarantees. Kamen et al [19] applied an indirect adaptive control technique to a BTT missile autopilot design.

Apkarian et al [69] applied linear parameter varying (LPV) techniques to the global control of the missile. This technique is the extension of the standard H_∞

synthesis technique. The proposed methodology produces an LPV controller that is automatically gain scheduled along the trajectories of the plant. Gratt et al [70] used feedback linearization for the autopilot design for the boost phase of the advance kinetic energy missile. Application of the feedback linearization methodology permitted an autopilot design without considering varying operating conditions. Wise et al [71] used nonlinear H_∞ optimal control to design a pitch plane flight control system for a high angle of attack agile missile. The nonlinear H_∞ control law was obtained by approximating the solution to the Hamilton-Jacobi-Isaacs equation. The solution to the partial differential equation was obtained by using the method of characteristics and was numerically approximated using successive approximations.

Carter and Shamma [72] used linear parameter varying transformations to design a gain scheduled autopilot for a bank-to-turn missile. The gain scheduled design did not require linearizations about operating points. This framework was applied to the design of a coupled longitudinal/lateral bank-to-turn missile autopilot. The pitch and roll-yaw dynamics were separated and robust controllers were designed using μ -synthesis for both the pitch and roll-yaw channels. Fu et al [73] proposed an adaptive robust neural network based control approach for a bank-to-turn missile autopilot design.

Zhu et al [74] designed a missile autopilot for the angle of attack and normal acceleration tracking using extended mean assignment (EMA) control technique for the linear time varying (LTV) systems. The EMA control technique is based on a new eigenvalue concept, called series-D (SD) eigenvalue for LTV systems. Geng et al [75] proposed a fuzzy neural network control system architecture called the fuzzy cerebellar model arithmetic computer (fuzzy CMAC) neural network. This fuzzy neural network architecture exploited a synergism between the original CMAC neural network and the theory of fuzzy logic controller.

1.3 Motivation

There are basically two schemes of design of a linear time invariant (LTI) controller which stabilizes a given LTI plant, and meet some design specifications. The first is based on analytical methods for determining a controller which is optimal

in some well defined sense, and the second is based on parameter optimization. The analytical methods have closed form solutions whereas the parameter optimization problems are usually solved by numerical methods.

The first scheme is called the optimal controller design. The most common examples are linear quadratic Gaussian (LQG) based designs, and H_∞ optimal controller designs. These analytical methods minimize a simple objective function for finding a controller. The weight matrices are, usually, specified in the objective function. The advantage of these optimal controllers is that they always find stabilizing controllers. The great disadvantage of these methods is that the design specifications are to be translated into objective function, and the weight matrices. In complex systems, it is difficult to fit all design specifications into objective function and also the translation of the actual design specifications into specification of weight matrices is difficult [50,51]. Similar comments apply to the other optimal controllers also. For example, in H_∞ optimal control method, the actual design specifications are to be translated into the weighting transfer matrices.

On the other hand, the parameter optimization methods for LTI feedback design start with the controller structures. Controller structure means a system model whose parameter values can be adjusted. The next step in the design using parameter optimization methods is to select an objective function that represents design specifications. An objective function can be formed by weighted sum or maximum of various performance indices. The weights define the relative importance of the various performances of the system. Certain explicit constraints may also be added.

After a controller structure, an objective function and some constraints have been specified, the design is formulated as nonlinear optimization problem. This problem can be solved using optimization methods. The following are the main advantages of the parameter optimization methods:

(i) A wide range of objective functions and constraints can be allowed than those available in analytical methods.

(ii) If the designer is certain that some controller of selected architecture will do the job, the parameters of the controller can be obtained using parameter optimization.

(iii) If a reasonable controller has been designed using analytical methods, it can be improved using parameter optimization methods.

(iv) The designer has the freedom as regards the structure of the controller.

However, the parameter optimization methods pose some problems :

(a) Initial guess is required in optimization methods. For simple systems, the initial guess is not a big problem but for complex systems it is a drawback.

(b) The nonlinear optimization problem may be nonconvex in nature. The general algorithms may provide only local optimal solution but not a globally optimal.

These drawbacks can be overcome by using recent techniques of Simulated Annealing (SA) and Genetic Algorithms (GA) [38, 52, 63]. These techniques provide global optimal or near global optimal solution.

The factorization approaches, initially presented by Youla et al [29, 32] and subsequently by Desoer et al [30, 44], provide simple parametrizations of controllers that stabilize a given plant. The controller parametrizations provide the choice of controller structure. The controller structure can be chosen through the choice of certain parametrization, and the controller design can easily be posed as optimization problem.

The design specifications of a feedback control system can be expressed as the frequency and time domain specifications or in other words, design specifications require the shaping of several frequency and time domain responses. These responses can be expressed as hard bound constraints. So all the design specifications can be expressed as hard bound constraints on the frequency and time domain responses. The objective function can be formed as a weighted sum or the maximum of various frequency and time domain performance functions.

From the literature survey, as in Section 1.2, it is clear that most of the autopilot designs for various kinds of missiles have used analytical methods. The BTT missile, shown in Fig. 1.1, is a fast maneuvering, high performance missile which is meant for air to ground applications. It has to function in uncertain and changing environments. This demands certain level of time domain and frequency domain responses from the missile system. The parametric methods of controller design with nonlinear optimization provide good framework for meeting the demanding requirements on

time domain and frequency domain performances. Moreover, the roll and yaw channels in the above configuration of the missile are coupled and require to keep sideslip small to avoid large roll rates. These constraints can be easily incorporated in the frequency domain and time domain performance functions. Parametric synthesis methods for autopilot design in this framework have not been reported in the literature.

Therefore, the motivations behind the work carried out in this thesis are :

(1) to explore the possibility of parametric synthesis of longitudinal (pitch) autopilot and develop design algorithm using nonlinear optimization methods.

(2) to explore the possibility of parametric synthesis of longitudinal autopilot and develop design algorithm in two degrees of freedom (TDOF) configuration using Simulated Annealing (SA) technique.

(3) to explore the possibility of parametric synthesis of lateral (roll-yaw) autopilot and develop the design algorithm using SA technique.

(4) to investigate the robustness of the designed autopilot.

1.4 Thesis Organisation

The first chapter introduces the control problem and autopilot design requirements for a BTT missile, presents brief literature survey on the subject, sets the motivation behind the research work carried out in this thesis.

In second chapter, a longitudinal autopilot has been designed based on pole-zero assignment using nonlinear optimization methods. The control law is based on the Youla parametrization in the ring of polynomials. The design problem has been posed as nonlinear optimization problem which has been solved using direct search methods of Simplex search, Powell's conjugate direction and Pattern search. The performance function includes the terms corresponding to the command tracking, overshoot, undershoot, gain and phase margins.

In third chapter, the longitudinal autopilot has been designed in two degrees of freedom (TDOF) configuration. The time and frequency domain performances have been achieved independently through the choice of two free parameters. These two free parameters are selected using closed loop model matching concept and the

frequency domain loop shaping using constrained optimization with Simulated Annealing technique, for achieving time domain and frequency domain responses, respectively.

In fourth chapter, the lateral (roll-yaw) autopilot has been designed for the stability axis roll rate command tracking using constrained optimization with simulated Annealing. The control law which is based on Youla parametrization facilitates input-output decoupling of roll and yaw channels as a result of which the body axis roll rate and yaw rate capabilities are achieved independently.

In fifth chapter, the robustness analysis has been carried out for neglected and mismodeled actuator dynamics and neglected sensor dynamics using singular values.

In sixth chapter, the thesis is concluded and the main findings and contributions are highlighted.

Chapter 2

Pitch Autopilot Synthesis Based on Pole-Zero Assignment with Nonlinear Optimization

2.1 Introduction

In control systems, the pole dominates the transient response and system stability [20-30], and, the zero of a system plays important role in the interaction between the system and environment [24-26]. So there have been many studies on the pole and zero assignment methods. Another strategy for control system design is the pole-zero assignment to minimize the control input signal of the system [25]. In optimal control theory [28], specially LQR and LQG, control input signal is minimized in the performance index.

One of the important results in the design of control systems is the parametrization of all stabilizing controllers in the unity feedback configuration [29,30].

With the development of modern computing facilities, these algebraic methods are advantageous in the following sense :

(i) The designer's level of subjective judgement is minimised.

(ii) Design goals, performance as well as stability, can straight way be incorporated in the performance index and the problem can be cast as parameter optimization problem which can be solved using optimization techniques. Thus parametrized controller can be constructed in a systematic way to assure stability as well as other design goals.

(iii) The algebraic methods permit assignment of poles and zeros through the selection of polynomials.

In this chapter, a parametrized longitudinal autopilot is designed using pole-zero assignment. The pitch dynamics form a single input multi output (SIMO) model. In the missile configuration, Fig.2.1, the rate feedback forms the inner loop whereas the acceleration feedback forms the outer loop. In this methodology one loop is designed at a time. While the inner pitch rate loop provides stabilization, damping and minimum input control, the outer acceleration loop is designed for acceleration command tracking with specified gain and phase margins.

The pole-zero assignment control law is developed based on the method by Tu [27], which uses Bongiorno and Youla's factorization approach [29] in the ring of polynomials.

The overall closed loop transfer function places a pair of dominant complex conjugate poles to achieve performance measures e.g. rise time, percentage overshoot and settling time etc. The remaining system poles and zeros are then selected via nonlinear optimization to give desired gain and phase margins. The performance index includes the terms corresponding to command tracking error, overshoot, undershoot, gain and phase margins. As this performance index is nondifferentiable, the gradient based optimization methods would provide poor results. Therefore, direct search methods of Simplex search, Powell's conjugate direction and Pattern search have been employed for optimization and their performance has been compared.

The structure of the chapter is as follows : in Section 2.2, the missile pitch dynamics is described. In section 2.3, the pole-zero assignment control law is discussed. In Section 2.4, the minimization of control input is described. In Section 2.5, the design algorithm is given and in Section 2.6, the design algorithm is implemented for the design of longitudinal autopilot. In Section 2.7, the design results are given and are compared with the results of other design methodologies. In Section 2.8, the chapter is concluded.

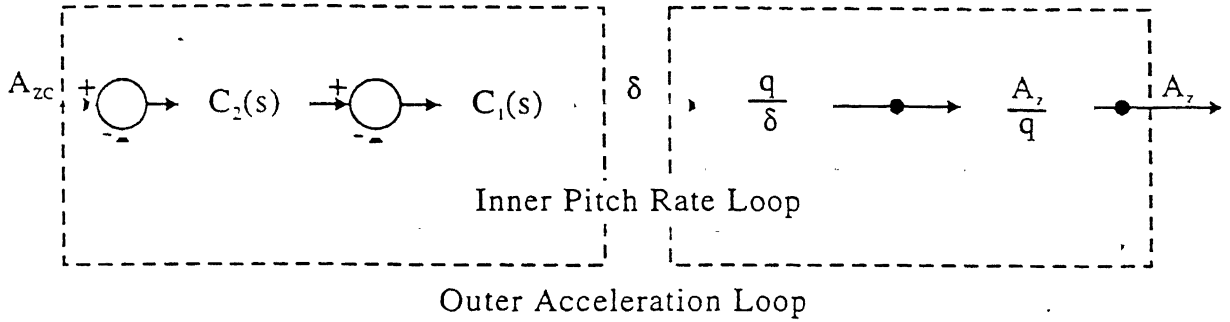


Figure 2.1 : Longitudinal Autopilot

2.2 Missile Pitch Dynamics

The details of the missile pitch dynamics, taken from [7,13], are described in Appendix 1. The equations governing missile pitch dynamics are rewritten as follows :

$$\begin{aligned}\dot{\alpha} &= Z_{\alpha} \cdot \alpha + Z_{\delta} \cdot \delta_e + q \\ \dot{q} &= M_{\alpha} \cdot \alpha + M_{\delta} \cdot \delta_e \\ \ddot{\delta}_e &= -2\xi\omega \dot{\delta}_e - \omega^2(\delta_e - \delta_{ec})\end{aligned}$$

where α , q , δ_e , ξ and ω are angle of attack, pitch rate, elevator fin deflection, fin actuator damping and natural frequency, respectively. The measured variables are normal acceleration, $A_z = VZ_{\alpha} \cdot \alpha + VZ_{\delta_e} \cdot \delta_e$ (ft/s^2) and the pitch rate q . The scalar control input, $u = \delta_{ec}(rad)$ is the elevator fin angle command. V is the missile velocity.

The transfer function matrix from the elevator fin command, δ_{ec} , to normal acceleration, A_z , and pitch rate, q , is given by :

$$G_p(s) = \begin{bmatrix} \frac{A_z}{\delta_{ec}} \\ \frac{q}{\delta_{ec}} \end{bmatrix} = \begin{bmatrix} \frac{\omega^2 V (Z_{\delta} \cdot s^2 + Z_{\alpha} M_{\delta} - Z_{\delta} M_{\alpha})}{(s^2 - Z_{\alpha} s - M_{\alpha})(s^2 + 2\xi\omega s + \omega^2)} \\ \frac{\omega^2 (M_{\delta} \cdot s + M_{\alpha} Z_{\delta} - M_{\delta} Z_{\alpha})}{(s^2 - Z_{\alpha} s - M_{\alpha})(s^2 + 2\xi\omega s + \omega^2)} \end{bmatrix}$$

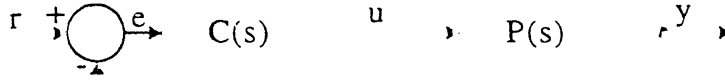


Figure 2.2 : Unity Feedback Configuration

2.3 Pole-Zero Assignment Control Law

Consider the unity feedback configuration shown in Fig.2.2

Let the plant be

$$P(s) = \frac{B(s)}{A(s)}, \quad (2.1)$$

where $A(s)$ and $B(s)$ are coprime polynomials.

The reference input is

$$R(s) = \frac{N(s)}{M(s)}, \quad (2.2)$$

where $M(s)$ and $N(s)$ are coprime polynomials.

The sensitivity function is given as

$$S(s) = \frac{1}{1 + P(s) C(s)} \quad (2.3)$$

and, the error is given by

$$E(s) = S(s) R(s) \quad (2.4)$$

Let $A(s)$, $B(s)$ and $M(s)$ be factorized as

$$A(s) = A_+(s) \cdot A_-(s) \quad (2.5)$$

$$B(s) = B_+(s) \cdot B_-(s) \quad (2.6)$$

$$M(s) = M_+(s) \cdot M_-(s) \quad (2.7)$$

where $A_+(s)$, $B_+(s)$ and $M_+(s)$ have all their zeros in $Re(s) \geq 0$ while $A_-(s)$, $B_-(s)$ and $M_-(s)$ have all their zeros in $Re(s) < 0$.

For a reference signal tracking and desired pole assignment, the sensitivity function must be of the form [27] :

$$S(s) = \frac{W(s) M_+(s)}{G(s)}, \quad (2.8)$$

where $G(s)$ is Hurwitz polynomial with desired closed loop poles and $W(s)$ is undetermined polynomial which should satisfy the internal stability constraints.

2.3.1 Definition [27]

The sensitivity function $S(s)$ is said to be internally stable if the closed loop system of Fig.2.2 is asymptotically stable for some choice of $C(s)$ ie. there is no pole-zero cancellation between $C(s)$ and $P(s)$ in $Re[s] \geq 0$.

The following Lemma gives conditions which guarantee internal stability of the sensitivity function.

2.3.2 Lemma [27]

The sensitivity function $S(s)$ is internally stable if and only if all the following conditions hold:

- (i) $S(s)$ is analytic in $Re[s] \geq 0$
- (ii) The numerator polynomial of $S(s)$ is divisible by $A_+(s)$.
- (iii) The numerator polynomial of $1-S(s)$ is divisible by $B_+(s)$.

Equation (2.8) and condition (ii) of the Lemma imply that the numerator of $S(s)$ must contain the least common multiple (LCM) of $A_+(s)$ and $M_+(s)$. ie.

$$S(s) = \frac{W(s) M_+(s)}{G(s)} = \frac{L(s) Z(s)}{G(s)}, \quad (2.9)$$

where $Z(s)$ is the least common multiple of $A_+(s)$ and $M_+(s)$ while $L(s)$ is undetermined polynomial and is used for loop shaping.

To satisfy the requirements of causality, $S(s)$ must be proper i.e.

$$\deg(G(s)) \geq \deg(L(s)) + \deg(Z(s)) \quad (2.10)$$

From the equation (2.9), we have

$$T(s) = 1 - S(s) = \frac{G(s) - L(s) Z(s)}{G(s)} \quad (2.11)$$

From condition (iii) of the Lemma, we have

$$\begin{aligned} H(s) &= G(s) - L(s) Z(s) \\ &= B_+(s) F(s) \end{aligned} \quad (2.12)$$

where, $F(s)$ is undetermined polynomial, the choice of which facilitates incorporation of additional zeros.

2.3.4 Theorem [27]

The solution of $L(s)$ in equation (2.12) exists if and only if $M_+(s)$ is coprime with $B_+(s)$.

The controller, thus, can be derived from the equation (2.3) as

$$\begin{aligned} C(s) &= \frac{1 - S(s)}{P(s) S(s)} \\ &= \frac{A(s) B_+(s) F(s)}{B(s) L(s) Z(s)} \end{aligned} \quad (2.13)$$

The output is given by

$$\begin{aligned} Y(s) &= (1 - S(s)) \cdot R(s) \\ &= \frac{B_+(s) F(s) N(s)}{G(s) M(s)} \end{aligned} \quad (2.14)$$

The closed loop transfer function is given by

$$T(s) = \frac{B_+(s) F(s)}{G(s)} \quad (2.15)$$

The loop transfer function, $L_i(s)$, at the input of plant, is given by

$$L_i(s) = P(s) C(s) = \frac{B_+(s) F(s)}{L(s) Z(s)} \quad (2.16)$$

The desired loop shaping and command tracking can be achieved by proper choice of $F(s)$, $L_i(s)$ and $G(s)$.

2.4 Minimisation of Control Input

The control input signal, $u(t)$, is minimized to save the control energy and to avoid saturation problems.

The L_2 norm of $u(t)$ is defined as [32]

$$\|u\|_2 = \left(\int_0^{\infty} u^2(t) dt \right)^{1/2}$$

If $u(t)$ is bounded for all values of $t \geq 0$; is zero for $t < 0$ and approaches zero at least as fast as $e^{-\epsilon t}$ as t approaches infinity, where ϵ is a small positive constant, then applying the Parseval theorem [39], L_2 norm of $u(t)$ becomes

$$\begin{aligned}
 \|u\|_2 &= \sqrt{\int_0^{\infty} u^2(t) dt} \\
 &= \frac{1}{2\pi j} \sqrt{\int_{-j\infty}^{j\infty} U(s) U(-s) ds} \\
 &\equiv \|U(s)\|_2.
 \end{aligned} \tag{2.17}$$

where $U(s)$ is the Laplace transform of $u(t)$, i.e $U(s)$ is stable with poles in $\text{Re}[s] < 0$.

2.5 Design Algorithm

The design algorithm is aimed at achieving closed loop pole-zero configurations for inner pitch rate loop and outer acceleration loop for the specified performance. The design is achieved in two parts: in Algorithm I, the inner pitch rate loop and in Algorithm II, the acceleration command tracking loop is designed.

In the design methodology given above, once the overall transfer function is chosen, the rest of the design for parametric controller is straight forward. The crux of the design is how to choose transfer functions for inner pitch rate loop and outer acceleration loop. The choices can be based on the minimization of the integral of time multiplied by absolute error (ITAE), quadratic performance index, model matching or computer simulations.

Some constraints are imposed on the bandwidth of the overall system or on the actuating signal. For the inner pitch rate loop, since our concern is with stabilization, damping and control input minimization, the proper choice would be to choose transfer function based on ITAE and impose constraint on $u(t)$.

Overall closed loop transfer function for the acceleration command tracking loop is obtained by model matching through nonlinear optimization and constraints are imposed on maximum overshoot, maximum undershoot, gain and phase margins.

Let the plant transfer functions for the inner and outer loops be denoted by $P_1(s)$ and $P_2(s)$, respectively. $T_1(s)$ and $T_2(s)$ denote closed loop transfer functions for inner and outer loops, respectively.

The L_2 norm of the control input, u , to the actuator due to unit step input is minimized. This saves the control energy and avoids saturation problems [27].

Now design algorithms for the pitch rate loop and acceleration command tracking loop are given as Algorithm I and Algorithm II, respectively.

2.5.1 Algorithm I : (for pitch rate loop)

Step 1

Optimal ITAE, expressed as polynomial in ω_0 is selected from the standard forms [33] for $U(s)$ to be strictly proper. The standard form of ITAE, however, is not available for all plant transfer functions. In such cases the idea of [34] may be used and a digital computer simulation may be used to obtain its optimal transfer function under the constraint on $u(t)$.

Step 2

By computer simulation, ω_0 is obtained to give $|u(t)| < 1.0$ for all $t \geq 0$.

Step 3

L_2 norm of $u(t)$ i.e. $\|u(t)\|_2$ is minimized using nonlinear programming under the constraint of equation (2.12) thus assigning the zeros of the system suitably.

Step 4

After ascertaining closed loop transfer function $T_1(s)$ and hence $L(s)$, $F(s)$ and $G(s)$ from equations (2.11), and (2.12), the controller $C_1(s)$ is parametrized using equation (2.13).

2.5.2 Algorithm II : (for acceleration command tracking loop)

Step 1

Choose the second order reference linear model whose time response behaviour is consistent with the specified performance measures of the missile system.

Step 2

Degree of the numerator and denominator polynomials, $n(s)$ and $m(s)$, of the closed loop transfer function $T_2(s)$ is selected such that :

$$(N_p - N_z)_{\text{closed loop system}} \geq (N_p - N_z)_{\text{open loop system}} \quad (2.18)$$

where N_p and N_z denote number of poles and zeros, respectively. i.e.

$$n(s) = (s + \alpha_1) (s + \alpha_2) \dots (s + \alpha_{N_z})$$

$$m(s) = (s + \beta_1) (s + \beta_2) \dots (s + \beta_{N_p})$$

An upper limit is placed on the selection of α_i and β_i to avoid numerical overflow during the optimization process and also because highly damped poles tend to affect the system dynamics adversely [35].

Step 3

Search for α_i and β_i .

The α_i and β_i are design variables denoted by the vector \bar{X} . They are selected via nonlinear optimization techniques.

The design variables are selected to minimize the following performance index

:

$$J = \sum_{i=1}^n \left[y_i(t) - y_i^d(t) \right]^2 + \lambda \left[\left(y_{\max} - y_{\max}^d \right)^2 + \langle y_{\min} \rangle^2 \right. \\ \left. + (\angle L_i(j\omega_c) + 180^\circ - \theta_{spec})^2 + (20 \log_{10} |L_i(j\omega_g)| - N)^2 \right] \quad (2.19)$$

where λ is the penalty factor; $y^d(t)$ is the desired time response ; $\langle y_{\min} \rangle^2$ is zero if $y_{\min} \geq 0$ or otherwise it equals $(y_{\min})^2$.

The first term in the penalty term provides a measure of the error for the percentage overshoot.

The third term in the penalty term accounts for phase margin ($\geq \theta_{spec}$). The phase margin specification is satisfied when the phase angle of $L_i(j\omega_c)$ is greater than or equal to $(180^\circ - \theta_{spec})$ at frequency ω_c when the magnitude of $L_i(j\omega_c)$ is equal to 0 dB. $L_i(j\omega)$ is the loop transfer function with loop broken at the input of actuator of the missile.

The last term in the penalty term imposes the constraint on the gain margin ($\geq N$ dB)

Step 4

After ascertaining closed loop transfer function, $T_2(s)$ and hence $L(s)$, $F(s)$ and $G(s)$ from the equations (2.11) and (2.12), the parametric controller $C_2(s)$ is obtained using equation (2.13).

2.6 Design Example

Design example has the model described in Section 2.2 of this chapter. The flight conditions studied here are the same as considered in [13], represented by $\alpha = 16^\circ$, Mach 0.8 and an altitude of 4000 ft. The nominal values of the dimensional aerodynamic stability derivatives are :

$$Z_\alpha = -1.3046 \text{ (1/s)} ; Z_\delta = -0.2142 \text{ (1/s)}$$

$$M_\alpha = 47.7109 \text{ (1/s}^2\text{)}; \text{ and } M_\delta = -104.8346 \text{ (1/s}^2\text{)}$$

The remaining system parameters are :

$$V = 886.78 \text{ (ft/s)}; \xi = 0.6, \omega = 113.0 \text{ (rad/s)}$$

The transfer function matrix, $G_p(s)$, is given by

$$G_p(s) = \begin{bmatrix} \frac{A_z}{\delta_{ec}} & \frac{-2.4254e6 (s + 26.196) (s - 26.196)}{(s + 67.8 + 90.4i) (s + 67.8 - 90.4i) (s + 7.5903) (s - 6.2857)} \\ \frac{q}{\delta_{ec}} & \frac{-1.3386e6 (s + 1.4021)}{(s + 67.8 + 90.4i) (s + 67.8 - 90.4i) (s + 7.5903) (s - 6.2857)} \end{bmatrix}$$

(2.20)

The transfer function from fin command δ_{ec} to A_z has a RHP zero and the plant has also a RHP pole. Thus the missile pitch plant is unstable and non-minimum phase.

Typical design specifications for such a missile can be stated as :

Design a parametric longitudinal autopilot to track the commanded acceleration maneuvers with a rise time (63%) less than 0.3 sec, overshoot less than 5%, initial undershoot less than 2.5%; The controller must provide gain and phase margins of (-6,+10)dB and ± 60 degrees, respectively. The controller bandwidth is to be restricted by high frequency unmodeled dynamics constraints (eg. unmodeled flexible modes and actuator nonlinearities).

The controller is synthesized using Algorithms I and II of the design algorithm discussed in Section 2.5.

2.6.1 Controller Synthesis for Pitch Rate Loop

Algorithm I is used for designing pitch rate loop.

For the inner pitch rate loop, the plant transfer function is

$$P_1(s) = \frac{-1.3386e6 (s + 1.4021)}{(s + 67.8 + 90.4i)(s + 67.8 - 90.4i)(s + 7.5903)(s - 6.2857)}$$

The controller $C_1(s)$ is designed with $\|u(t)\|_2 < 1.0$, for all $t \geq 0$.

From Fig. 2.2 the control input $U(s)$, can be written in terms of sensitivity function $S(s)$ as

$$U(s) = C(s) S(s) R(s).$$

Substituting the values of $R(s)$, $S(s)$ and $C(s)$ from equations (2.2), (2.9) and (2.13), it reduces to

$$U(s) = \frac{A(s) F(s) N(s)}{B_-(s) G(s) M(s)} \quad (2.21)$$

Factorizing the plant transfer function $P_1(s)$ according to equations (2.5), (2.6) and (2.7), we get

$$B_+(s) = 1.0$$

$$B_-(s) = -1.3386e6(s+1.4021)$$

$$A_+(s) = (s-6.2857)$$

$$A_-(s) = (s+67.8+90.4i)(s+67.8-90.4i)(s+7.5903)$$

$$Z(s) = s(s-6.2857)$$

$$M_+(s) = s$$

$$M(s) = 1.$$

The $U(s)$ given by equation (2.21), fully contains the closed loop transfer function given by equation (2.15). Substituting the above factors into equation (2.21), it is clear that, $\deg(G(s)) - \deg(F(s))$ should be at least 4 for the $U(s)$ to be strictly proper. Therefore, with one zero, the optimal ITAE is taken of the form

$$T_1(s) = \frac{k(s + \gamma)}{(s^5 + 2.8\omega_0 s^4 + 5\omega_0^2 s^3 + 5.5\omega_0^3 s^2 + 3.4\omega_0^4 s + \omega_0^5)} \quad (2.22)$$

The standard form for fifth order ITAE as given above is taken from [33]. To satisfy the equation (2.12), the $L(s)$ and $F(s)$ are chosen of the following forms:

$$L(s) = s^3 + l_1 s^2 + l_2 s + l_3$$

$$F(s) = f_1 s + f_2.$$

Then $H(s)$, given by equation (2.12) is

$$\begin{aligned} H(s) &= G(s) - L(s)Z(s) \\ &= (s^5 + 2.8\omega_0 s^4 + 5\omega_0^2 s^3 + 5.5\omega_0^3 s^2 + 3.4\omega_0^4 s + \omega_0^5) - (s^2 - 6.2857s)(s^3 + l_1 s^2 + l_2 s + l_3) \\ &= B_+(s)F(s) \\ &= F(s) \\ &= f_1 s + f_2 \end{aligned}$$

This gives,

$$\left. \begin{aligned} 2.8\omega_0 &= l_1 - 6.2857 \\ 5\omega_0^2 &= l_2 - 6.2857 l_1 \\ 5.5\omega_0^3 &= l_3 - 6.2857 l_2 \\ 3.4\omega_0^4 + 6.2857 l_3 &= f_1 \\ \omega_0^5 &= f_2 \end{aligned} \right\} \quad (2.23)$$

The control input to the plant turns out to be

$$U(s) = \frac{(s + 67.8 + 90.4i)(s + 67.8 - 90.4i)(s + 7.5903)(s - 6.2857)(f_1 s + f_2)}{-1.3386e6 s(s + 1.4021)(s^5 + 2.8\omega_0 s^4 + 5\omega_0^2 s^3 + 5.5\omega_0^3 s^2 + 3.4\omega_0^4 s + \omega_0^5)} \quad (2.24)$$

Now the problem is formulated as nonlinear optimization problem to minimize the L_2 -norm of $u(t)$ i.e. $\|U(s)\|_2$ under the constraints of equations (2.23). To obtain

the initial guess for ω_0 , $\gamma = 1.4021$ is chosen which is existing zero of the plant. Computer simulation is used to find out the initial guess on ω_0 to get $\|u(t)\|_2 < 1.0$.

Simplex search with multiple restarts with $\lambda = 50.0$, has the solution vector $(\omega_0, l_1, l_2, l_3, f_1, f_2)$ as $\{9.9988, 34.42, 716.245, 10000.2, 96843.0, 9.994e4\}$. This gives :

$$T_1(s) = \frac{96843 (s + 1.032)}{(s^5 + 27.997 s^4 + 499.88 s^3 + 5498 s^2 + 33984 s + 99940)} \quad (2.25)$$

and

$$C_1(s) = \frac{-7.2346 e^{-2} (s + 7.5903) (s + 67.8 + 90.4i) (s + 67.8 - 90.4i)}{s(s + 1.4021) (s^3 + 34.43 s^2 + 716.245 s + 10000.2)} \quad (2.26)$$

2.6.2. Controller Synthesis for Outer Acceleration Loop

For the outer acceleration loop, the plant transfer function becomes :

$$P_2(s) = \frac{A_z}{q} \cdot T_1(s) \quad (2.27)$$

$$= \left(\frac{A_z / \delta_{ec}}{q / \delta_{ec}} \right) \cdot T_1(s) \quad (2.28)$$

$$= \frac{1.7547e5 (s + 26.196) (s - 26.196) (s + 1.032)}{(s + 1.4021) (s^5 + 27.997 s^4 + 499.88 s^3 + 5498 s^2 + 33984 s + 99940)} \quad (2.29)$$

As the RHP zero is beyond the bandwidth of the system, there is no need to assign the zeros. However, LHP zeros can be assigned to new locations to get desired overshoot and settling time.

The second order linear system which meets the time response specifications (desired), is given by $\frac{50}{(s^2 + 10s + 50)}$.

The zeros of the closed loop system are maintained at $\alpha_1, \alpha_2 = \pm 26.196$. Additional minimum four number of poles are required to satisfy the criterion.

$$(N_p - N_z)_{\text{closed loop system}} \geq (N_p - N_z)_{\text{open loop system}} \quad (2.30)$$

These additional four poles are placed at $-p_1, -p_2, -p_3$ and $-p_4$ to give :

$$m(s) = (s^2 + 10s + 50) (s + p_1) (s + p_2) (s + p_3) (s + p_4) \quad (2.31)$$

The optimum set of independent variables $\bar{X} = \{p_1, p_2, p_3, p_4\}$ is searched such that the performance index J given by equation (2.19) is minimum.

As J is nondifferentiable the gradient based optimization methods will give poor results. The direct search methods for nonlinear optimization are the ones which are suitable. For optimization of the performance index J , three direct search methods namely, Simplex search, Powell's conjugate direction and Pattern search have been applied and their performances have been compared.

The Simplex method is due to Nelder and Mead [35]. This method is very robust but not very efficient in terms of the number of function evaluations needed for function minimization. The Powell's conjugate direction method [37] is faster than simplex search. In this method the basic idea is to create a set of N linearly independent search directions, starting each time from the previous best point. Hooke-Jeeves Pattern search method [38] works by creating a set of search directions, iteratively.

Solutions obtained using these techniques with different values of λ and starting solutions are shown in the Table 2.1. The results are fairly insensitive to the type of optimization technique employed as well as to the starting solution.

The optimal solution vector $\{p_1, p_2, p_3, p_4\}$ using Simplex search with multiple restarts ($\lambda = 10$) is obtained as $\{41.223, 41.243, 41.236, 41.214\}$.

This results in the closed loop transfer function

$$T_2(s) = \frac{-2.1079e5 s^2 + 1.4465e8}{(s^2 + 10s + 50) (s + 41.223) (s + 41.243) (s + 41.236) (s + 41.214)} \quad (2.32)$$

The corresponding controller is

$$C_2(s) = \frac{-1.2013 (s + 1.4021) (s - 26.196) (s^5 + 27.997s^4 + 499.88s^3 + 5498s^2 + 33984s + 99940)}{s(s + 1.032)(s^5 + 1.7508e2 s^4 + 1.192e4 s^3 + 3.9161e5 s^2 + 6.43419e6 s + 4.3067e7)} \dots (2.33)$$

Table 2.1

Variation of solution vector $\bar{X} = (p_1, p_2, p_3, p_4)$ with respect to starting solution and penalty factor (λ).

λ	Starting Solution	Simplex Search		Powell's conjugate Direction		Pattern Search	
		Variable	J	Variable	J	Variable	J
1.0	30.0	41.532	2.471	45.778	2.192	41.326	2.496
	30.0	40.885		45.893		41.168	
	30.0	41.087		45.491		38.116	
	30.0	41.165		41.727		40.616	
1.0	50.0	41.500	2.464	45.148	2.190	41.502	2.465
	50.0	41.539		44.619		41.681	
	50.0	41.451		44.794		40.980	
	50.0	41.497		44.963		41.550	
1.0	10.0	41.528	2.4635	45.323	2.190	41.632	2.479
	30.0	41.516		44.631		41.568	
	50.0	41.495		44.337		40.630	
	100.0	41.511		45.135		39.678	
5.0	30.0	41.339	10.687	42.330	10.428	41.832	10.731
	30.0	41.164		42.637		41.681	
	30.0	41.298		42.032		41.916	
	30.0	41.301		41.152		41.682	
5.0	50.0	41.261	10.653	42.010	10.426	41.326	10.826
	50.0	41.329		41.724		41.613	
	50.0	41.265		41.723		43.816	
	50.0	41.321		42.317		43.126	
5.0	10.0	41.336	10.686	42.213	10.426	43.629	10.7
	30.0	41.303		42.192		41.668	
	50.0	41.296		41.965		41.239	
	100.0	41.276		42.018		41.199	
10.0	30.0	41.223	20.96	41.683	20.703	41.261	20.96
	30.0	41.243		41.777		41.363	
	30.0	41.236		41.500		41.268	
	30.0	41.214		40.934		40.932	
10.0	50.0	41.286	20.96	42.105	20.702	41.218	20.958
	50.0	41.304		41.585		41.206	
	50.0	41.200		41.442		41.266	
	50.0	41.242		41.743		41.267	
10.0	10.0	41.267	20.95	41.807	20.701	41.268	20.958
	30.0	41.269		41.633		41.206	
	50.0	41.270		41.607		41.266	
	100.0	41.267		41.344		41.267	

λ	Starting Solution	Simplex Search		Powell's conjugate direction		Pattern Search	
		Variable	J	Variable	J	Variable	J
20.0	30.0	41.254	41.507	41.602	41.249	41.256	41.507
	30.0	41.256		41.691		40.682	
	30.0	41.263		41.382		40.732	
	30.0	41.239		41.009		41.558	
20.0	50.0	41.257	41.506	41.470	41.248	41.256	41.523
	50.0	41.254		41.407		41.367	
	50.0	41.252		41.306		40.676	
	50.0	41.255		41.432		40.326	
20.0	10.0	41.266	41.506	41.375	41.247	41.326	41.506
	30.0	41.268		41.482		41.236	
	50.0	41.270		41.603		41.266	
	100.0	41.267		41.414		41.260	
50.0	30.0	41.237	103.144	41.352	102.888	41.268	103.146
	30.0	41.139		41.490		40.263	
	30.0	41.176		41.287		41.319	
	30.0	41.298		40.868		41.238	
50.0	50.0	41.242	103.143	41.412	102.885	41.249	103.145
	50.0	41.226		41.203		41.321	
	50.0	41.181		41.256		41.386	
	50.0	41.255		41.179		41.256	
50.0	10.0	41.249	103.144	41.273	102.885	41.268	103.145
	30.0	41.249		41.368		41.232	
	50.0	41.246		41.523		41.169	
	100.0	41.247		41.251		40.681	
100.0	30.0	41.236	205.879	41.295	205.624	41.257	205.908
	30.0	41.238		41.505		41.263	
	30.0	41.208		41.191		41.256	
	30.0	41.766		40.755		40.931	
100.0	50.0	41.249	205.871	41.222	205.614	41.251	205.908
	50.0	41.243		41.056		41.267	
	50.0	41.268		40.997		41.259	
	50.0	41.273		41.253		40.328	
100.0	10.0	41.216	205.873	41.320	205.612	40.691	205.924
	30.0	41.328		41.252		40.326	
	50.0	41.242		41.351		41.369	
	100.0	41.532		41.307		41.245	

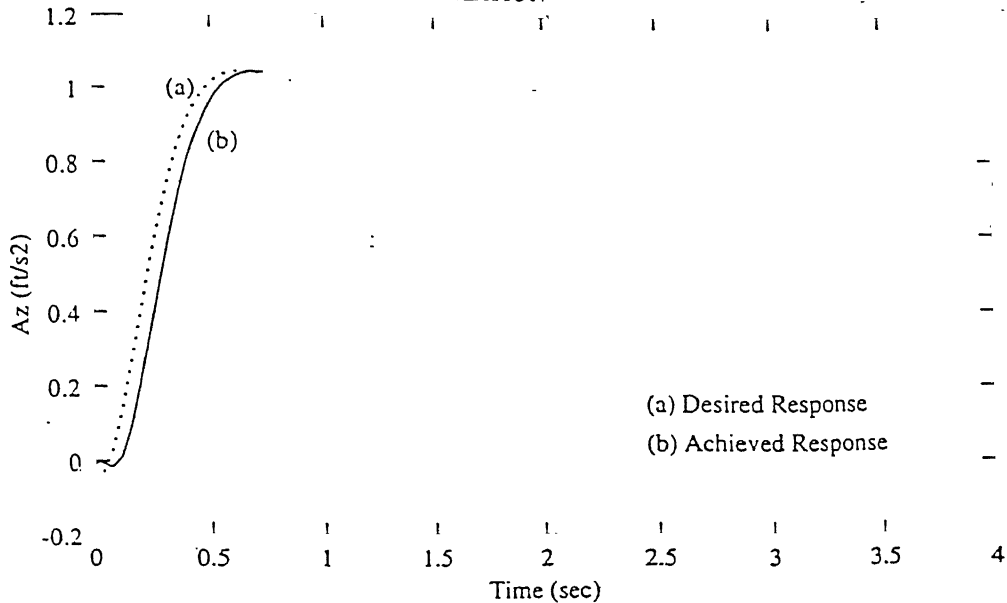


Figure 2.3 : Unit Step Response

2.7 Results and Discussion

Achieved design specifications with above solution vector are:

Gain Margin	= (-10.88, ∞) dB
Phase Margin	= ± 63.95 Deg
Loop gain cross over frequency	= 6.9 Hz.
Rise time (63%)	= 0.32 sec
Maximum overshoot	= 4.06%
Initial undershoot	= 1.53%
Settling time (95%)	= 0.52 sec.
Maximum fin deflection	= 0.945 Deg/G
Maximum fin rate	= 5.96 Deg/s/G

Unit step responses of the model and the present design methodology are shown in Fig.2.3. Nyquist plot of loop transfer function is shown in Fig.2.4. The elevator fin deflection is shown in Fig.2.5.

The time and frequency response specifications achieved in the present design are compared with the other autopilot designs listed in Table 2.2, which is drawn from [13], having the same missile model. Design specifications achieved in the present design are comparable with any other design methodology.

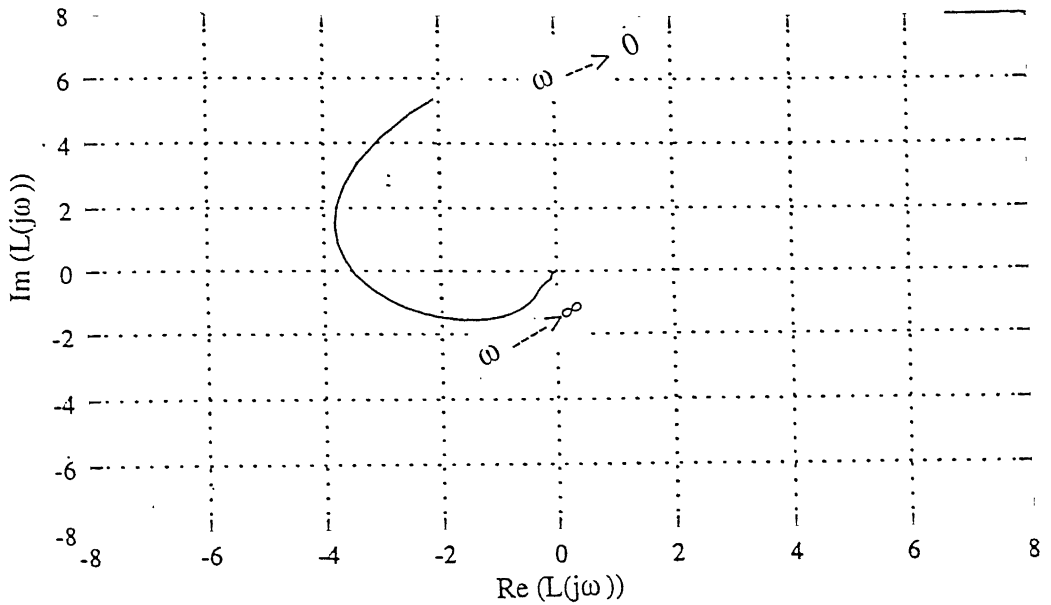


Figure 2.4 : Nyquist Plot

Table 2.2
Autopilot Design

*	63% Rise Time	95% Settling Time	% Initial Under shoot	% Over- shoot	Max Fin Angle, Deg/G	Max Fin Rate, Deg/s/G	Gain Margin (dB)	Phase Margin (Deg)	Loop Gain Freq. (Hz)	States
K_{CL}	0.385	0.961	-8.3	-0.4	0.928	52.5	-11,7.3	± 33	5.2	2
K_{LQR}	0.238	0.347	-4.0	4.2	0.854	15.0	-6,+ ∞	± 60	3.7	1
K_{∞}	0.213	0.514	-10.2	0.0	1.136	61.4	-5,6.3	± 30	4.8	6
K_{μ}	0.329	0.784	-2.4	0.0	0.668	8.0	-8,10	± 39	3.4	27
$K_{ref\mu}$	0.213	0.784	-2.4	0.0	0.668	8.0	-8,10	± 39	3.4	22
$K_{\infty SF}$	0.213	0.514	-9.3	0.0	1.053	34.4	-6,+ ∞	± 40	24.0	2
K_{SPPC}	0.213	0.514	-9.3	0.0	1.053	34.4	-6,+ ∞	± 40	4.7	4
K_{PPC}	0.213	0.514	-9.3	0.0	1.053	34.4	-6,+ ∞	± 40	52.1	2

* This column represents controllers designed using Classical, Linear Quadratic, DGKF Algorithm, μ -Synthesis, Reduced Order μ -Synthesis, H_{∞} State Feedback, Strictly Proper Projective Control and Proper Projective Control techniques, respectively .

2.8 Conclusions

In this chapter parametrized longitudinal autopilot for missile has been designed using pole-zero assignment. The design technique employed Youla parametrization of stabilizing compensator which facilitated incorporation of poles and zeros through polynomials. The crux of the design is finding out the overall closed loop transfer functions which meet the design specifications. Direct search methods of nonlinear optimization have been found very suitable for selection of the closed loop transfer functions. For pitch rate loop ITAE optimal transfer function under the constraint of L_2 -norm on $u(t)$ was chosen. For outer acceleration command tracking loop, objective function having the terms corresponding to tracking error, maximum overshoot, undershoot, gain and phase margins has been minimized to achieve the overall closed loop transfer function. Once these transfer functions are selected, the rest of the design is straight forward.

The element of subjective judgement or requirement of hit and trial is much less as compared to other techniques. The design of parametric controller, in the frame work of algebraic theory, using optimization techniques is very potent area. The designer's level of subjective judgement on the design reduces. The design is more transparent and the algorithms lead to controller from desired specifications in a systematic way.

Disadvantages of the methodology are (i) order of compensator is high (ii) use of conventional direct search methods for nonlinear optimization does not guarantee global optimum solution but only local optimum. But this is not a serious disadvantage in the sense that the solutions finally achieved have been found reasonably insensitive to the starting solutions. In fact even where the starting solutions were chosen well beyond dominant pole configuration, the final solution converged almost to the same value. Regarding high order of controllers, the model reduction techniques can be applied to reduce the order of the designed compensator.

Chapter 3

A Two Degrees of Freedom Parametric Longitudinal Autopilot Synthesis using Model Matching and Constrained Optimization with Simulated Annealing

3.1 Introduction

The objective of the control system design is to select the controller such that the closed loop system is stable and has the desired characteristics with respect to the reference command, disturbance, sensor noise, sensitivity and robust stability for parameter perturbations. In control systems with one degree of freedom configuration, it is not possible to cope up simultaneously with the two problems of :

- (i) attaining a desired system response with reference to command tracking and
- (ii) achieving feedback properties to handle plant parameter variations and/or disturbances acting on the plant [40].

It has been pointed out by Desoer et al [41] that properties with respect to the reference command and closed loop characteristics could be independently specified using a two degrees of freedom (TDOF) structure.

In this chapter, longitudinal autopilot has been designed using parametrization of stabilizing controllers with two degrees of freedom configuration given by Hara [42]. This parametrization gives possible classes of stabilizing controllers with two degrees of freedom configuration using fractional representation approach. The possible

classes of controllers and realizable characteristics are provided by two free independent parameters of proper stable rational matrices. This two degrees of freedom configuration is for the case in which the measured variables are not necessarily coincident with the controlled outputs. The missile pitch dynamics form the similar system with one controlled output (pitch acceleration) and two measured variables (pitch rate and pitch acceleration).

This parametrization of stabilizing controllers with two degrees of freedom configuration is superior to others given by Yoshikawa et al [43] and Vidyasagar [44] in the sense that the properties with respect to the reference command depend only on one parameter, $K_1(s)$, and the closed loop properties depend only on another one, $K_2(s)$. This facilitates independent shapings of time domain and frequency domain responses by proper selection of $K_1(s)$ and $K_2(s)$, respectively. All the objectives of the autopilot design can be expressed as the hard bound constraints on time domain and frequency domain responses. Hard bound constraints on the time domain are in terms of the rise time, peak overshoot, undershoot, settling time, steady state error and on the control input. The main frequency domain hard bound constraints are related with disturbance rejection over the bandwidth of the feedback system and stability robustness to plant uncertainty and parameter variations. Stability robustness constraints are equivalent to the classical gain and phase margins.

In this chapter, the time response shaping has been carried out using closed loop model matching concept [45,46]. This technique reduces the nonlinear optimization problem to a problem of linear simultaneous algebraic equations in terms of solution variables.

The frequency domain response shaping has been carried out by casting the design problem as constrained optimization problem which has been solved using Simulated Annealing (SA) technique [52]. Constrained frequency domain optimization problem requires tuning of bounds on the performance functions during optimization process. This approach of frequency response shaping is superior to unconstrained H_∞ minimization approaches [47-49] because the latter suffer from the following drawbacks :

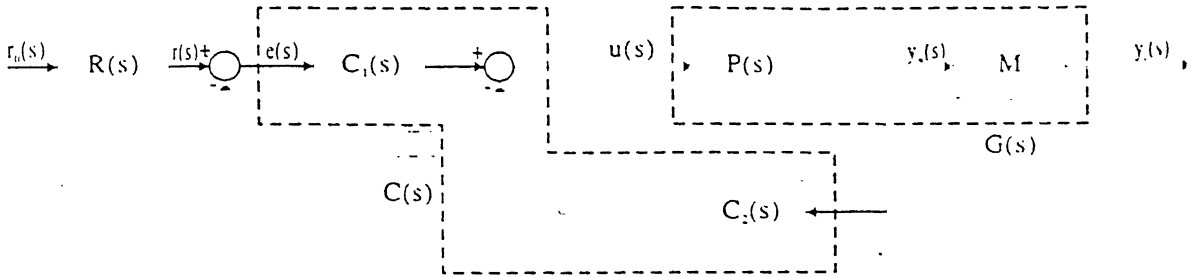


Figure 3.1 : Feedback Control System with Two Degrees of Freedom

$$X(s) N(s) + Y(s) D(s) = I_m$$

$$(ii) \text{ rank } [N^T(\lambda) D^T(\lambda)] = m; \forall \lambda \in C_e^+$$

where C_e^+ denotes the extended right half plane, ie. $\{s : \text{Re } s \geq 0\} \cup \{\infty\}$. In this case, ND^{-1} is referred to as right coprime factorization of H . The left coprime factorization is defined analogously.

3.2.2 Two Degrees of Freedom Configuration

The two degrees of freedom configuration of the control system, given by Hara [42], is shown in the Fig.3.1. $P(s) \in R_{sp}^{q \times m}$, $C(s) = [C_1(s) \ C_2(s)] \in R_p^{m \times (p+q)}$ and $R(s) = \alpha(s) I = \psi \phi^{-1} I \in R_{sp}^{p \times p}$ denote the plant, the controller and the reference command generator, respectively. The signals r , e , u , y_m and y_c represent the reference, error, control input, measured output and controlled output, respectively. The matrix M is assumed of the form $M = [I_p \ 0]$ and the total plant is defined by

$$G(s) = \begin{bmatrix} d & -MP(s) \\ & P(s) \end{bmatrix}$$

With the internal model $I/\phi(s)$ for the reference command at the error channel, the servo system is shown in the Fig.3.2. Consider the augmented system of the total plant $G(s)$ and the internal model $I/\phi(s)$ which is represented by [42],

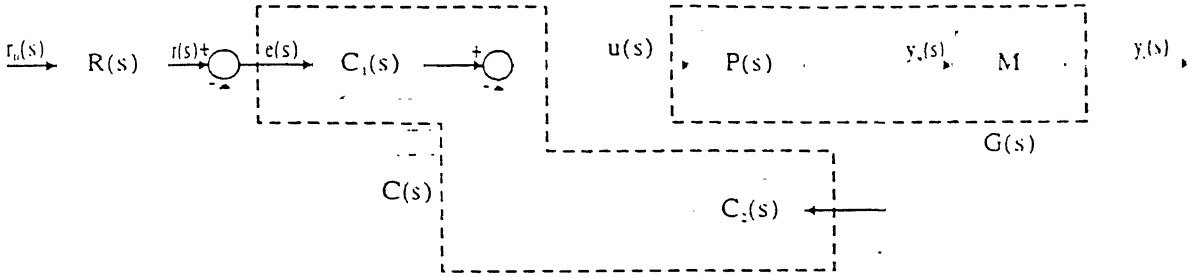


Figure 3.1 : Feedback Control System with Two Degrees of Freedom

$$X(s) N(s) + Y(s) D(s) = I_m$$

$$(ii) \text{ rank } [N^T(\lambda) D^T(\lambda)] = m; \forall \lambda \in C_e^+$$

where C_e^+ denotes the extended right half plane, ie. $\{s : \text{Re } s \geq 0\} \cup \{\infty\}$. In this case, ND^{-1} is referred to as right coprime factorization of H . The left coprime factorization is defined analogously.

3.2.2 Two Degrees of Freedom Configuration

The two degrees of freedom configuration of the control system, given by Hara [42], is shown in the Fig.3.1. $P(s) \in R_{sp}^{q \times m}$, $C(s) = [C_1(s) \ C_2(s)] \in R_p^{m \times (p+q)}$ and $R(s) = \alpha(s) I = \psi \phi^{-1} I \in R_{sp}^{p \times p}$ denote the plant, the controller and the reference command generator, respectively. The signals r , e , u , y_m and y_c represent the reference, error, control input, measured output and controlled output, respectively. The matrix M is assumed of the form $M = [I_p \ 0]$ and the total plant is defined by

$$G(s) = \begin{bmatrix} d & - \\ MP(s) & - \\ & P(s) \end{bmatrix}$$

With the internal model $I/\phi(s)$ for the reference command at the error channel, the servo system is shown in the Fig.3.2. Consider the augmented system of the total plant $G(s)$ and the internal model $I/\phi(s)$ which is represented by [42],

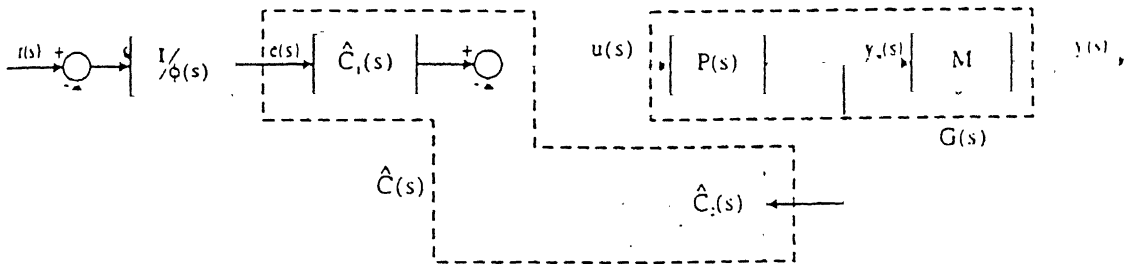


Figure 3.2 : Servo System with Two Degrees of Freedom

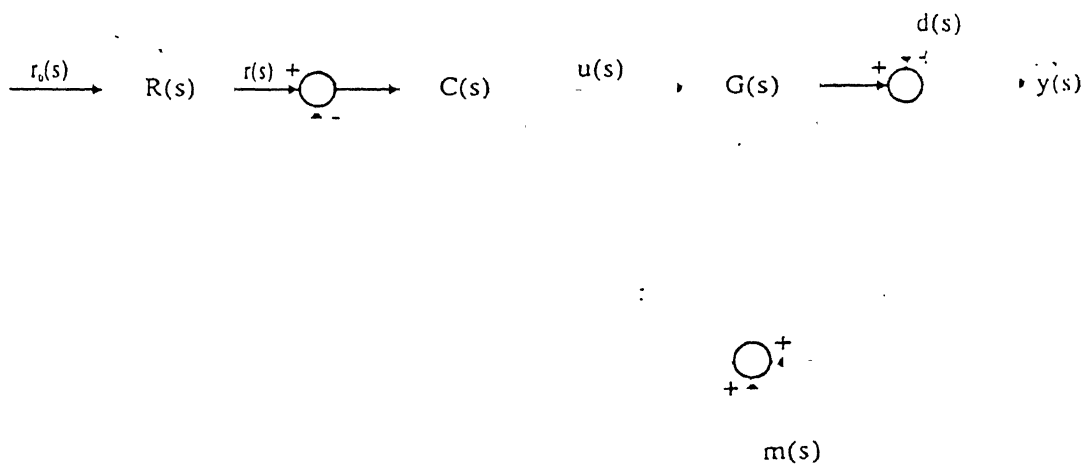


Figure 3.3 : Standard Feedback Configuration

$$G_e(s) = \frac{MP(s)/\phi(s)}{P(s)} \quad (3.1)$$

The $C(s) = [\hat{C}_1(s)/\phi(s) \quad \hat{C}_2(s)]$ is a servo controller for $G(s)$ if $\hat{C}(s) = [\hat{C}_1(s) \quad \hat{C}_2(s)]$ stabilizes the augmented system $G_e(s)$ under the assumptions of solvability condition (A2.5) or (A2.6) (given in Appendix 2), which assures no unstable pole-zero cancellation between $G(s)$ and $1/\phi(s)$ [42]. Hence the class of controllers $\hat{C}(s)$ that stabilize $G_e(s)$, is investigated.

3.2.3 The Class of Stabilizing Controllers

In the following, the class of stabilizing controllers is given by the Lemma 3.1 which is taken from [42]. Other details pertaining to the parametrization of controllers for the present TDOF configuration, which are based on [42], are relegated to Appendix 2.

Lemma 3.1

Suppose that solvability condition (A2.5) or (A2.6) holds. The controller $\hat{C}(s) = [\hat{C}_1(s) \quad \hat{C}_2(s)]$ which stabilizes $G_e(s)$ is given by

$$\hat{C}_1(s) = (Y - K_2 \tilde{N})^{-1} (X_1 + \phi K_1) \quad (3.2)$$

$$\hat{C}_2(s) = (Y - K_2 \tilde{N})^{-1} ([-K_1 \quad X_2] + K_2 \tilde{D}) \quad (3.3)$$

for any $K_1(s) \in R^{m \times p}$ and $K_2(s) \in R^{m \times q}$.

Furthermore, the attainable transfer characteristics are expressed as

$$H_{er}(s) = \phi (\tilde{Y}_1 \tilde{D}_1 - \hat{N} K_1) \quad (3.4)$$

$$H_{yr}(s) = \hat{N} (X_1 + \phi K_1) \quad (3.5)$$

$$H_{ur}(s) = \tilde{X} \tilde{D}_1 + D \hat{D} K_1 \quad (3.6)$$

$$S_i(s) = D \hat{D} (Y - K_2 \tilde{N}) \quad (3.7)$$

$$S_0(s) = \frac{\phi (\tilde{Y}_1 - \hat{N} K_2)}{\tilde{Y}_2 - N_2 \hat{D} K_2} \tilde{D} \quad (3.8)$$

where $H_{er}(s)$, $H_{yr}(s)$ and $H_{ur}(s)$ are the transfer function matrices from r to e , r to y_c and r to u , respectively, and $S_i(s)$ and $S_o(s)$ represent the relative sensitivity matrices at the input (u) and the output (y_m) channels of the plant, $P(s)$, respectively.

Remark 3.1

Setting $\phi(s) = 1$ in Lemma 3.1, we have the results for TDOF regulator systems.

Remark 3.2

It can be noted from equations (3.4) - (3.8) that the properties with respect to the reference command and sensitivity characteristics depend only on $K_1(s)$ and $K_2(s)$, respectively and these two types of characteristics can be specified independently in the control system design.

3.3 Design For Pitch Acceleration Command Tracking – using Closed Loop Model Matching Concept

3.3.1 General

Closed loop system in pitch channel is required to track reference acceleration command. The typical time response specifications for a command tracking system are rise time, peak overshoot, undershoot, settling time and steady state error. Moreover, the command input signals can drive the missile plant outside the linearization region which may lead to performance deterioration or even instability. So design specifications should include some measure of maximum actuator deflection and maximum actuator rate.

In TDOF parametrization used here, the reference command tracking depends on parameter $K_1(s)$. Thus the design objective is to select proper $K_1(s)$ which will give the desired tracking performance. The closed loop model matching concept [45,46] has been used here for determining $K_1(s)$.

3.3.2 Problem Formulation

In this Section, the reference command tracking problem is formulated as closed loop model matching problem. With internal model present in the Fig. 3.2 for the reference command in two degrees of freedom configuration, the equation (3.5) is rewritten as

$$H_{yr}(s) = \hat{N} (X_1 + \phi K_1) \quad . \quad (3.9)$$

The cost function in closed loop model matching problem is defined as a mean square error function [45,46]

$$J = \int_{\omega_1}^{\omega_2} \left| H_{yr}^d(j\omega) - H_{yr}(j\omega) \right|^2 d\omega \quad . \quad (3.10)$$

Here, $H_{yr}^d(j\omega)$ is the desired closed loop transfer function. (ω_1, ω_2) is the frequency interval of interest over which the closed loop model matching is to be achieved.

Let

$$H_{yr}(j\omega) = \frac{Z_1}{Z_2}$$

$$H_{yr}^d(j\omega) = \frac{H_1}{H_2} = \frac{R_1 + R_2 j}{S_1 + S_2 j} \quad (3.11a)$$

$$N_1(j\omega) = \frac{C_1 + C_2 j}{g_1 + g_2 j} \quad (3.11b)$$

$$X_1(j\omega) = \frac{d_1 + d_2 j}{g_1 + g_2 j} \quad (3.12)$$

$$K_1(j\omega) = \frac{A_1 + A_2 j}{B_1 + B_2 j} \quad (3.13)$$

$$= \frac{\sum_{i=0}^m a_i (j\omega)^i}{1 + \sum_{i=1}^n b_i (j\omega)^i} \quad (3.14)$$

Here, the aim is to solve for unknowns a_i 's and b_i 's. One approach may be to set $\nabla J_{a,b} = 0$ and solve a set of nonlinear simultaneous equations. In this approach, rather than minimising equation (3.10) ie. the quantity

$$\int_{\omega_1}^{\omega_2} \left| \left(H_1 Z_2 - H_2 Z_1 \right) / H_2 Z_2 \right|^2 d\omega,$$

the quantity $\int_{\omega_1}^{\omega_2} \left| H_1 Z_2 - H_2 Z_1 \right|^2 d\omega$ is minimized. If a solution exists, the

minimum value of this quantity will always be zero. Therefore, under optimal conditions $H_1 Z_2 = H_2 Z_1$, provided that polynomials on both sides of this equation are of the same order.

Upon substitution of equations (3.9) and (3.11) - (3.14), and multiplying the resultant integrand by its common denominator, the following equation is obtained.

$$J = \int_{\omega_1}^{\omega_2} \left[\left(B_1 C - B_2 D - P A_1 + Q A_2 \right)^2 + \left(B_1 D + B_2 C - P A_2 - Q A_1 \right)^2 \right] d\omega \quad (3.15)$$

where,

$$A_1 = a_0 - a_2 \omega^2 + a_4 \omega^4 - \dots \quad (3.16)$$

$$A_2 = a_1 \omega - a_3 \omega^3 + a_5 \omega^5 - \dots \quad (3.17)$$

$$B_1 = b_0 - b_2 \omega^2 + b_4 \omega^4 - \dots \quad (3.18)$$

$$B_2 = b_1 \omega - b_3 \omega^3 + b_5 \omega^5 - \dots \quad (3.19)$$

$$P = (S_1 C_1 - S_2 C_2) g_1 - (S_1 C_2 + S_2 C_1) g_2 \quad (3.20)$$

$$Q = (S_1 C_2 + S_2 C_1) g_1 + (S_1 C_1 - S_2 C_2) g_2 \quad (3.21)$$

$$C = E - G \quad (3.22)$$

$$D = F - H \quad (3.23)$$

$$E = R_1 (g_1^2 - g_2^2) - 2 R_2 g_1 g_2 \quad (3.24)$$

$$F = 2 R_1 g_1 g_2 + R_2 (g_1^2 - g_2^2) \quad (3.25)$$

$$G = (S_1 C_1 - S_2 C_2) d_1 - (S_1 C_2 + S_2 C_1) d_2 \quad (3.26)$$

$$H = (S_1 C_2 + S_2 C_1) d_1 + (S_1 C_1 - S_2 C_2) d_2 \quad (3.27)$$

On setting

$$\nabla J_{a,b} = 0,$$

a set of linear algebraic equations is obtained. These equations can be written in the matrix form as

$$XY = I \quad (3.28)$$

where,

$$X = \begin{bmatrix} U_0 & 0 & -U_2 & 0 & \dots & W_1 & V_2 & -W_3 & -V_4 & \dots \\ 0 & U_2 & 0 & -U_4 & \dots & -V_2 & W_3 & V_4 & -W_5 & \dots \\ -U_2 & 0 & U_4 & 0 & \dots & -W_3 & -V_4 & W_5 & V_6 & \dots \\ 0 & U_4 & 0 & U_6 & \dots & V_4 & -W_5 & -V_6 & W_7 & \dots \\ \vdots & \vdots & \vdots & \vdots & \ddots & \vdots & \vdots & \vdots & \vdots & \ddots \\ W_1 & -V_2 & -W_3 & V_4 & \dots & Z_2 & 0 & -Z_4 & 0 & \dots \\ V_2 & W_3 & -V_4 & -W_5 & \dots & 0 & Z_4 & 0 & -Z_6 & \dots \\ -W_3 & V_4 & W_5 & -V_6 & \dots & -Z_4 & 0 & Z_6 & 0 & \dots \\ -V_4 & -W_5 & V_6 & W_7 & \dots & 0 & -Z_6 & 0 & Z_8 & \dots \\ \vdots & \vdots & \vdots & \vdots & \ddots & \vdots & \vdots & \vdots & \vdots & \ddots \\ \vdots & \vdots & \vdots & \vdots & \ddots & \vdots & \vdots & \vdots & \vdots & \ddots \\ \vdots & \vdots & \vdots & \vdots & \ddots & \vdots & \vdots & \vdots & \vdots & \ddots \end{bmatrix}$$

(3.29)

$$Y = \begin{bmatrix} a_0 \\ a_1 \\ a_2 \\ a_3 \\ \vdots \\ \vdots \\ \vdots \\ b_1 \\ b_2 \\ b_3 \\ b_4 \\ \vdots \\ \vdots \\ \vdots \end{bmatrix}; \quad Z = \begin{bmatrix} V_0 \\ W_1 \\ -V_2 \\ -W_3 \\ \vdots \\ \vdots \\ \vdots \\ 0 \\ Z_2 \\ 0 \\ Z_4 \\ \vdots \\ \vdots \\ \vdots \end{bmatrix} \quad (3.30)$$

where,

$$U_i = \int_{\omega_1}^{\omega_2} \omega^i (P^2 + Q^2) d\omega \quad (3.31)$$

$$W_i = \int_{\omega_1}^{\omega_2} \omega^i (PD - QC) d\omega \quad (3.32)$$

$$V_i = \int_{\omega_1}^{\omega_2} \omega^i (PC + QD) d\omega \quad (3.33)$$

$$Z_i = \int_{\omega_1}^{\omega_2} \omega^i (C^2 + D^2) d\omega \quad (3.34)$$

$K_1(s)$ can be obtained for the closed loop model matching problem by solving the above set of equations. The above formulation considers only acceleration command tracking problem. A large control signal at actuator may have large actuator deflection and if the rate of rise of control signal is large, it may produce large actuator rate which may drive the missile plant out of linearity zone and even may lead to instability.

This problem can be eliminated by introducing in the cost function the

term $\int_{\omega_1}^{\omega_2} |H_{ur}|^2 d\omega$, which may be interpreted as square of L_2 -norm of the control

signal due to a unit impulse within the frequency range (ω_1, ω_2) . The modified cost function can now be written as.

$$J' = \int_{\omega_1}^{\omega_2} |H_{yr} - H_{yr}^d|^2 d\omega + k \int_{\omega_1}^{\omega_2} |H_{ur}|^2 d\omega. \quad (3.35)$$

Upon substitution and after some manipulations on earlier lines, cost function reduces to

$$\begin{aligned}
J' = \int_{\omega_1}^{\omega_2} & \left\{ \left[\left(-PA_1 + QA_2 + B_1C - B_2D \right)^2 + \left(-PA_2 - QA_1 + B_1D + B_2C \right)^2 \right] \right. \\
& \left. + k \left[\left(d_1B_1 - d_2B_2 + g_1A_1 - g_2A_2 \right)^2 + \left(d_1B_2 + d_2B_1 + g_1A_2 + g_2A_1 \right)^2 \right] \right\} d\omega
\end{aligned} \quad (3.36)$$

On setting $\nabla J'_{a,b} = 0$, the equations in the same form ie $XY = Z$ are obtained with modified U_i , W_i , V_i and Z_i 's. In this case, these are given by

$$U_{i,m} = \int_{\omega_1}^{\omega_2} \omega^i \left[\left(P^2 + Q^2 \right) + k \left(g_1^2 + g_2^2 \right) \right] d\omega \quad (3.37)$$

$$W_{i,m} = \int_{\omega_1}^{\omega_2} \omega^i \left[\left(PD - QC \right) + k \left(-g_1d_2 + g_2d_1 \right) \right] d\omega \quad (3.38)$$

$$V_{i,m} = \int_{\omega_1}^{\omega_2} \omega^i \left[\left(PC + QD \right) + k \left(-g_1d_1 - g_2d_2 \right) \right] d\omega \quad (3.39)$$

$$Z_{i,m} = \int_{\omega_1}^{\omega_2} \omega^i \left[\left(C^2 + D^2 \right) + k \left(d_1^2 + d_2^2 \right) \right] d\omega \quad (3.40)$$

X , Y and Z will have the same form as given in equations (3.29) and (3.30) with the difference that $U_{i,m}$, $W_{i,m}$, $V_{i,m}$ and $Z_{i,m}$, will replace the respective terms U_i , W_i , V_i , and Z_i in equations (3.29) and (3.30).

By varying the value of k , a tradeoff is established between reference acceleration command tracking and control signal (u), and its rate (\dot{u}).

3.3.3 Algorithm

For implementing the above approach the following algorithm is developed for selecting $K_1(s)$ to achieve the desired tracking response:

Step 1

Select a second order transfer function that gives the desired time response characteristics. Take this as the desired transfer function.

Step 2

Determine the plant and its Bezout coprime factors.

Step 3

Set $\delta_{k_{1n}} = \delta_{k_{1m}} = 0$ and $k = 0$ (δ denotes the degree of polynomial)

Step 4

Check, if $\delta(H_1 Z_2) = \delta(H_2 Z_1)$. If yes, go to Step 5; otherwise increment $\delta_{k_{1n}}$ and $\delta_{k_{1m}}$ till $\delta(H_1 Z_2) = \delta(H_2 Z_1)$ is satisfied.

Step 5

Check if $K_1(s)$ is stable. If yes, go to Step 6; otherwise increment $\delta_{k_{1n}}$ and $\delta_{k_{1m}}$ and go to Step 4.

Step 6

Evaluate tracking response. If satisfactory, go to Step 7; otherwise increment $\delta_{k_{1n}}$ and $\delta_{k_{1m}}$, and go to Step 4.

Step 7

Evaluate actuator deflection and actuator rate. If satisfactory, stop search for $K_1(s)$; otherwise go to Step 8.

Step 8

Take $k \neq 0$, and solve for $K_1(s)$ using equation (3.28) with $U_{i,m}$, $V_{i,m}$, $W_{i,m}$ and $Z_{i,m}$, as obtained from equations (3.37)-(3.40).

Step 9

Evaluate tracking response. If satisfactory, stop search for $K_1(s)$; otherwise modify k and repeat Step 8 until satisfactory tradeoff is obtained between tracking response and, actuator deflection and actuator rate. If satisfactory trade off is not obtained, increment $\delta_{k_{1n}}$ and $\delta_{k_{1m}}$ and go to Step 4.

The problem is posed as constrained optimization problem and is solved using Simulated Annealing (SA) technique. SA technique is a global optimization technique which finds out global optimum in the presence of many local optima.

3.4.2 Frequency Domain Performance Specifications

(i) Disturbance Rejection

Disturbance and measurement noise rejection can be obtained by keeping $|S_i(j\omega)|$ small at lower frequencies and $|T_i(j\omega)|$ small over higher frequency range, respectively. So good disturbance rejection over the bandwidth of the feedback system can be achieved by keeping the $|S_i(j\omega)|$ small over the bandwidth $(0, \omega_c)$.

Hence we define the following performance function to capture the above mentioned constraint.

$$\phi_1(K_2) \triangleq \sup_{\omega \in [0, \infty]} \{ |S_i(j\omega)| - b_f(\omega) \} \quad (3.41)$$

where $b_f(\omega)$ is a continuous bound function.

Therefore, the disturbance rejection performance requirements can be formulated in terms of the following inequality

$$\phi_1(K_2) \leq 0 \quad (3.42)$$

A simple choice for the bound function would be to set [49] :

$$0 < b_f(\omega) = b_{f1} < 1, \quad \text{if } \omega < \omega_c \quad (3.43)$$

$$b_f(\omega) = b_{f2} > 1, \quad \text{if } \omega > \omega_c \quad (3.44)$$

It follows from the extension of Bode's integral theorem to multivariable systems [49,54,55], that if the sensitivity is made lower at some frequencies, the penalty is a higher peak value of the sensitivity at some higher frequency. So $b_f(\omega)$ must exceed over some frequency range beyond ω_c

Some time, the time response specifications of the selected transfer function may not be achievable even after a large number of iterations. In such case, modify the desired transfer function and repeat all the steps.

3.4 Design For Shaping Frequency Domain Responses

3.4.1 General

Feedback in a closed loop system is required to achieve various desirable properties, such as stability, disturbance attenuation and low sensitivity to changes in the plant. Since all these properties depend on the shape of various responses in the feedback loop, the simultaneous loop shaping of several frequency domain responses is essential.

In the present approach of frequency response shapings, constrained optimization technique has been used. The various frequency domain hard bound constraints on the performance functions are defined and the problem is posed as constrained optimization problem. These bounds are tuned during optimization to achieve satisfactory performance. The main frequency domain hard bounds are related with disturbance rejection over the bandwidth of the feedback system and stability robustness to plant uncertainties and parameter variations. If no hidden modes are present, then the closed loop stability can be inferred from the stability of either the output or input sensitivity functions [53]. In missile pitch dynamics, no hidden modes are assumed to be present. So the loop shaping has been done with the loop broken at the input of the plant. Since the pitch dynamics form a Single Input Multi Output (SIMO) system, with one input and two outputs, the loop transfer function, when the loop is broken at the input of the plant, turns out to be scalar transfer function. Robust stability constraint has been imposed in terms of M-circle constraint [51], which provides robustness against parameter variations and sector bounded time varying nonlinearities. M-circle constraint guarantees given classical gain and phase margins. Apart from the above frequency domain constraints, other constraints are incorporated to capture the desired sensitivity and complementary sensitivity functions responses.

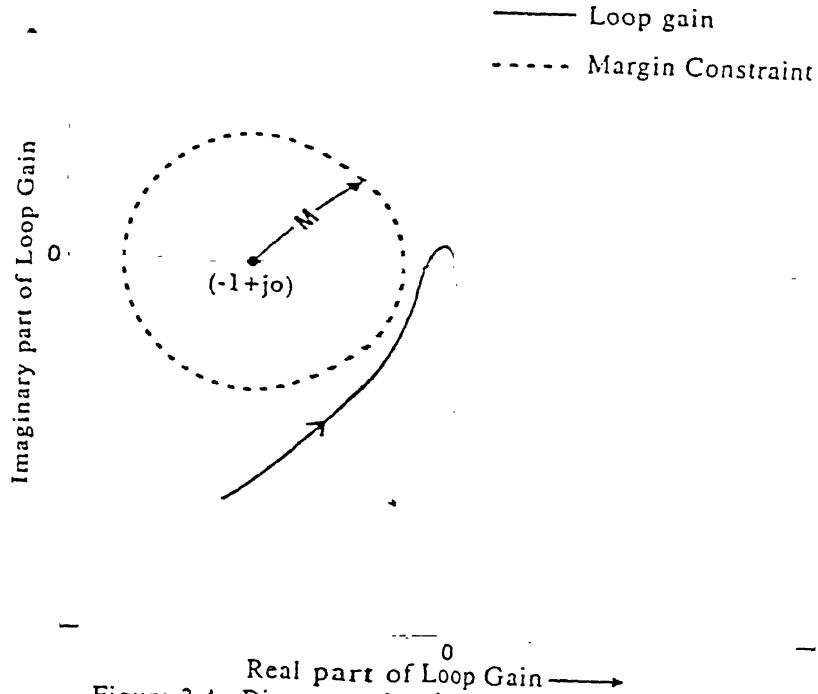


Figure 3.4 : Diagram showing M-Circle constraint

(ii) M-circle Constraint For Robust Stability

M-circle constraint provides an useful way of specifying stability margins [51]. The loop margin, M , is simply the minimum distance in the complex plane between the Nyquist plot of the loop gain and the critical point $(-1 + j0)$:

$$M = \min_{\omega} |1 + L_i(j\omega)|. \quad (3.45)$$

Here, $L_i(j\omega)$ is the loop transfer function with the loop broken at the input of the plant. The M-circle constraint requires the Nyquist plot of $L_i(j\omega)$ to maintain at least a distance of M (the M-circle radius) from the critical point $(-1 + j0)$, as shown in Fig.3.4. This will provide guaranteed gain and phase margins.

Therefore, a classification of minimum loop margin,

$$M \geq M_{\min} \quad (3.46)$$

can be interpreted as robustness specification [51], as shown in Fig. 3.5. The perturbed loop gain is $L(s) = L_i(s) + \Delta(s)$, where $\Delta(s)$ is a stable transfer function. Such a perturbation is called additive loop gain perturbation.

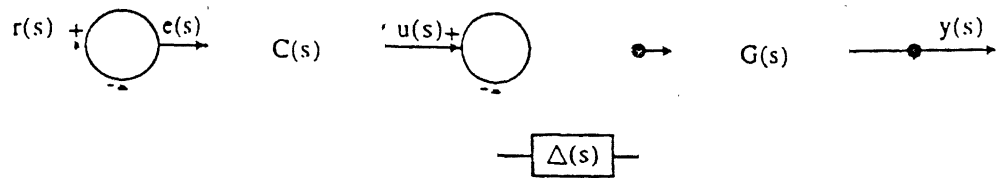


Figure 3.5 : The Perturbed Plant for Loop Margin Constraint

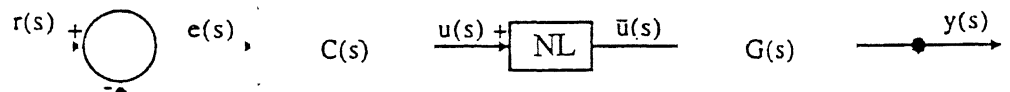


Figure 3.6 : System with a Time Varying Nonlinearity

The closed-loop system is stable for all stable Δ such that $\|\Delta\|_\infty < \frac{1}{M_{\min}}$.

In other words, meeting a minimum loop margin specification is equivalent to guaranteeing stability of the closed loop system despite additive perturbations of the nominal loop gains by any stable transfer function with magnitude less than $1/M$ for all frequencies.

The loop margin, M , is related with the sensitivity function as follows [51] :

$$M = \min_{\omega} |1 + L_i(j\omega)| \quad (3.47)$$

$$= \max_{\omega} \frac{1}{|1 + L_i(j\omega)|} \quad (3.48)$$

$$= \frac{1}{\|S_i(s)\|_\infty} \quad (3.49)$$

Thus small loop margin corresponds to peaking of the sensitivity function at some frequency. The equation can also be expressed as

$$\|S_i(s)\|_\infty \leq \frac{1}{M_{\min}} \quad (3.50)$$

using the inequality given by equation (3.46).

Another interpretation of M-circle constraint can be based on circle criterion which provides sufficient condition for closed loop stability despite certain nonlinear plant perturbations [51]. The perturbations are time varying memoryless nonlinearities in the actuator which can be expressed as $\bar{u} = f(u(t), t)$ (Fig.3.6). The time varying memoryless nonlinearity $f(\cdot)$ satisfies a sector condition : roughly speaking, $f(\cdot)$ multiplies u by at least a and at most b , i.e. for all t ,

$$ax^2 \leq xf(x, t) \leq bx^2, \quad (3.51)$$

where we assume $0 < a \leq 1 \leq b$. This is shown graphically in Fig.3.7.

The circle theorem states that if the nominal system is closed loop stable and the Nyquist plot of the nominal loop gain remains outside the circle symmetric with respect to the real axis and passing through the points $1/b$ and $1/a$, then the perturbed closed loop system of the Fig.3.6 will be stable.

The circle theorem yields another interpretation of (3.46) : constraints expressed by equations (3.46) and therefore (3.49) hold if and only if the circle criterion is

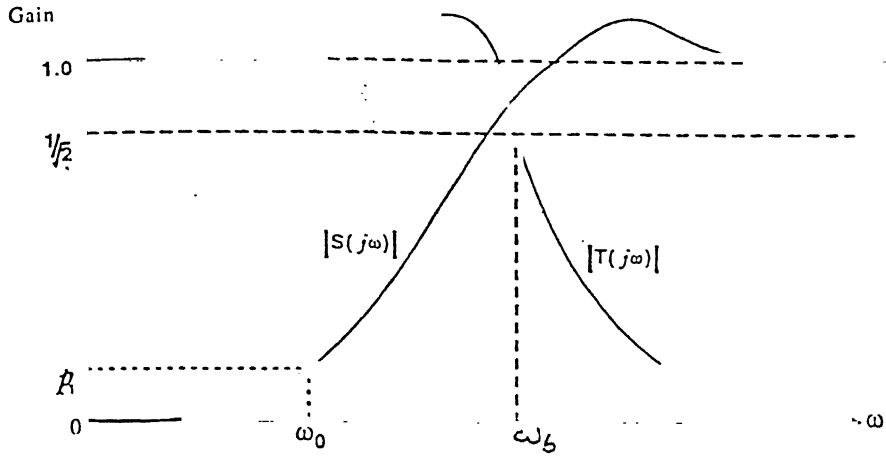


Figure 3.8 : Typical gain Characteristics of sensitivity and complementary sensitivity functions

extends over a much wider frequency range. Therefore, $|S_i(j\omega)|$ is kept small at low frequencies (for $0 \leq \omega \leq \omega_0$, say) and $|T_i(j\omega)|$ is kept small at high frequencies (for $\omega > \omega_b$, say).

Though performance functions $\phi_1(K_2)$ and $\phi_2(K_2)$, already defined, both put constraints on $|S_i(s)|$ in various frequency ranges, a few additional performance functions are required to cover more frequency points/ranges and capture the typical shapes of $|S_i(j\omega)|$ and $|T_i(j\omega)|$ as shown in Fig.3.8.

In a very low frequency interval $0 \leq \omega \leq \omega_0$, (where ω_0 is much lesser than ω_c) we require that :

$$|S_i(j\omega)| < p_1, \quad \text{for } 0 \leq \omega \leq \omega_0 \quad (3.54)$$

and we have

$$|T_i(j\omega)| \approx 1, \quad \text{for } 0 < \omega \leq \omega_0 \quad (3.55)$$

Here $p_1 (<< 1)$ is the bound on $|S_i(j\omega)|$ in the frequency range $0 \leq \omega \leq \omega_0$.

We define the performance functions $\phi_3(K_2)$, $\phi_4(K_2)$ corresponding to equation (3.54) and (3.55) as :

$$\phi_3(K_2) \triangleq \sup_{\omega \in [0, \omega_0]} \{|S_i(j\omega)| - p_1\} \quad (3.56)$$

$$\phi_4(K_2) \triangleq \sup_{\omega \in [0, \omega_0]} \{|T_i(j\omega)| - p_2\} \quad (3.57)$$

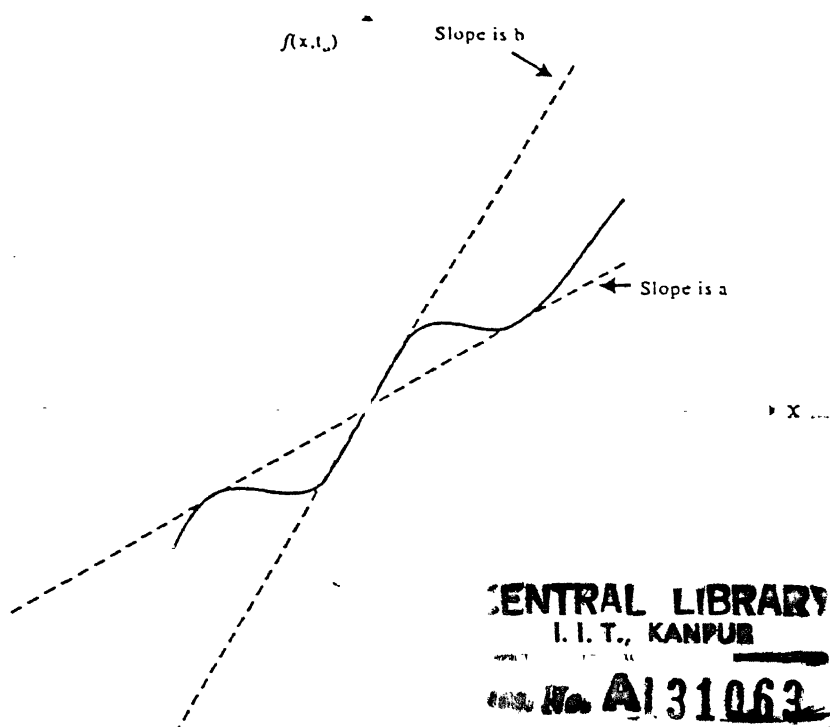


Figure 3.7 : An Example of a Sector $[a,b]$ Nonlinearity $f(x,t)$

satisfied for nonlinearities in sector $[1/(1+M), 1/(1-M)]$. Thus constraint (3.49) can be viewed as guaranteeing stability despite time-varying memoryless nonlinear perturbations in the loop.

Thus, the M-circle constraint performance specification can be defined as

$$\phi_2(K_2) \triangleq \sup_{\omega \in [0, \infty)} \left| S_i(j\omega) \right| - \frac{1}{M_{\min}} \quad (3.52)$$

Therefore, for meeting the M-circle constraint we require that

$$\phi_2(K_2) \leq 0 \quad (3.53)$$

(iii) Input Sensitivity And Complementary Sensitivity Shapings

It has been shown in [48] that many essential design requirements can be achieved by shaping of sensitivity and complementary sensitivity functions. The unavoidable trade off between these two is given by equation (A3.14) of Appendix 3. In practice, the conflict between keeping $T(s)$ small and keeping $S(s)$ small is resolved by making one small at some frequencies and the other small at other frequencies. Usually, the spectrum of reference signals and disturbance signals are

Here p_2 is constant and provides bound on the $|T_1(j\omega)|$ in the frequency interval $(0, \omega_0)$

The bandwidth of the feedback loop, ω_b , is defined as the lowest frequency such that

$$|T_i(j\omega_b)| = |T_i(0)|/\sqrt{2} = 0.707 \quad (3.58)$$

Performance function corresponding to the value of $T_i(j\omega)$ at bandwidth is defined as

$$\phi_5(K_2) \stackrel{\Delta}{=} \{ |T(j\omega_b)| - 0.707 \} \quad (3.59)$$

The loop bandwidth, ω_b , is usually very close to '0 dB crossover frequency' ω_c of the loop transfer function $L_i(s)$ ($= C(s)G(s)$). For acceptable designs, loop bandwidth can be estimated in terms of crossover frequency by the relation[32]:

$$\omega_c \leq \omega_b \leq 2\omega_c. \quad (3.60)$$

Therefore, we define, correspondingly, a performance function

$$\phi_6(K_2) \stackrel{\Delta}{=} \{ |L(j\omega_c)| - 1 \} \quad (3.61)$$

Permissible peak of $|S_i(j\omega)|$ has been specified in performance function $\phi_1(K_2)$ and also in the M-circle constraint $\phi_2(K_2)$. Permissible peak of the $|T_i(j\omega)|$ is specified by another performance function :

$$\phi_7(K_2) \stackrel{\Delta}{=} \sup_{\omega \in [0, \omega_b]} \{ |T_i(j\omega)| - p_t \} \quad (3.62)$$

where, p_t is the bound on $|T_i(j\omega)|$ in the frequency interval $\omega \in [0, \omega_b]$.

Another performance function is required to capture the shape of $|T_i(j\omega)|$ beyond the frequencies greater than ω_b . It is required that

$$|T_i(j\omega)| > p_h, \quad \text{for } \omega > \omega_h. \quad (3.63)$$

The corresponding performance function is defined as

$$\phi_8(K_2) \stackrel{\Delta}{=} \sup_{\omega > \omega_h} \{ |T_i(j\omega)| - p_h \}$$

Therefore, to capture the shapes of $|S_i(j\omega)|$ and $|T_i(j\omega)|$ at various frequencies, we require.

$$\phi_3(K_2) \leq 0 \quad (3.64)$$

$$\phi_4 (K_2) \leq 0 \quad (3.65)$$

$$\phi_5 (K_2) = 0 \quad (3.66)$$

$$\phi_6 (K_2) = 0 \quad (3.67)$$

$$\phi_7 (K_2) \leq 0 \quad (3.68)$$

$$\phi_8 (K_2) \leq 0 \quad (3.69)$$

3.4.3 Objective Function

All the design requirements in the design for the frequency domain loop shaping are expressed in the form of either equalities or inequalities . Weighted sum objective function with external penalty is used in the following form :

$$\phi (K_2) = \frac{\Delta}{K_2} \{ \sum_i \lambda_i < \phi_i (K_2) >^2 + \sum_j \lambda_j [\phi_j (K_2)]^2 \} \quad (3.70)$$

where $\phi_i (K_2)$ and $\phi_j (K_2)$ are the performance functionals with inequality and equality constraints, respectively. In the first term on the RHS of the above performance function , $< \alpha > = \alpha$, when inequality is violated; it is zero, otherwise. Second term on the RHS is used to handle equality constraints. Since the feasible point always satisfies $\phi_j (K_2) = 0$, any infeasible point is penalized by an amount proportionate to the square of the constraint violation . λ_i and λ_j are the non-negative scalar weight factors.

During the optimization process, the λ_i and λ_j , and bounds are tuned to achieve the optimal solution. Here, $\phi_1(K_2)$, $\phi_2(K_2)$, $\phi_3(K_2)$, $\phi_4(K_2)$, and $\phi_7(K_2)$ are the performance functionals with inequality whereas $\phi_5 (K_2)$ and $\phi_6 (K_2)$ are the performance functionals with equality.

3.4.4 Simulated Annealing Technique

Simulated Annealing (SA) is a global optimization technique that distinguishes between different local minima. Starting from an initial point, the algorithm takes a step and the function is evaluated. When minimising a function any downhill step is accepted and the process repeats from this new point. An uphill step may be accepted. Thus, it can escape from local minima. This uphill decision is made by the

Metropolis Criterion [52,58]. As the optimization process proceeds, the length of the steps declines and the algorithm closes in on the global minimum. The SA algorithm [52] with some modifications as in [63], has been used for optimization, details of which are given in Appendix 4. The SA algorithm used here is applicable to the functions which do not need to be smooth or even continuous in their domain.

3.5 Example

Consider the same missile pitch dynamics model as taken in Example 2.6 of Chapter 2.

Typical design objectives for the autopilot can be stated in terms of the time and frequency response specifications as follows:

Design an autopilot to track the commanded acceleration maneuvers with a (63%) rise time less than 0.3 secs, overshoot less than 5%, undershoot less than 2.5%, (95%) settling time less than 1 sec. The autopilot must provide the gain margins of (-6, +10) dB and phase margins of ± 40 degrees. The autopilot bandwidth is to be restricted by the high frequency unmodeled dynamics constraints (e.g. unmodeled flexible modes and actuator nonlinearities).

The present design approach facilitates independent time response and frequency response shapings. Now time response and frequency response designs are taken up separately to determine $K_1(s)$ and $K_2(s)$, respectively.

3.5.1 Design For Acceleration Command Tracking

For the closed loop model matching, the desired closed loop transfer function is chosen of the second order given by,

$$H_{yr}^d = \frac{55}{(s^2 + 10.5s + 55)}, \quad (3.71)$$

which gives the desired time response.

The left and right coprime factors and the corresponding elements of the Bezout identity, are obtained by the algorithm of Nett et al [59] which requires to solve

only two pole placement problems. These doubly coprime factors are the solution of the following equation

$$\begin{bmatrix} Y(s) & X(s) \\ -\bar{N}(s) & \bar{D}(s) \end{bmatrix} \begin{bmatrix} D(s) & -\bar{X}(s) \\ N(s) & \bar{Y}(s) \end{bmatrix} = \begin{bmatrix} I & 0 \\ 0 & I \end{bmatrix} \quad (3.72)$$

These two pole placement problems have been solved with arbitrary pole locations at $-67.8 \pm 90.4i$, -10.713 , -1.563 .

The stable coprime factors relevant to the design of time and frequency responses are given below :

$$G = s^4 + 147.88s^3 + 14450.0s^2 + 1.5902e5s + 2.1381e5 \quad (3.73)$$

$$X_1 = \frac{x_1}{G}, \quad (3.74)$$

where

$$x_1 = 8.8098e-3s^3 + 1.219s^2 + 1.1852e2s + 7.745e2$$

$$N_1 = \frac{n_1}{G}, \quad (3.75)$$

where

$$n_1 = -2.4254e6s^2 + 1.6644e9$$

$$D = \frac{d}{G}, \quad (3.76)$$

where

$$d = s^4 + 136.9s^3 + 12898s^2 + 10189s - 609220$$

$$Y = \frac{y}{G},$$

where

$$y = s^4 + 1.5885e2s^3 + 1.6123e4s^2 + 3.468e5s + 2.1485e6$$

$$\bar{N} = \begin{bmatrix} \bar{N}_1 \\ \bar{N}_2 \end{bmatrix} = \frac{1}{G} \begin{bmatrix} \tilde{n}_1 \\ \tilde{n}_2 \end{bmatrix},$$

where \tilde{n}_1 and \tilde{n}_2 are given by :

$$\tilde{n}_1 = -2.4254e6s^2 + 5.6313e6s + 5.6372e8$$

$$\tilde{n}_2 = -1.4693e6s - 1.5737e7$$

$$\bar{D} = \begin{bmatrix} \bar{D}_{11} & \bar{D}_{12} \\ \bar{D}_{21} & \bar{D}_{22} \end{bmatrix} = \frac{1}{G} \begin{bmatrix} \tilde{d}_{11} & \tilde{d}_{12} \\ \tilde{d}_{21} & \tilde{d}_{22} \end{bmatrix}, \quad (3.77)$$

where \tilde{d}_{11} , \tilde{d}_{12} , \tilde{d}_{21} and \tilde{d}_{22} are given by :

$$\bar{d}_{11} = s^4 + 1.415e2 s^3 + 1.3328e4 s^2 + 4.9972e4 s + 6.6777 e5$$

$$\bar{d}_{12} = 2.9054e3 s^3 + 3.8518e5 s^2 + 3.0566e7 s + 2.7443e7$$

$$\bar{d}_{21} = 3.9573e - 2 s^3 + 7.3586 s^2 + 6.1302e2 s + 5.5711e3$$

$$\bar{d}_{22} = s^4 + 1.4328e2 s^3 + 1.4107e4 s^2 + 1.3584e5 s + 3.3886e4$$

For regulator systems, $\varphi(s)=1$, and for the class of step reference input signals, the solvability condition given by equation (A2.5) is satisfied for all $\varphi(s) = \frac{s}{s + \alpha}$, if no root of n_1 is at the origin and G does not have any root at $s = -\alpha$.

Now decomposing the factors into real and imaginary parts as defined in equations (3.11) - (3.13), we get

$$C_1 = 2.4254e6 \omega^2 + 1.6644e9 \quad (3.78)$$

$$C_2 = 0.0 \quad (3.79)$$

$$g_1 = \omega^4 - 14450 \omega^2 + 2.1381e5 \quad (3.80)$$

$$g_2 = 1.5902e5 \omega - 147.88 \omega^3 \quad (3.81)$$

$$d_1 = 7.7475e2 - 1.219 \omega^2 \quad (3.82)$$

$$d_2 = 1.1852e2 \omega - 8.8098e-3 \omega^3 \quad (3.83)$$

$$R_1 = 55.0 \quad (3.84)$$

$$R_2 = 0 \quad (3.85)$$

$$S_1 = 55 - \omega^2 \quad (3.86)$$

$$S_2 = 10.5 \omega \quad (3.87)$$

These equations are substituted in equations (3.20) - (3.27) to evaluate the integrals given by equations (3.31) - (3.34). U_i, V_i, W_i and Z_i 's are found out by evaluation of integrals given by equations (3.31)- (3.34) in the frequency interval (ω_1, ω_2) . The solution vector, Y , in equation (3.28) is $Y = [a_0, a_1, a_2, \dots, b_0, b_1, b_2, \dots]^T$. These a_i 's and b_i 's are the coefficients of numerator and denominator of $K_1(s)$, respectively. The matrix X and vector Z in equation (3.28) have entries made of U_i, V_i, W_i and Z_i 's. The order of the system of equations depends on the number of a_i 's and b_i 's to be found out for the selection of $K_1(s)$. The number of a_i 's and b_i 's depends on the degrees of the numerator ($\delta_{k_{1m}}$) and denominator ($\delta_{k_{1n}}$) of $K_1(s)$.

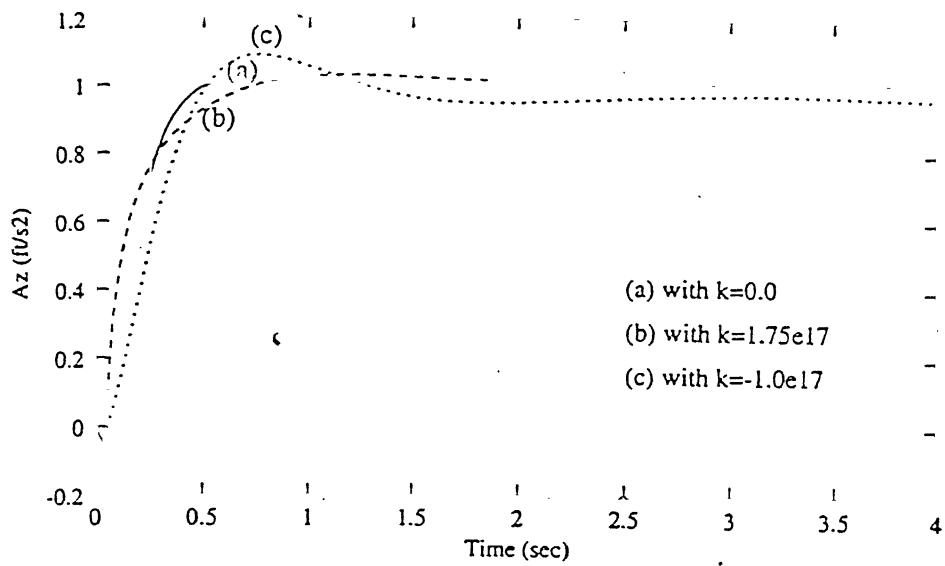


Figure 3.9 : Unit Step Responses

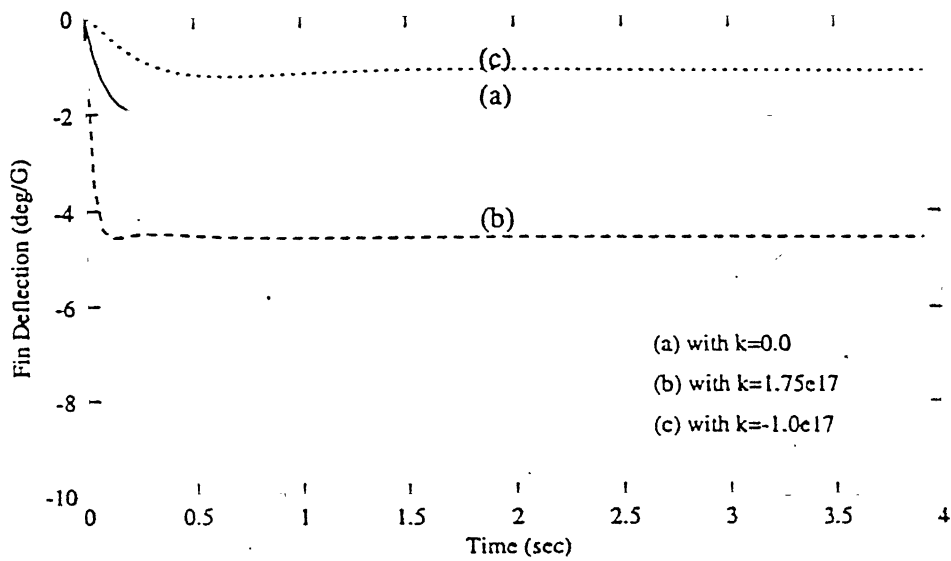


Figure 3.10 : Elevator Fin Deflection

Since $K_{21}(s)$ and $K_{22}(s)$ are proper stable rational functions, the numerator and denominator will have the same degree i.e. $m=n$.

The gain and phase margin constraints are imposed by the M-circle constraint given by equation (3.50). $M_{\min} = 0.7$ guarantees gain margins of $(-4.6, +10.4)$ dB and the phase margins of ± 41 degrees, approximately. Initially the design is aimed at achieving $\omega_c=30$ rad/sec and $\omega_b=50$ rad/sec.

For frequency shaping design the objective function given by equation (3.70) is minimized to get solution vector, $\{a'_i, b'_i, c'_i\}$ using Simulated Annealing algorithm given in Appendix 4. Scalar weight factors have been used in the objective function. Initially weight factors, $\lambda_i, i=1, \dots, 8$, were taken unity. The following initial values of the bounds were taken:

$$b_{f1} = 0.4, \text{ at } \omega < \omega_c$$

$$b_{f2} = 1.4$$

$$p_1 = 0.2, \text{ at } \omega_0 = 5 \text{ rad/s}$$

$$p_2 = 1.0$$

$$p_t = 1.5$$

The following parameters were used for running Simulated Annealing algorithm given in Appendix 4:

$$N_s = 20$$

$$N_T = 60$$

$$C_i = 2, \quad i = 1, \dots, n$$

$$N_e = 4.0$$

$$r_T = 0.85$$

The SA algorithm was run for various initial guesses of the design variables but irrespective of initial guess solution converged. The starting temperature of 1.5×10^4 gave optimal solution. The implementation of SA algorithm given in Appendix 4 was run. Only one run of the SA algorithm was found necessary to get converged solution. However, the convergence of the algorithm dependend on the initial temperature selected. The above temperature value was selected using the criteria described in [52]. This value of temperature was arrived at after running many trial runs. Once the temperature parameter was selected, the program was run for the design variables. After each run, the performance of the design was evaluated. Accordingly, the

non-negative scalar weights and bounds were modified to get satisfactory design specifications. The following set of scalar weight factors and bounds gave satisfactory performance :

Scalar weight factors :

$$\lambda_1 = 42.0$$

$$\lambda_2 = 1.0$$

$$\lambda_3 = 11.0$$

$$\lambda_4 = 300.0$$

$$\lambda_5 = 350.0$$

$$\lambda_6 = 30.0$$

$$\lambda_7 = 50.0$$

$$\lambda_8 = 50.0$$

and bounds :

$$b_{f1} = 0.55$$

$$b_{f2} = 1.3$$

$$p_1 = 0.4$$

$$p_2 = 1.0$$

$$p_t = 1.4$$

$$p_h = 0.7, \text{ at } \omega_h = \omega_b$$

And the values of ω_b and ω_c were to be adjusted to 42 and 25 rad/sec respectively. This gives the following values of $K_{21}(s)$ and $K_{22}(s)$

$$K_{21}(s) = \frac{-1.11478e-2 s^2 + 2.7772487e5 s + 2.974556e6}{s^2 + 300 s + 22500.0} \quad (3.93)$$

$$K_{22}(s) = \frac{-4.584468e5 s^2 + 1.064291e6 s + 1.06549519e8}{s^2 + 300 s + 22500.0} \quad (3.94)$$

With $\phi(s) = \frac{s}{s + 2.563}$, and on substituting the values of $K_1(s)$, $K_{21}(s)$ and $K_{22}(s)$, alongwith the values of X, Y, \tilde{N}, X_2 and \tilde{D} the $C_1(s)$ and $C_2(s) = [C_{21}(s) \quad C_{22}(s)]$, are given by

$$C_1(s) = \frac{(5.3286e-5 s^9 + 2.4079e-2 s^8 + 4.4272 s^7 + 4.43376e2 s^6 + 2.1544e4 s^5 + 2.8027e5 s^4 + 1.5815e6 s^3 + 1.021e7 s^2 + 4.1629e7 s + 4.4678e7)}{(7.1342e-2 s^9 + 3.367e1 s^8 + 4.658e3 s^7 + 5.4447e5 s^6 + 2.0602e7 s^5 + 2.5557e8 s^4 + 1.3692e9 s^3 + 3.939e9 s^2 + 5.9876e9 s + 3.6226e9)} \quad (3.95)$$

$$C_{21}(s) = \frac{(-8.4859e-4 s^8 + 1.8519e4 s^7 + 2.9732e6 s^6 + 3.0444e8 s^5 + 6.6739e9 s^4 + 7.216e10 s^3 + 5.4172e11 s^2 + 2.3444e12 s + 2.5799e12)}{(7.1342e-2 s^8 + 3.3487e1 s^7 + 4.5722e3 s^6 + 5.3275e5 s^5 + 1.9236e7 s^4 + 2.0627e8 s^3 + 8.4055e8 s^2 + 1.7847e9 s + 1.4134e9)} \quad (3.96)$$

$$C_{22}(s) = \frac{(-3.2707e4 s^8 - 4.9548e6 s^7 - 4.3437e8 s^6 + 1.8414e9 s^5 + 8.6124e11 s^4 + 1.6617e13 s^3 + 1.0232e14 s^2 + 1.7712e14 s + 8.524e13)}{(7.1342e-2 s^8 + 3.3487e1 s^7 + 4.5722e3 s^6 + 5.3275e5 s^5 + 1.9236e7 s^4 + 2.0627e8 s^3 + 8.4055e8 s^2 + 1.7847e9 s + 1.4134e9)} \quad (3.97)$$

The following design specifications are achieved using the present frequency response shaping approach :

$$\text{Gain Margins} = (-12.316, +14.8) \text{ dB}$$

$$\text{Phase Margins} = \pm 82.2 \text{ deg}$$

$$\text{Gain Crossover Freq.} = 5.7932 \text{ Hz.}$$

The frequency response shapings are shown in the Fig.3.11 for Nyquist plot of $L_i(j\omega)$, in the Fig. 3.12 for Bode Magnitude plot of $L_i(j\omega)$ to show loop shaping near the gain crossover frequency, and in the Fig.3.13 for gain characteristics of $S_i(j\omega)$ and $T_i(j\omega)$.

3.5.3 Results and Discussion

Achieved time domain performance specifications are shown in the Table 3.1 and the frequency domain specifications are given in Section 3.5.2. The specifications achieved using present design methodology are comparable with the other designs reported in Table 2.2 of Chapter 2, which uses the same missile dynamics. Since in the present design approach, the time domain and frequency domain specifications have been achieved independently, any set of design specifications listed in Table

2.2 can be achieved by suitably selecting the desired closed loop transfer function.

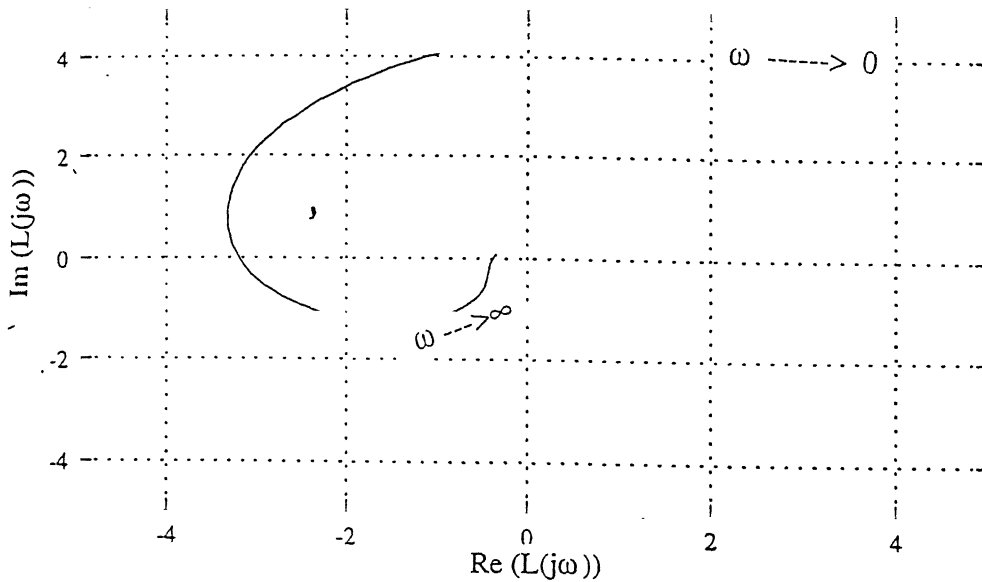


Figure 3.11 : Nyquist Plot

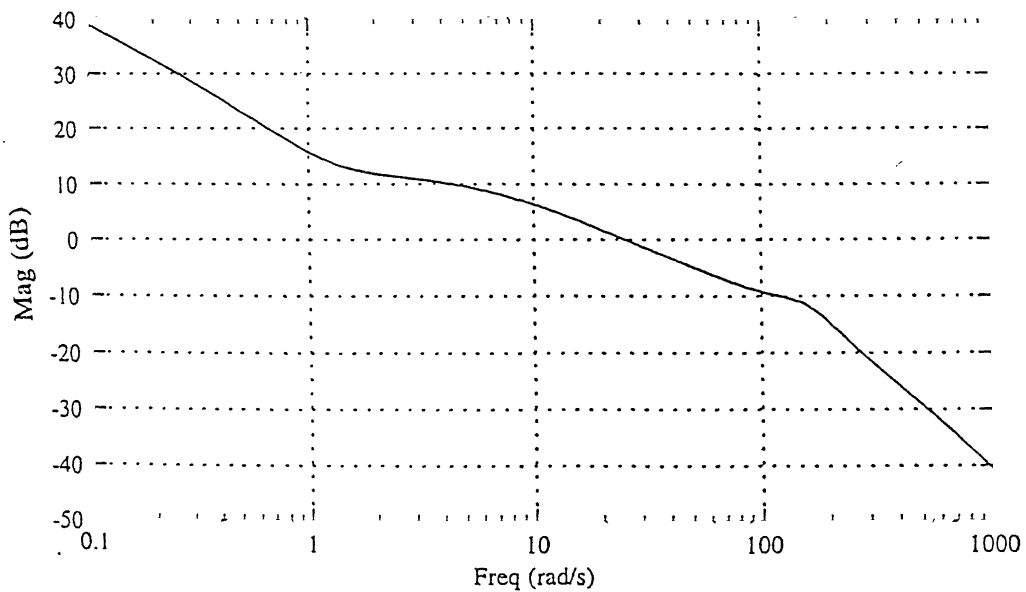


Figure 3.12 : Bode Magnitude Plot with the Loop Broken at the Input of the Plant

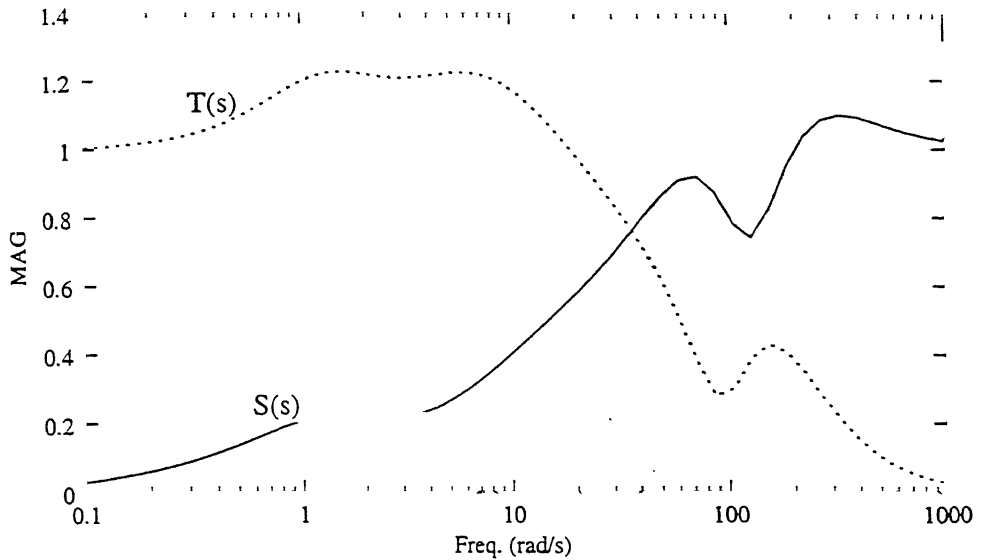


Figure 3.13 : Sensitivity and Complementary Sensitivity Functions at the Plant Input

parameter k in the acceleration command tracking design, and bounds and scalar weight factors in the frequency response shaping.

3.6 Conclusions

The design approach developed in this chapter provides a systematic procedure for the acceleration command tracking design and frequency response design. Since the time and frequency response designs are independent to each other, wide variety of design specifications can be achieved through present design methodology. Simulated Annealing (SA) technique of optimization has proved to be very suitable for solving the constrained optimization problem.

Chapter 4

Synthesis of Decoupled Roll-Yaw (Lateral) Autopilot using Constrained Optimization with Simulated Annealing

4.1 Introduction

Due to highly asymmetric BTT missile configuration, strong roll-yaw coupling is present. A BTT missile is first rolled to desired orientation and then required magnitude of force is achieved by adjusting the angle of attack (α). If some sideslip is present, then in conjunction with the angle of attack large roll moments will be generated which are undesirable. So ideally, the sideslip should be zero. The lateral (roll-yaw) autopilot requires the closed loop system to command roll rate (stability axis) while keeping the sideslip small.

In MIMO systems where input-output coupling is present, the decoupling methods [20, 33, 44] facilitate individual channel design. After decoupling, diagonal closed loop transfer function matrix is obtained.

As discussed in Chapter 2, in a control system the pole dominates transient response as well as stability [20-23] and the zero of a system plays major role in the interaction between the system and its external environment [24-26]. So wide variety of specifications can be achieved by assigning poles and zeros. After the input-output decoupling of the system, the poles and zeros can be suitably assigned to achieve the desired performance while maintaining stability of the closed loop system.

The H_∞ -norm based constraints on the closed loop transfer function and sensitivity function have been found useful for specifying the robust stability against parameter variations and time varying nonlinearities [51]. M-circle concept [51], which is related with the sensitivity function, is convenient for imposing robust stability constraint against the plant parameter variations and the sector bound time varying nonlinearities.

The roll-yaw channel of the BTT asymmetric missile considered here use roll and yaw rates for feedback. In its maneuver the missile is required to roll and then develop an angle of attack to intercept the target. So the roll rate is commanded. The roll rate commanded for the model under study is the stability axis roll rate p_s . At the same time the lateral autopilot is required to minimise the sideslip (β).

The roll-yaw autopilot designed here is based on the decoupling approach studied in [60, 61]. The choice of the sensitivity function and hence the closed loop transfer function is made on the basis of time domain and frequency domain performance specifications e.g. tracking performance, sideslip, actuator effort, robust stability against parameter variations, uncertainties and time varying nonlinearities, disturbance rejection etc. The H_∞ -norm based constraints are imposed and the problem is formulated as nonlinear optimization problem with constraints. This optimization problem aims at finding the coefficients of the polynomials involved in sensitivity and closed loop transfer functions which in turn will give parametrization of the controller. The problem so formulated is solved using Simulated Annealing (SA) technique [52]. The SA algorithm used here is found to give global optimal or near global optimal solution. Other details of SA technique are given in Chapter 3 and Appendix 4.

The structure of the chapter is as follows : in section 4.2, the roll-yaw missile dynamics and closed loop design goals are described ; the control law based on decoupling and pole-zero assignment is discussed in Section 4.3. In Section 4.4, the time domain and frequency domain performance specifications are described and the design problem is formulated as optimization problem in Section 4.5. The design methodology and design algorithm are developed in Sections 4.6 and 4.7, respectively. The design algorithm is implemented in Section 4.8 and the Chapter is concluded in Section 4.9.

4.2 Roll-Yaw Missile Dynamics And Closed Loop Design Goals

The roll-yaw missile dynamics involves the dynamical equations in sideslip (β), roll rate (p), yaw rate (r), and actuator deflections. The linearized roll-yaw dynamics for the BTT missile, taken from [62], which is same as in [7], is described in Appendix 1. The governing equations are :

$$\dot{\beta} = p \sin(\alpha) - r \cos(\alpha) + Y_{\beta} \cdot \beta + Y_{\delta_a} \cdot \delta_a + Y_{\delta_r} \cdot \delta_r \quad (4.1)$$

$$\dot{p} = L_{\beta} \cdot \beta + L_{\delta_a} \cdot \delta_a + L_{\delta_r} \cdot \delta_r \quad (4.2)$$

$$\dot{r} = N_{\beta} \cdot \beta + N_{\delta_a} \cdot \delta_a + N_{\delta_r} \cdot \delta_r \quad (4.3)$$

$$\dot{\delta}_a = -2 \xi \omega \dot{\delta}_a - \omega^2 (\delta_a - \delta_{ac}) \quad (4.4)$$

$$\dot{\delta}_r = -2 \xi \omega \dot{\delta}_r - \omega^2 (\delta_r - \delta_{rc}) \quad (4.5)$$

The roll rate (p) and the yaw rate (r) are measured outputs and have been used for feedback. In the state-space representation, the missile dynamics, in roll-yaw, can be expressed as :

$$\dot{\bar{X}} = A \bar{X} + B \bar{U} \quad (4.6)$$

$$\bar{Y} = C \bar{X} \quad (4.7)$$

where,

$$\bar{X} = [\beta, p, r, \phi, \psi, \delta_a, \dot{\delta}_a, \delta_r, \dot{\delta}_r]^T \quad (4.8)$$

$$\bar{Y} = [p, r]^T \quad (4.9)$$

$$\bar{U} = [\delta_{ac}, \delta_{rc}]^T \quad (4.10)$$

The various variables and stability derivatives used here are explained in Appendix 1. ψ and ϕ are integrals of yaw rate and roll rate, respectively.

The lateral (roll-yaw) autopilot is required to command stability axis roll rate and minimize induced sideslip. The stability axis co-ordinate system is defined as the transformation of the body axes to the stability axes using angle of attack (α) [7]. Thus roll rate in stability axis (p_s) is given by

$$p_s = p \cos(\alpha) + r \sin(\alpha) . \quad (4.11)$$

4.3 Control Law Based on Decoupling and Pole-Zero Assignment

Consider the multivariable feedback system shown in Fig.4.1, where P and $C \in C^{n \times n}$ denote the plant and controller transfer function matrices, respectively.

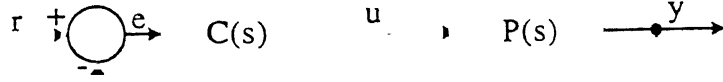


Figure 4.1 : Multivariable Feedback Control System

Let the plant of the system be factored as

$$P(s) = A^{-1}(s) B(s) = B_1(s) A_1(s)^{-1}, \quad (4.12)$$

where, the pairs $(A(s), B(s))$ and $(B_1(s), A_1(s))$ are the left and right coprime polynomial matrix factorizations of the plant, respectively.

The sensitivity matrix, with the loop broken at the output of the plant, is given by,

$$S(s) = (I + P(s) C(s))^{-1} \quad (4.13)$$

and then, the tracking error, $E(s)$, is given by,

$$E(s) = S(s) R(s) \quad (4.14)$$

where, $R(s)$ is the reference signal. Let the reference signal be

$R(s) = [r_1(s), r_2(s), \dots, r_n(s)]^T$ and let the zeros of the polynomial $m_i(s)$ be the poles of $r_i(s)$ in $\text{Re}[s] \geq 0$, for $i = 1, \dots, n$.

For the input-output decoupling, reference signal tracking and desired closed-loop pole assignment, the sensitivity matrix must be of the form.

$$\begin{aligned} S(s) &= \text{diag} [s_1(s), \dots, s_n(s)] \\ &= \text{diag} \begin{bmatrix} \frac{w_1(s) m_1(s)}{g_1(s)}, \dots, \frac{w_n(s) m_n(s)}{g_n(s)} \end{bmatrix} \end{aligned} \quad (4.15)$$

where, $g_i(s)$, $i = 1, \dots, n$, are Hurwitz polynomials with desired closed-loop poles and $w_i(s)$, $i = 1, \dots, n$, are undetermined polynomials which should be determined to satisfy the internal stability constraints.

In the following, Lemma 1 and Lemma 2 due to [61], are stated without proof. These provide pole-zero assignment control law which satisfies internal stability of the multivariable feedback system.

Lemma 1

Suppose $\det(A(s))$ and $\det(B_1(s))$ have no common zeros in $\text{Re}[s] \geq 0$. Then $S(s)$ is internally stable if and only if $S(s)$ is analytical in $\text{Re}[s] \geq 0$ and for some appropriately dimensioned stable rational matrices $X(s)$ and $Y(s)$

$$S(s) = Y(s) A(s) \quad (4.16)$$

$$I - S(s) = B_1(s) X(s) \quad (4.17)$$

From equations (4.16) and (4.17), we have

$$Y(s) = S(s) A^{-1}(s) \quad (4.18)$$

$$X(s) = B_1^{-1}(s) (I - S(s)) \quad (4.19)$$

Equivalently, $S(s)$ is internally stable if and only if $S(s)$, $S(s) A^{-1}(s)$ and $B_1^{-1}(s) (I - S(s))$ are analytic in $\text{Re}[s] \geq 0$.

REMARK : If $S(s)$ satisfies the internal stability requirements, then the controller can be directly obtained from (4.13) as

$$C(s) = P^{-1}(s) S^{-1}(s) (I - S(s)) \quad (4.20)$$

Assume,

$$A^{-1}(s) = \begin{bmatrix} a_{11}(s) & \dots & a_{1n}(s) \\ \vdots & & \vdots \\ a_{n1}(s) & \dots & a_{nn}(s) \end{bmatrix} \quad (4.21)$$

and

$$B_1^{-1}(s) = \begin{bmatrix} b_{11}(s) & \dots & b_{1n}(s) \\ \vdots & & \vdots \\ b_{n1}(s) & \dots & b_{nn}(s) \end{bmatrix} \quad (4.22)$$

From equations (4.15), (4.21) and (4.22), we obtain

$$S(s) A^{-1}(s) = \begin{bmatrix} s_1(s) & a_{11}(s) & \dots & \dots & s_1(s) & a_{1n}(s) \\ \vdots & \vdots & & & \vdots & \vdots \\ s_n(s) & a_{n1}(s) & \dots & \dots & s_n(s) & a_{nn}(s) \end{bmatrix} \quad (4.23)$$

and,

$$B_1^{-1}(s) (I - S(s)) = \begin{bmatrix} (1 - s_1(s)) & b_{11}(s) & \dots & \dots & (1 - s_n(s)) & b_{1n}(s) \\ \vdots & \vdots & & & \vdots & \vdots \\ (1 - s_1(s)) & b_{n1}(s) & \dots & \dots & (1 - s_n(s)) & b_{nn}(s) \end{bmatrix} \quad (4.24)$$

Define the polynomials

$$\gamma_i(s) = \prod_{l=1}^{\lambda_i} (s - p_{il})^{\sigma_{il}}, \quad i = 1, \dots, n \quad (4.25)$$

where, λ_i is the number of distinct poles p_{il} of the i_{th} row of $A^{-1}(s)$ in $\text{Re}[s] \geq 0$ and σ_{il} is the greatest multiplicity of each pole p_{il} which appears in any element of the i_{th} row of $A^{-1}(s)$. Similarly, we define the polynomials.

$$\Omega_i(s) = \prod_{l=1}^{\delta_i} (s - q_{il})^{\eta_{il}}, \quad i = 1, \dots, n \quad (4.26)$$

where δ_i is the number of distinct poles q_{il} of the i_{th} column $B_1^{-1}(s)$ in $\text{Re}[s] \geq 0$ and η_{il} is the greatest multiplicity of each pole q_{il} which appears in any element of the i_{th} column of $B_1^{-1}(s)$. Then following Lemma is obtained :

Lemma 2

For the system shown in Fig.4.1, if $\gamma_i(s)$ and $\Omega_i(s)$ are coprime for $i = 1, \dots, n$, then $S(s) = \text{diag} [s_1(s), \dots, s_n(s)]$ is internally stable if and only if the following conditions hold :

- (i) $s_i(s)$ is analytic in $\text{Re}[s] \geq 0$, for $i = 1, \dots, n$;
- (ii) the numerator polynomial of $s_i(s)$ is divisible by $\gamma_i(s)$, for $i = 1, \dots, n$;
- (iii) the numerator polynomial of $1 - s_i(s)$ is divisible by $\Omega_i(s)$,

for $i = 1, \dots, n$.

REMARK

If there exists any pair $(\gamma_i(s), \Omega_i(s))$ which is not coprime, then it is impossible for $S(s)$ to achieve the internal stability.

From the condition (ii) of Lemma 2, the numerator polynomial of $S_i(s)$ must contain $\gamma_i(s)$, and from the equation (4.15), the numerator of $s_i(s)$ must also contain $m_i(s)$. Thus the numerator of $s_i(s)$ must contain the least common multiple of $\gamma_i(s)$ and $m_i(s)$ for $i = 1, \dots, n$ ie.

$$\begin{aligned} S(s) &= \text{diag} \begin{bmatrix} \frac{w_1(s) m_1(s)}{g_1(s)}, \dots, \frac{w_n(s) m_n(s)}{g_n(s)} \end{bmatrix} \\ &= \text{diag} \begin{bmatrix} \frac{l_1(s) z_1(s)}{g_1(s)}, \dots, \frac{l_n(s) z_n(s)}{g_n(s)} \end{bmatrix} \end{aligned} \quad (4.27)$$

where $z_i(s)$, $i = 1, \dots, n$ are the least common multiples of $\gamma_i(s)$ and $m_i(s)$ while $l_i(s)$, $i = 1, \dots, n$ are undetermined polynomials. To satisfy the requirement of causality of the closed-loop system, the sensitivity matrix must be proper, i.e.

$$\deg(g_i(s)) \geq \deg(l_i(s)) + \deg(z_i(s)) \quad (4.28)$$

From equation (4.27) we have

$$\begin{aligned} t_i(s) &= 1 - s_i(s) \\ &= \frac{g_i(s) - l_i(s) z_i(s)}{g_i(s)} \end{aligned} \quad (4.29)$$

and from condition (iii) of Lemma 2, the numerator of $1 - s_i(s)$ must contain $\Omega_i(s)$. Thus we have

$$h_i(s) = g_i(s) - l_i(s) z_i(s) = \Omega_i(s) f_i(s), \quad i = 1, \dots, n \quad (4.30)$$

where $f_i(s)$, $i = 1, \dots, n$ are undetermined polynomials.

The following Lemma, given as Theorem 1 in [61], provides the condition on existence of $l_i(s)$.

Lemma 3

The solution of $l_i(s)$ in equation (4.30) exists if and only if $m_i(s)$ is coprime with $\Omega_i(s)$, for $i = 1, \dots, n$, respectively

REMARK

If $l_i(s)$ exists and the number of undetermined parameters of $l_i(s)$ is equal to $\deg(\Omega_i(s))$, then the solution of $l_i(s)$ in equation (4.30) is unique for $(\Omega_i(s))$, for $i = 1, \dots, n$, respectively.

By solving equation (4.30), we obtain $l_i(s)$, i.e. $S(s)$ is obtained. Then the controller can be derived using equation (4.20).

Moreover, if $l_i(s)$ exists and the number of undetermined parameters of $l_i(s)$ is greater than $\deg(\Omega_i(s))$, then no unique solution of $l_i(s)$ exists for $i = 1, \dots, n$, respectively. This leads to an over parametrized solution and the free parameters of $l_i(s)$ can be determined according to some specific performance criterion.

In the design here, $l_i(s)$, $f_i(s)$ and $g_i(s)$ are obtained by solving nonlinear optimization problem formulated in Section 4.5 for the desired performance requirements.

4.4 Performance Specifications

In the following, the time domain and frequency domain performance specifications are expressed by performance functions $\phi_i(R)$, where R is the solution vector for the optimization problem.

4.4.1 Time Domain Performance Specifications

(i) Command Tracking

Good tracking performance can be achieved by minimising the error between desired response and actual response. Let $y_{ij}^d(t)$ and $y_{ij}(t)$ be the discretized desired and actual responses, respectively, for the i_{th} channel for the discrete point j , $j = 1, \dots, nn$. Then the performance function for command tracking is defined as :

$$\phi_1(R) \triangleq \sum_{j=1}^{nn} \left[y_{ij}(t) - y_{ij}^d(t) \right]^2. \quad (4.31)$$

In order to get desired overshoot, another performance function $\phi_2(R)$ is defined for the error in desired overshoot ($y_{i, \max}^d$) and the actual overshoot ($y_{i, \max}$) and is given by

$$\phi_2(R) \triangleq (y_{i, \max} - y_{i, \max}^d) . \quad (4.32)$$

The corresponding performance constraints are

$$\phi_1(R) = 0 \quad (4.33)$$

$$\phi_2(R) = 0 \quad (4.34)$$

(ii) Control Input

The L_2 -norm of the control input signal $u_i(t)$ for the i_{th} channel, is minimized to save the control energy and to avoid saturation problems.

The L_2 -norm of $u_i(t)$ is defined as [32]

$$\|u_i\|_2 = \left(\int_{-\infty}^{\infty} u_i^2(t) dt \right)^{1/2} \quad (4.35)$$

This L_2 -norm can be calculated using Parseval theorem [39] as given by the equation (2.17) of the Chapter 2. The corresponding performance function is defined as

$$\phi_3(R) \triangleq \{ \|u_i(t)\|_2 - U_{i0} \} , \quad (4.36)$$

where U_{i0} is a constant which puts upper limit on L_2 -norm of $u_i(t)$ for the i_{th} input-output channel of the closed loop system. The corresponding performance constraint is

$$\phi_3(R) \leq 0. \quad (4.37)$$

(iii) Sideslip

The sideslip is kept small to avoid large roll moments. The performance function for the sideslip is defined as

$$\phi_4(R) \triangleq \max_{t \in [0, t_f]} \{ |\beta(t)| - b_s \} \quad (4.38)$$

where b_s is a constant which puts upper limit on the magnitude of permissible sideslip. t_f is the time during which the sideslip is to be kept small. The corresponding performance constraint is given by

$$\phi_4(R) \leq 0. \quad (4.39)$$

4.4.2 Frequency Domain Performance Specifications

(i) Robust Stability

Robust stability specification is based on M-circle constraint [51].

The details of the M-circle constraint are explained in the Section 3.4.2 of the Chapter 3. The M-circle constraint, based on loop margin, imposes gain and phase margin restrictions in terms of M-circle radius. This constraint provides robust stability against plant parameter variations and time-varying nonlinearities.

The performance specification, based on M-circle constraint for robust stability is defined as :

$$\phi_5(R) \triangleq \sup_{\omega \in [0, \infty)} \left\{ |S_{0i}(j\omega)| - \frac{1}{M_{\min}} \right\} \quad (4.40)$$

where, M_{\min} is the minimum radius of the M-circle.

The corresponding performance constraint is given by

$$\phi_5(R) \leq 0. \quad (4.41)$$

(ii) Sensitivity and Complementary Sensitivity Shapings

It has been shown in [48] and discussed in Section 3.3.2 of the Chapter 3 that many design specifications, time domain as well as frequency domain, can be achieved by proper shaping of the sensitivity and complementary sensitivity functions.

Here, the sensitivity and complementary sensitivity functions at the output of the plant have been taken for the shaping. The performance requirements are the same as discussed in Section 3.4.2 of the Chapter 3. These are restated as follows:

The spectrum of reference signals and disturbance signals are concentrated at low frequencies, while the spectrum of the measurement noises extends over a much wider frequency range. Therefore, $|S(j\omega)|$ is kept small at low frequencies (for $0 \leq \omega \leq \omega_0$, say) and $|T(j\omega)|$ is kept small at high frequencies (for $\omega > \omega_b$, say).

In a very low frequency interval $0 \leq \omega \leq \omega_0$ (where ω_0 is much lesser than the cut-off frequency), we require that :

$$|S_{0i}(j\omega)| < p_1, \text{ for } 0 \leq \omega \leq \omega_0 \quad (4.42)$$

and

$$|T_{0i}(j\omega)| \approx 1, \text{ for } 0 < \omega \leq \omega_0. \quad (4.43)$$

Here, $S_{0i}(j\omega)$ and $T_{0i}(j\omega)$ are the sensitivity and complementary sensitivity functions, respectively, at the plant output for the i th channel. p_1 ($\ll 1$) is a constant and puts upper bound on $S_{0i}(j\omega)$ in the frequency range $0 \leq \omega \leq \omega_0$.

We define the performance functions $\phi_6(R)$ and $\phi_7(R)$ corresponding to equations (4.42) and (4.43) respectively, as

$$\phi_6(R) \triangleq \sup_{\omega \in [0, \omega_0]} \{|S_{0i}(j\omega) - p_1|\} \quad (4.44)$$

$$\phi_7(R) \triangleq \sup_{\omega \in [0, \omega_0]} \{|T_{0i}(j\omega) - p_2|\} \quad (4.45)$$

Here, p_2 is a constant which puts upper bound on $|T_{0i}(j\omega)|$ required in the frequency range $(0, \omega_0)$.

The value of $|T_{0i}(j\omega)|$ at the bandwidth (ω_b) is given by

$$|T_{0i}(j\omega_b)| = |T_{0i}(0)|/\sqrt{2} = 0.707 \quad (4.46)$$

and the corresponding performance function is defined as

$$\phi_8(R) \triangleq \{|T_{0i}(j\omega_b)| - 0.707\} \quad (4.47)$$

The loop transfer function, L_{0i} , with the loop broken at the output of the plant, is $P(s)C(s)$. The performance function corresponding to the value of loop transfer function at crossover frequency, ω_c , is given by

$$\phi_9(R) \triangleq \{|L_{0i}(j\omega_c)| - 1\} \quad (4.48)$$

The permissible peak of the $|S_{0i}(j\omega)|$ has been specified in the performance function $\phi_5(R)$ of the robust stability given by equation (4.40). The permissible peak of $|T_{0i}(j\omega)|$ is specified by another performance function.

$$\phi_{10}(R) \triangleq \sup_{\omega \in [0, \omega_b]} \{|T_{0i}(j\omega)| - p_t\}, \quad (4.49)$$

where p_t is the bound on $|T_{0i}(j\omega)|$ in the frequency interval $\omega \in [0, \omega_b]$.

Therefore, to capture the desired shapes of $|S_{0i}(j\omega)|$ and $|T_{0i}(j\omega)|$ at various frequencies, we require.

$$\phi_6(R) \leq 0 \quad (4.50)$$

$$\phi_7(R) \leq 0 \quad (4.51)$$

$$\phi_8(R) = 0 \quad (4.52)$$

$$\phi_9(R) = 0 \quad (4.53)$$

$$\phi_{10}(R) \leq 0 \quad (4.54)$$

(iii) Disturbance and Measurement Noise Rejection

As given by equation (A3.6) in Appendix 3, the disturbance and measurement noise rejections can be obtained by keeping $|S_{0i}(j\omega)|$ small over lower frequencies and $|T_{0i}(j\omega)|$ small over higher frequencies, respectively. By proper sensitivity and complementary sensitivity shapings, both the disturbance and measurement noise rejections are achieved. However, explicit bounds on $|S_{0i}(j\omega)|$ and $|T_{0i}(j\omega)|$ need to be put.

Good disturbance rejection over the bandwidth of the feedback system can be achieved by keeping $|S_{0i}(j\omega)|$ small over the bandwidth $(0, \omega_c)$.

Hence, we define the following performance function for achieving disturbance rejection.

$$\phi_{11}(R) \stackrel{\Delta}{=} \sup_{\omega \in [0, \infty]} \{ |S_i(j\omega)| - b_f(\omega) \}, \quad (4.55)$$

where $b_f(\omega)$ is a continuous bound. The corresponding performance constraint is

$$\phi_{11}(R) \leq 0. \quad (4.56)$$

The choice of $b_f(\omega)$ has been discussed in Section 3.4.2 of Chapter 3. The bound $b_f(\omega)$ is given by equations (3.43) and (3.44) of Chapter 3. For the sake of completeness of the specification, these equations are given below :

$$\begin{aligned} 0 < b_f &= b_{f1} < 1, & \text{if } \omega \leq \omega_c \\ b_f &= b_{f2} > 1, & \text{if } \omega > \omega_c \end{aligned}$$

For the measurement noise rejection, the performance specification is given by

$$\phi_{12}(R) \stackrel{\Delta}{=} \sup_{\omega > \omega_b} \{ |T_{0i}(j\omega)| - c_f \}, \quad (4.57)$$

where c_f is a constant which puts the upper bound on $|T_{0i}(j\omega)|$ for frequencies $\omega > \omega_b$.

The corresponding performance constraint is given by

$$\phi_{12}(R) \leq 0. \quad (4.58)$$

4.5 Formulation of the Design Problem

4.5.1 Objective Function

The objective function used, is the weighted sum objective function, same as was used in Section 3.4.3 of Chapter 3. It is given by the equation (3.70) of Chapter 3. Here, the performance functions governing the inequalities are $\phi_3(R)$, $\phi_4(R)$, $\phi_5(R)$, $\phi_6(R)$, $\phi_7(R)$, $\phi_{10}(R)$, $\phi_{11}(R)$ and $\phi_{12}(R)$, and the performance functions governing the equalities are given by $\phi_1(R)$, $\phi_2(R)$, $\phi_8(R)$ and $\phi_9(R)$.

4.5.2 Simulated Annealing (SA) Technique

As discussed in the Section 3.4.4 of the Chapter 3, the SA technique guarantees global optimal or near global optimal solution. The same SA algorithm as was used in Chapter 3, is applied to solve the optimization problem, defined in Section 4.5.1.

4.6 Design Methodology

The closed-loop design goals for the roll-yaw MIMO system are to command stability axis roll rate (p_s) and to minimize the side slip. The stability axis roll rate is given by equation (4.11). The control law discussed in the Section 4.3 provides input-output decoupling of the MIMO system. This facilitates independent tracking of body axis roll rate (p) and yaw rate (r). As given by equation (4.11), the command of the stability axis roll rate implies tracking of the body axis roll rate and yaw rate, i.e.

$$p_{sc} = p_c \cos(\alpha) + r_c \sin(\alpha) \quad (4.59)$$

where p_{sc} , p_c and r_c are stability axis roll rate command, body axis roll rate command and yaw rate command respectively. In the present scheme of the autopilot design, p and r are used for feedback. Hence, the reference signal (r) here, is

$\begin{bmatrix} p_c \\ r_c \end{bmatrix}$ and the measured output is $\begin{bmatrix} p \\ r \end{bmatrix}$. Therefore, the roll-yaw missile dynamics form a MIMO system with two inputs and two outputs.

With input-output decoupling, the closed loop transfer function matrix is diagonal. The diagonal entries are the closed loop transfer functions for the individual channels and are given by equation (4.29).

The sensitivity function matrix, $S(s)$, given by equation (4.27) is also diagonal.

Therefore, the performance specifications, both time domain and frequency domain, can be achieved for each channel independently by proper selection of $s_i(s)$ and $t_i(s)$. The pole-zero assignment is used to get proper $s_i(s)$ and $t_i(s)$. As is evident from equations (4.27) and (4.29), the choice of poles and zeros for both $s_i(s)$ and $t_i(s)$ is dependent on the choice of the polynomials $l_i(s)$ and $g_i(s)$. The polynomial $l_i(s)$, in turn, is related with the polynomial $f_i(s)$ by equation (4.30). Therefore, pole-zero assignment problem boils down to the selection of $g_i(s)$, $l_i(s)$ and $f_i(s)$ to achieve the desired design specifications.

The performance specifications are written as time domain and frequency domain specifications and the problem is posed as optimization problem. The objective function of the optimization problem is given by equation (3.70). of Chapter 3.

This optimization problem, which is nonlinear, nonconvex and nondifferentiable in nature, is solved by SA technique to get $g_i(s)$, $l_i(s)$ and $f_i(s)$. The solution vector of the optimization problem consists of the unknown coefficients of polynomials $g_i(s)$, $l_i(s)$ and $f_i(s)$.

4.7 Design Algorithm

Following are the steps in the design algorithm:

Step 1

Perform the factorization $P(s) = A^{-1}(s) B(s) = B_1(s) A_1^{-1}(s)$, as given in equation (4.12) and calculate $A^{-1}(s)$ and $B_1^{-1}(s)$. Then determine $\gamma_i(s)$ and $\Omega_i(s)$ as

given by equations (4.25) and (4.26), respectively. Determine $m_i(s)$ and $z_i(s)$ as in equations (4.15) and (4.27), respectively.

Step 2

Identify first order transfer function or second order transfer function with two complex conjugate poles and no zeros, to get desired unit step responses for body axis roll rate (p) and yaw rate (r). Let these responses be $y_1^d(t)$ and $y_2^d(t)$, respectively.

Step 3

Specify the closed loop time domain and frequency domain performance specifications, including hard bounds, as given by equations (4.31)-(4.58).

Step 4

Using the performance functions as specified in Step 3, form the objective function with constraints, as given by equation (3.70).

Step 5

Set SA parameters and initial guess for the solution vector R. Choose initial values of non-negative scalar weight factors depending on the importance of design specifications.

Step 6

Run the SA algorithm to get optimal solution vector, R, consisting of unknown coefficients of $g_i(s)$, $l_i(s)$ and $f_i(s)$.

Step 7

Evaluate the performance with the solution as obtained in Step 5. If satisfactory, go to Step 9; otherwise go to Step 8.

Step 8

Modify the bounds on time domain and frequency domain performance specifications, and also modify the non-negative scalar weight factors depending on the accuracy desired. Reset SA parameters, if required. Go to Step 6.

Step 9

Obtain the controller, $C(s)$, as given by equation (4.20).

4.8 Design Examples

Two design examples are worked out. The Example 1 relates with the BTT missile [7,62] for which both the longitudinal and lateral autopilots are designed in this thesis. Example 2 is for the HAVE DASH II [17], which is also a BTT missile, and is worked out to show the applicability of the design algorithm to other BTT missiles.

4.8.1 Example 1

The design example takes the roll-yaw missile dynamics described in Section 4.2 of this Chapter. The flight conditions studied here are the same as considered for missile pitch dynamics, represented by $\alpha = 16^\circ$, Mach 0.8 and an altitude of 4000 ft. The nominal values of the dimensional aerodynamic stability derivatives for this flight condition, taken from [62], are reproduced below :

$$Y_{\beta} = -0.0052 (1/s)$$

$$Y_{\delta a} = 0.1338 (1/s)$$

$$Y_{\delta r} = -0.1004 (1/s)$$

$$L_{\beta} = 556.8 (1/s^2)$$

$$L_{\delta a} = 70.2 (1/s)$$

$$L_{\delta r} = -1079.0 (1/s^2)$$

$$N_{\beta} = 5.679 (1/s^2)$$

$$N_{\delta a} = -57.03 (1/s^2)$$

$$N_{\delta r} = 5.7471 (1/s^2)$$

The natural frequency and damping of the rudder and aileron, are taken the same as that of elevator, ie. $\omega = 113 \text{ rad/s}$ and $\xi = 0.6$.

The transfer function matrix of the roll-yaw dynamics with the state space description of equations (4.6)-(4.10), is given by

$$P(s) = \begin{bmatrix} P_{11}(s) & P_{12}(s) \\ P_{21}(s) & P_{22}(s) \end{bmatrix} \quad (4.60)$$

where,

$$P_{11}(s) = \frac{p}{\delta_{ac}} = \frac{8.9638e5 (s + 5.3323e-1 + 2.0976e1i) (s + 5.3323e-1 - 2.0976e1i)}{s (s + 67.8 - 90.4i) (s + 67.8 + 90.4i) (s + 12.169) (s - 12.164)}$$

$$P_{12}(s) = \frac{p}{\delta_{rc}} = \frac{-2.3993e7 (s + 1.7476e-2 + 2.6638i) (s + 1.7476e-2 - 2.6638i)}{s (s + 67.8 + 90.4i) (s + 67.8 - 90.4i) (s + 12.169) (s - 12.164)}$$

$$P_{21}(s) = \frac{r}{\delta_{ac}} = \frac{-7.2822e5 (s + 12.462) (s - 12.47)}{s (s + 67.8 + 90.4i) (s + 67.8 - 90.4i) (s + 12.169) (s - 12.164)}$$

and

$$P_{22}(s) = \frac{r}{\delta_{rc}} = \frac{7.3385e4 (s - 25.84) (s + 25.746)}{s (s + 67.8 + 90.4i) (s + 67.8 - 90.4i) (s + 12.169) (s - 12.164)}$$

The plant transfer function matrix is unstable with one pole in RHP at 12.164.

Typical design specifications for a lateral autopilot can be stated as :

Design a lateral autopilot to command stability axis roll rate with the steady state accuracy of 0.5%, time constant less than 0.2 sec, overshoot less than 20%. The sideslip should not be more than 5 degrees. The rudder and aileron should have deflections less than 60 degrees and fin rates should not exceed 400 deg/s. In each channel the autopilot must provide the minimum gain margins of (-6,+10)dB and the minimum phase margins of ± 40 degrees. The autopilot bandwidth is to be restricted by the high frequency unmodeled dynamics constraints, e.g. unmodeled flexible modes and actuator nonlinearities.

The lateral autopilot is synthesised using the design algorithm given in Section 4.6.

Performing the factorizations of $P(s)$, as in equation (4.2), we get

$$A^{-1}(s) = \frac{1}{D_a(s)} \begin{bmatrix} a_{11}(s) & a_{12}(s) \\ a_{21}(s) & a_{22}(s) \end{bmatrix} \quad (4.61)$$

$$B^{-1}(s) = \frac{1}{D_b(s)} \begin{bmatrix} b_{11}(s) & b_{12}(s) \\ b_{21}(s) & b_{22}(s) \end{bmatrix} \quad (4.62)$$

and

$$A_1(s) = \frac{1}{D_d(s)} \begin{bmatrix} d_{11}(s) & d_{12}(s) \\ d_{21}(s) & d_{22}(s) \end{bmatrix} \quad (4.63)$$

$$a_{11}(s) = (s + 6.3452) (s + 4.2883) (s + 3.279e-1 + 1.8396i) (s + 3.279e-1 - 1.8396i) (s + 2.25)$$

$$a_{12}(s) = 2.4439e2 (s + 6.0918) (s + 3.9701) (s - 2.0071) (s - 2.1524)$$

$$\begin{aligned}
a_{21}(s) &= 2.2054e-2 (s + 6.7987e1) (s + 5.8929) (s + 3.8432) (s + 1.8052) \\
a_{22}(s) &= (s - 11.1930) (s + 13.674) (s + 5.9762) (s + 4.0148) (s + 1.9937) \\
b_{11}(s) &= 8.9838e5 (s + 5.8916) (s + 3.9556) (s + 2.0848) (s + 51.565) \\
b_{12}(s) &= -2.3993e7 (s + 9.9317e-1) (s + 6.2841) (s + 2.816) (s + 4.5923) \\
b_{21}(s) &= -7.2822e5 (s + 6.0829) (s + 4.027) (s + 1.9577) (s - 1.5996e-1) \\
b_{22}(s) &= 7.3385e4 (s - 3.7299e2) (s + 5.7005) (s + 3.4262) (s + 1.033) \\
d_{11}(s) &= (s + 67.8 + 90.4i) (s + 67.8 - 90.4i) (s + 6.0741) (s + 4.022) (s + 1.9736) \\
&\quad (s - 7.3366e2 - 3.0956i) (s - 7.3366e-2 + 3.0956i) \\
d_{12}(s) &= 3.8175e1 (s + 67.8 + 90.4i) (s + 67.8 - 90.4i) (s + 5.7341) (s + 3.513) \\
&\quad (s + 1.099) (s - 1.9576) \\
d_{21}(s) &= 2.0049e-2 (s + 1.1118e3) (s + 67.8 + 90.4i) (s + 67.8 - 90.4i) (s + 6.0477) \\
&\quad (s + 4.0142) (s + 1.9802)
\end{aligned}$$

and

$$d_{22}(s) = (s + 67.8 + 90.4i) (s + 67.8 - 90.4i) (s - 10.173) (s + 5.8298) (s + 3.6546) (s + 1.1314)$$

where,

$$D_d(s) = D(s) = (s + 1) (s + 2) (s + 3) (s + 4) (s + 5) (s + 6) (s + 7)$$

$$D_a(s) = s (s + 67.8 + 90.4i) (s + 67.8 - 90.4i) (s + 12.169) (s + 12.169) (s + 12.164) D(s)$$

$$D_b(s) = 1.7406e13 (s + 1.8054e-2) D(s)$$

From the matrices $A^{-1}(s)$ and $B_1^{-1}(s)$ we get the following values of polynomials $\gamma_1(s)$, $\gamma_2(s)$, $\Omega_1(s)$, and $\Omega_2(s)$, using the equations (4.25) and (4.26):

$$\gamma_1(s) = \gamma_2(s) = s(s - 12.164) \quad (4.64)$$

$$\Omega_1(s) = \Omega_2(s) = 1 \quad (4.65)$$

Hence, we get

$$m_1(s) = m_2(s) = s \quad (4.66)$$

and,

$$z_1(s) = z_2(s) = z(s) = s(s - 12.164). \quad (4.67)$$

The second order closed loop transfer function of $\frac{60}{s^2 + 10s + 60}$ provides the desired time response. The closed loop transfer functions for both roll rate and yaw rate channels are taken of 5th order, same as that of the plant, satisfying the inequality (2.18) for the poles and zeros of the closed loop and open-loop systems. For the controller given by the equation (4.20) to be proper, the closed loop systems in both roll rate and yaw rate channels should have two zeros.

Here, we have $\Omega_1(s) = \Omega_2(s) = 1$. Therefore, to satisfy the conditions (ii) and (iii) of Lemma 2, the requirements of proper controller and causality of the closed loop system as given in equations (4.20) and (4.28) respectively, we choose $l_1(s)$, $l_2(s)$, $f_1(s)$ and $f_2(s)$ in the following forms:

$$l_1(s) = s^3 + a_2 s^2 + a_1 s + a_0 \quad (4.68)$$

$$l_2(s) = s^3 + a'_2 s^2 + a'_1 s + a'_0 \quad (4.69)$$

$$f_1(s) = b_2 s^2 + b_1 s + b_0 \quad (4.70)$$

and

$$f_2(s) = b'_2 s^2 + b'_1 s + b'_0 \quad (4.71)$$

Let $g_1(s)$ and $g_2(s)$ be given by

$$g_1(s) = s^5 + g_4 s^4 + g_3 s^3 + g_2 s^2 + g_1 s + g_0 \quad (4.72)$$

$$g_2(s) = s^5 + g'_4 s^4 + g'_3 s^3 + g'_2 s^2 + g'_1 s + g'_0 \quad (4.73)$$

The $g_1(s)$, $g_2(s)$, $l_1(s)$, $l_2(s)$, $f_1(s)$ and $f_2(s)$ are related by the equality given in equation (4.30). The coefficients of all these polynomials are unknown. If all these coefficients are taken as design variables, in the optimization problem certain equality constraints among a_i , a'_i , b_i , b'_i , g_i and g'_i will be involved to satisfy the equation (4.30). To avoid this problem, the design variables have been taken as a_i , a'_i , b_i and b'_i . Then, g_i and g'_i are calculated therefrom, putting the restriction that the poles of $g_1(s)$ and $g_2(s)$ should lie in the LHP. Therefore, the solution vector, R , of the optimization problem is given by,

$$R = [a_i, a'_i, b_i, b'_i]^T, \forall i = 1, \dots, 2 \quad (4.74)$$

The gain and phase margin constraints are imposed by M-circle constraint given by equation (4.39). $M_{\min} = 0.7$ guarantees gain margins of $(-4.6, +10.4)$ dB and the phase margins of ± 41 degrees, approximately. Initially, the design was aimed at achieving $\omega_c = 25$ rad/s and $\omega_b = 45$ rad/s.

The following initial bounds were taken:

$$U_{10} = 1.0$$

$$U_{20} = 1.0$$

$$\begin{aligned}
 b_s &= 1.0 \\
 b_{f1} &= 0.4, \text{ for } \omega < \omega_c \\
 b_{f2} &= 1.4 \\
 p_1 &= 0.2, \text{ for } \omega_0 = 5 \text{ rad/s} \\
 p_2 &= 1.0 \\
 \text{and } p_t &= 1.5 \\
 c_f &= 0.7 .
 \end{aligned}$$

The following parameters were set to run the Simulated Annealing algorithm, given in Appendix 4 :

$$\begin{aligned}
 N_s &= 20 \\
 N_T &= 50 \\
 C_i &= 2, \quad i = 1, \dots, n \\
 N_\epsilon &= 4.0
 \end{aligned}$$

and,

$$r_T = 0.85$$

The SA algorithm was run for different initial guesses. Initially, for the pole locations, one complex conjugate pole pair was taken as $(s+5\pm 5.9161i)$, which are the poles of the desired second order transfer function as in Step 2 of the design algorithm. The other poles were taken so that the above pole pair was in the dominant mode as compared to the remaining poles. Initial values of a_i , a'_i , b_i and b'_i were chosen to satisfy the equation (4.30). The bounds were set on a_i , a'_i , b_i and b'_i to have only positive real values.

Initially, a set of scalar weight factors was selected and convergence of the SA algorithm was studied. The SA algorithm was run for various values of the temperature parameter. As the starting temperature was increased, the solution improved. But, with increase of starting temperature speed of execution reduced. The starting temperature of $2.5e12$ gave optimal solution within reasonable execution time. Only one run was required for the converged solution.

After each run, the performance of the design was evaluated with solution vector. And scalar weight factors and bounds were tuned, if required. The scalar weight factors were modified.

The scalar weight factors $\lambda_1, \lambda_2, \lambda_3, \lambda_4, \lambda_5, \lambda_6, \lambda_7, \lambda_8, \lambda_9, \lambda_{10}, \lambda_{11}$ and λ_{12} with the respective values of 1, 50, 100, 10, 100, 200, 200, 150, 30, 50, 42 and 50 gave satisfactory performance for both the body roll rate and yaw rate channels. Finally, the solution converged with the bounds :

$$U_{10} = 1.0$$

$$U_{20} = 0.5$$

$$b_s = 1.0$$

$$b_{f1} = 0.55$$

$$b_{f2} = 1.4$$

$$p_1 = 0.4, \text{ for } \omega_0 = 10 \text{ rad/s}$$

$$p_2 = 1.0$$

$$p_t = 1.4$$

and,

$$c_f = 0.7 .$$

The values of the ω_b and ω_c were to be adjusted to 52 and 30 rad/s for both the roll rate and yaw rate channels .

The following polynomials were obtained with the solution vector R:

$$l_1(s) = s^3 + 1.2314e2 s^2 + 2.7633e5 s + 1.4508e6 \quad (4.75)$$

$$l_2(s) = s^3 + 8.3684e1 s^2 + 2.7897e5 s + 1.0592e6 \quad (4.76)$$

$$f_1(s) = 1.5885e7 s^2 + 1.1742e8 s + 2.8716e8 \quad (4.77)$$

$$f_2(s) = 8.7777e5 s^4 + 1.2409e8 s^3 + 1.1926e10 s^2 + 1.9908e11 s + 5.3544e11 \quad (4.78)$$

$$g_1(s) = s^5 + 1.1098e2 s^4 + 2.7483e5 s^3 + 1.3975e7 s^2 + 9.9772e7 s + 2.8716e8 \quad (4.79)$$

and,

$$g_2(s) = s^5 + 7.152e1 s^4 + 2.7795e5 s^3 + 1.2662e7 s^2 + 8.049e7 s + 3.851e8 \quad (4.80)$$

The corresponding controller, $C(s)$, is given by the equation (4.20), as

$$C(s) = P^{-1}(s) S^{-1}(s) [S(s) - I]$$

$$= [B_1(s) A_1^{-1}(s)]^{-1} [I - S^{-1}(s)]$$

$$= A_1(s) B_1^{-1}(s) [I - S^{-1}(s)]$$

$$= A_1(s) B_1^{-1}(s) \left\{ \begin{bmatrix} 1 & 0 & - & g_1(s) & 0 \\ & & - & l_1(s)z_1(s) & g_2(s) \\ 0 & 1 & & 0 & l_2(s)z_2(s) \end{bmatrix} \right\}$$

$$= A_1(s) B_1^{-1}(s) \left\{ \begin{bmatrix} 1 & 0 \\ 0 & 1 \end{bmatrix} - \begin{bmatrix} \frac{g(s)}{l_1(s)z(s)} & 0 \\ 0 & \frac{g(s)}{l_2(s)z(s)} \end{bmatrix} \right\}$$

On substituting the values of $A_1(s)$, $B_1^{-1}(s)$, $g_1(s)$, $g_2(s)$, $l_1(s)$, $l_2(s)$ and $z(s)$ from equations (4.62), (4.63), (4.79), (4.80), (4.75), (4.76) and (4.67), respectively, we get

$$C(s) = \begin{bmatrix} \frac{C_{11}(s)}{D_{C1}(s)} & \frac{C_{12}(s)}{D_{C2}(s)} \\ \frac{C_{21}(s)}{D_{C1}(s)} & \frac{C_{22}(s)}{D_{C2}(s)} \end{bmatrix}, \quad (4.81)$$

where,

$$C_{11}(s) = 1.1657e12 s^6 + 1.6658e14 s^5 + 1.5283e16 s^4 + 4.838e14 s^3 - 1.0435e19 s^2 \\ - 7.5124e19 s - 1.7901e20$$

$$C_{12}(s) = 3.598e14 s^6 + 5.1042e16 s^5 + 4.9116e18 s^4 + 3.0393e19 s^3 + 1.5385e20 s^2 \\ - 1.741e20 s - 4.1495e20$$

$$C_{22}(s) = 1.3442e13 s^6 + 1.9208e15 s^5 + 1.9129e17 s^4 + 2.1505e18 s^3 + 8.6317e19 s^2 \\ + 4.9586e20 s + 1.9407e21$$

$$C_{21}(s) = 1.1568e13 s^6 + 1.654e15 s^5 + 1.577e17 s^4 + 8.6185e17 s^3 - 2.2127e19 s^2 \\ - 1.741e20 s - 4.1495e20$$

$$D_{c1}(s) = 1.7406e15 s^6 + 1.932e15 s^5 + 4.7838e18 s^4 - 3.3168e19 s^3 - 3.0778e20 s^2 - 5.5458e18 s$$

$$D_{c2}(s) = 1.7406e13 s^6 + 1.2452e15 s^5 + 4.8381e15 s^4 - 4.0542e15 s^3 - 2.25e20 s^2 - 4.0489e18 s$$

The unit step responses for p and r are shown in Fig.4.2. Fig.4.3 shows the control deflections to unit step command and the sideslip is shown in Fig.4.4.

Bode magnitude plots to indicate loop shapings near ω_c for the loop transfer functions broken at the output channels of p and r are shown in Fig.4.5. Fig.4.6 and Fig.4.7 show the gain characteristics of $S_0(j\omega)$ and $T_0(j\omega)$ at the output of p and r channels, respectively. The time domain and frequency domain performance specifications achieved with the designed autopilot are shown in Table 4.1. The maximum sideslip is 0.128 degrees.

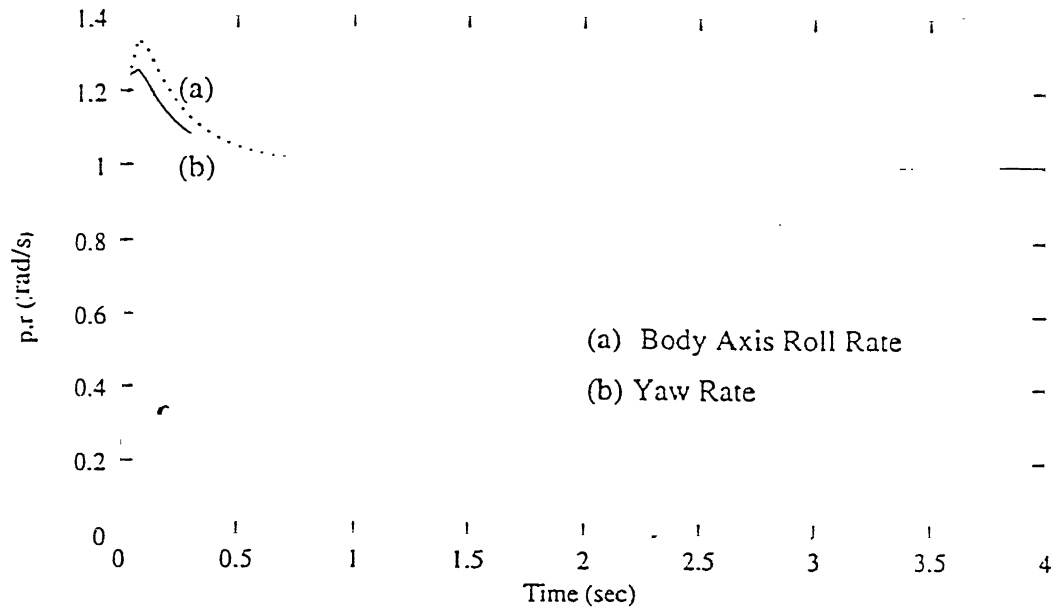


Figure 4.2 : Unit Step responses for Body Axis Roll Rate and Yaw Rate

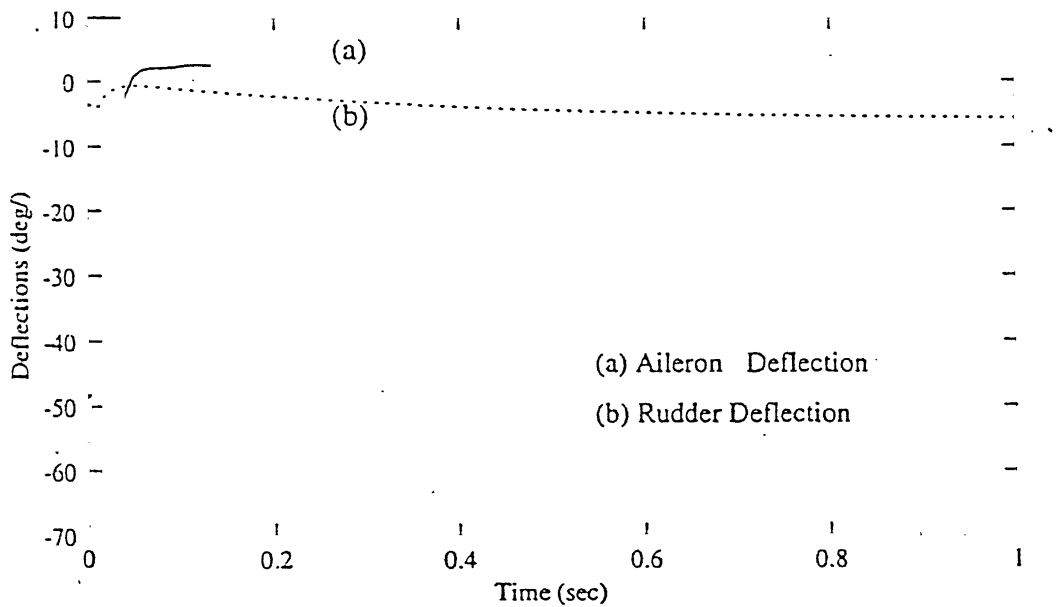


Figure 4.3 : Control Deflections

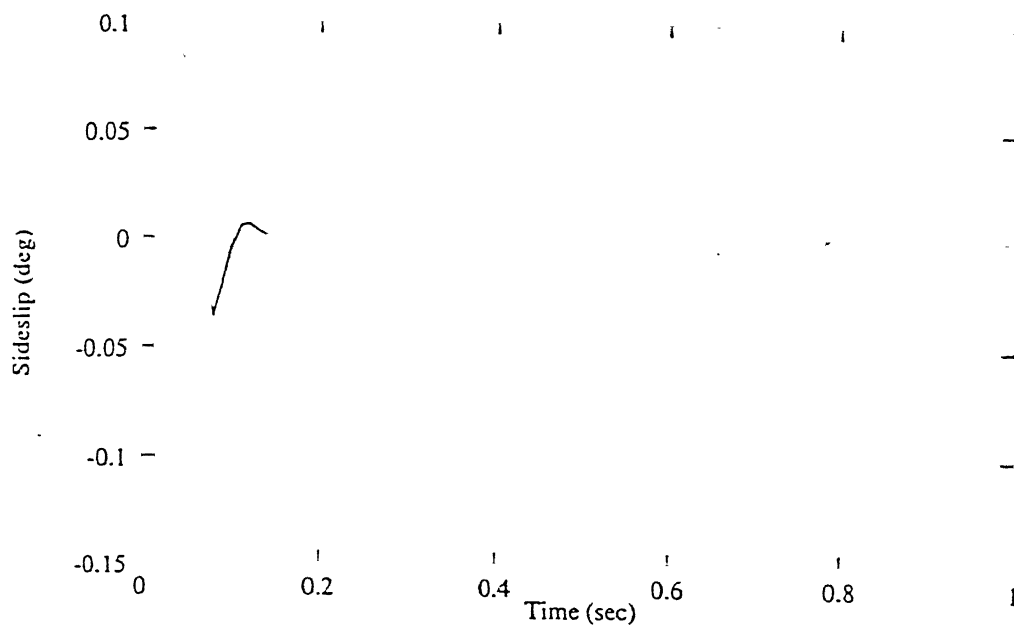


Figure 4.4 : Sideslip

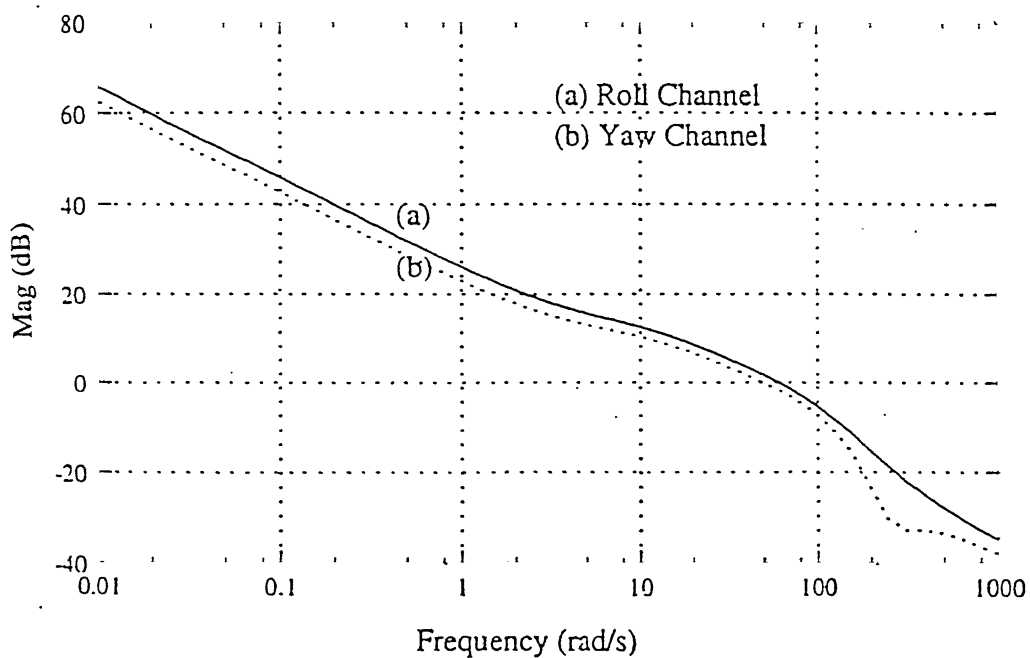


Figure 4.5 : Bode Magnitude Plots for Roll and Yaw Channels

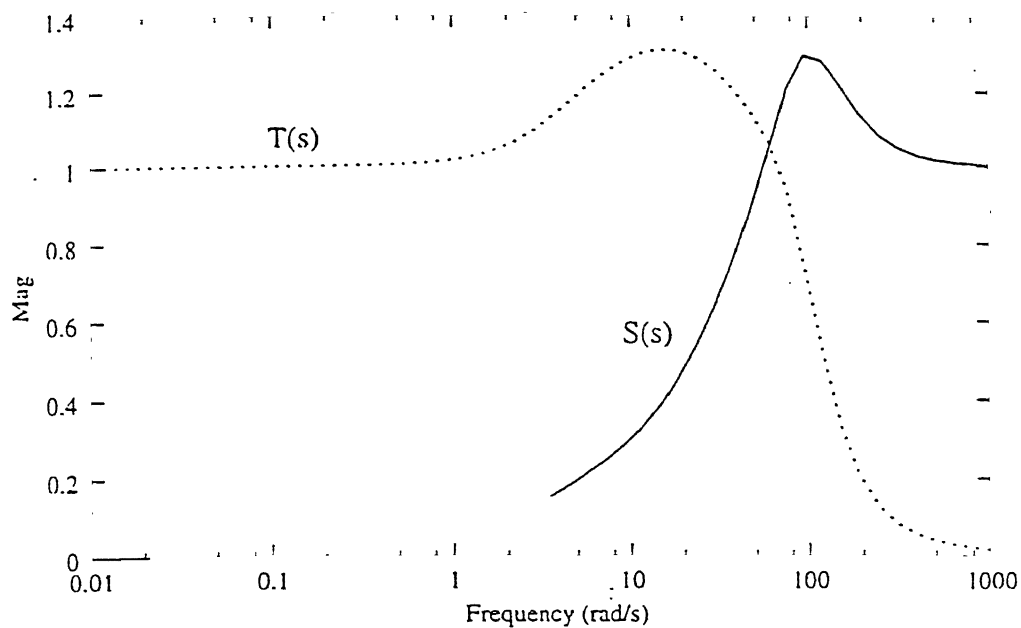


Figure 4.6 : Sensitivity and Complementary Sensitivity Functions for Roll Channel at the Output.

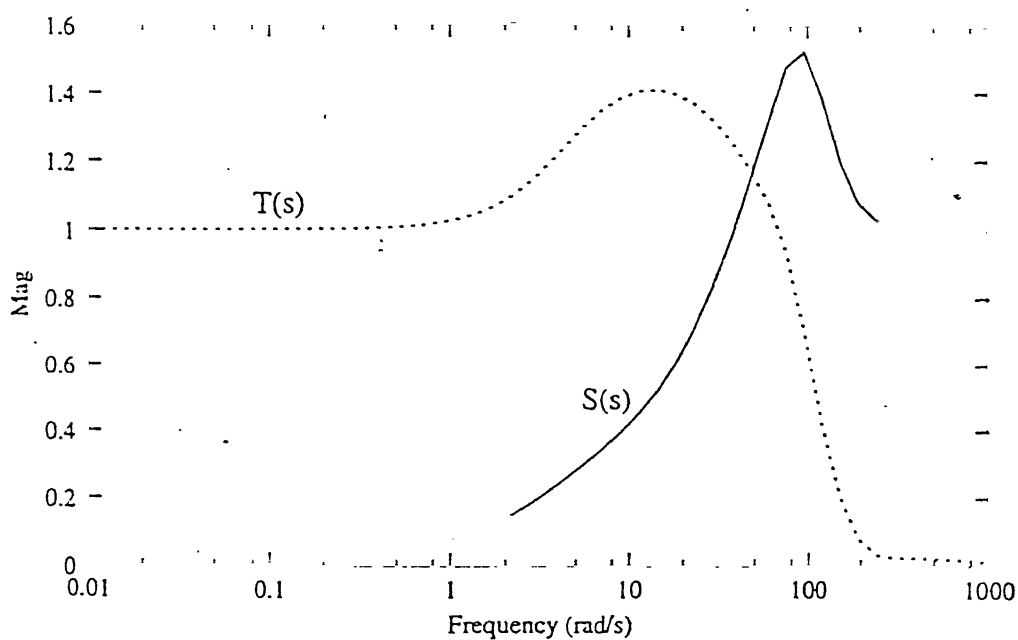


Figure 4.7 : Sensitivity and Complementary Sensitivity Functions for Yaw Channel at the Output

Table 4.1
Time Domain and Frequency Domain Performance for the Body Axis Roll Rate and Yaw Rate (Example 1)

Channel	Rise Time (s)	Overshoot (%)	Settling Time (s)	Fin Deflection (deg)	Fin Rate (deg/s)	Gain Margin (dB)	Phase Margin (deg)	Gain Crossover Freq. (Hz)
Body Axis Roll Rate	0.04	25.5	0.4	20.7	469	-11.3,+8.4	± 74.3	9.1
Yaw Rate	0.04	31.8	0.48	1.42	144	-10.6,+7.2	± 73.3	8.4

Normally for the BTT missile, the maneuvering capability required in yaw is very small. The stability axis roll rate command tracking response can be obtained with combination of step responses of p and r using equation (4.11). If we take one to one combination of unit step responses for p and r , as shown in Fig.4.5. we get the unit step response for p_s as shown in Fig.4.8. The design methodology facilitates any combination of p and r to get unit step response for p_s . Thus, the present design methodology facilitates stability axis roll rate command tracking design for any capability in yaw.

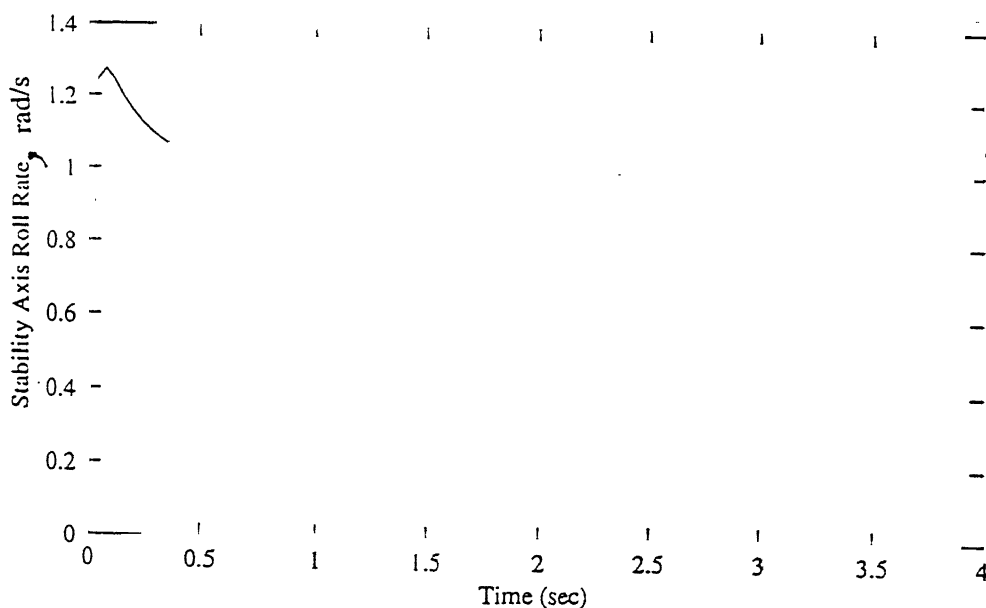


Figure 4.8 : Unit step Response for Stability Axis Roll Rate

Most of the design specifications have been reasonably achieved using present methodology of design except the overshoot. The RHP pole of the transfer function matrix of the roll yaw plant occurs in the polynomials $z_1(s)$ and $z_2(s)$. The zeros of the closed loop transfer functions for body axis roll rate and yaw rate channels are given by the roots of the polynomials $f_1(s)$ and $f_2(s)$, respectively. Due to RHP pole occurring in $z_1(s)$ and $z_2(s)$, the zeros of $f_1(s)$ and $f_2(s)$ can not be assigned arbitrarily, as given by equation (4.30). As a result of which this RHP root forces the time responses in both p and r to be very fast and thus producing large overshoot. In both body axis roll rate and yaw rate unit step responses, the time constant is less than 0.1 sec and overshoot is more than 25%.

By varying the bounds on performance functions and scalar weight factors, different sets of design specifications can be achieved.

4.8.2 Example 2

In this Section, roll-yaw autopilot has been designed for the HAVE DASH II missile system. HAVE DASH II is a high performance BTT missile. The missile model has been taken from [17]. The linearized roll-yaw dynamics are described by

$$\dot{\beta} = p_s \sin(\alpha) - r \cos(\alpha) + Y_{\beta} \cdot \beta + \left(\frac{g}{V \cos(\theta_0)} \right) \cdot \varphi + Y_{\delta_a} \cdot \delta_a + Y_{\delta_r} \cdot \delta_r \quad (4.82)$$

$$\dot{p}_s = L_{\beta} \cdot \beta + L_{\delta_a} \cdot \delta_a + L_{\delta_r} \cdot \delta_r \quad (4.83)$$

$$\dot{r} = N_{\beta} \cdot \beta + N_{\delta_a} \cdot \delta_a + N_{\delta_r} \cdot \delta_r \quad (4.84)$$

$$\dot{\varphi} = p_s \quad (4.85)$$

$$\dot{\delta}_a = -\omega (\delta_a - \delta_{ac}) \quad (4.86)$$

$$\dot{\delta}_r = -\omega (\delta_r - \delta_{rc}) \quad (4.87)$$

Here, p_s is the stability axis roll rate ; θ_0 is the missile pitch attitude angle. The stability derivatives and other variables occurring in the above equations have already been explained with reference to roll-yaw missile model in Example 1.

The missile is assumed to fly at 40,000 ft, Mach=2.75, $\alpha = 10^0$. At this flight condition the stability derivatives are as follows :

$$Y_{\beta} = -0.2980 (1/s)$$

$$Y_{\delta_a} = 0.0025 (1/s)$$

$$Y_{\delta r} = 0.1021 (1/s)$$

$$L_{\beta} = -2075.6121 (1/s^2)$$

$$L_{\delta a} = -2631.4756 (1/s)$$

$$L_{\delta r} = -486.4590 (1/s^2)$$

$$N_{\beta} = 8.1743 (1/s^2)$$

$$N_{\delta a} = 4.2661 (1/s^2)$$

$$N_{\delta r} = -117.2795 (1/s^2)$$

A stability axis roll rate command of 90 deg/s has been taken between 2.0 to 4.0 secs. The body yaw rate for coordination is

$$r_c = p_{sc} \sin(\alpha) = 90 \sin(10) = 15.62 \text{ deg/s}$$

The p_s and r are the measured variables and have been used for feedback. Therefore, the transfer function matrix of the roll-yaw dynamics, given by equation (4.60), is

$$P(s) = \begin{bmatrix} P_{11}(s) & P_{12}(s) \\ P_{21}(s) & P_{22}(s) \end{bmatrix} \quad (4.88)$$

where,

$$\begin{aligned} p_{11} &= \frac{r}{\delta_{rc}} \\ &= \frac{-2.111e4 (s + 1.1083e-1 + 1.9139e1 i) (s + 1.1083e-1 - 1.9139e1 i) (s + 6.9224e-2)}{s (s + 1.1514e-1 + 1.9195e1 i) (s + 1.1514e-1 - 1.9195e1 i) (s + 6.7711e-2) (s + 180)} \\ p_{12} &= \frac{r}{\delta_{ac}} \\ &= \frac{7.679e2 (s - 22.581) (s + 2.2814e1) (s + 6.9218e-2)}{s (s + 1.1514e-1 + 1.9195e1 i) (s + 1.1514e-1 - 1.9195e1 i) (s + 6.7711e-2) (s + 180)} \\ p_{21} &= \frac{p}{\delta_{rc}} \\ &= \frac{-8.7563e4 s (s + 3.6682e-1 + 2.2377e1 i) (s + 3.6682e-1 - 2.2377e1 i)}{s (s + 1.1514e-1 + 1.9195e1 i) (s + 1.1514e-1 - 1.9195e1 i) (s + 6.7711e-2) (s + 180)} \\ p_{22} &= \frac{p}{\delta_{ac}} \\ &= \frac{-4.7367e5 s (s + 1.4999e-1 + 2.1711 i) (s + 1.4999e-1 - 2.1711 i)}{s (s + 1.1514e-1 + 1.9195e1 i) (s + 1.1514e-1 - 1.9195e1 i) (s + 6.7711e-2) (s + 180)} \end{aligned}$$

The lateral autopilot is synthesised using the design algorithm given in Section 4.6. Performing the factorizations of $P(s)$ as in equation (4.2), we get

$$A^{-1}(s) = \frac{1}{D_a(s)} \begin{bmatrix} a_{11}(s) & a_{12}(s) \\ a_{21}(s) & a_{22}(s) \end{bmatrix} \quad (4.89)$$

$$B_1^{-1} = \frac{1}{D_b(s)} \begin{bmatrix} b_{11}(s) & b_{12}(s) \\ b_{21}(s) & b_{22}(s) \end{bmatrix} \quad (4.90)$$

and

$$A_1(s) = \frac{1}{D_d(s)} \begin{bmatrix} d_{11}(s) & d_{12}(s) \\ d_{21}(s) & d_{22}(s) \end{bmatrix} \quad (4.91)$$

where,

$$\begin{aligned} a_{11}(s) &= (s + 180)(s + 4.9913)(s - 1.0658 + 1.8822e1 i)(s - 1.0658 - 1.8822e1 i) \\ &\quad (s + 2.9624)(s + 6.9853e-2) \\ a_{12}(s) &= -2.797e-2(s + 180)(s + 4.9915e1)(s + 5.0049)(s + 2.996424)(s + 7.0434e-2) \\ a_{21}(s) &= 5.9443e2 s(s + 180)(s + 6.8887)(s + 4.3131)(s + 2.4318) \\ a_{22}(s) &= s(s + 180)(s + 5.5126)(s + 3.5144 + 1.294 i)(s + 3.5144 - 1.294 i)(s + 2.8646) \\ b_{11}(s) &= -4.7367e5 s(s + 5.4015)(s + 3.6279)(s + 1.8407) \\ b_{12}(s) &= -7.679e2(s + 9.1862e2)(s + 4.6042)(s + 2.3435)(s + 3.7581e-1) \\ b_{21}(s) &= -8.7563e4 s(s + 5.2832)(s + 3.4884)(s + 1.7445) \\ b_{22}(s) &= -2.111e4(s + 4.7494)(s - 3.4097)(s + 2.5327)(s + 3.9942e-1) \\ d_{11}(s) &= (s + 7.195e-1 + 2.267 i)(s + 7.195e-1 - 2.267 i)(s + 180)(s - 4.33)(s + 4.7335) \\ d_{12}(s) &= -3.3064e1(s + 5.1521e-1 + 2.5312 i)(s + 5.1521e-1 - 2.5312 i)(s + 180) \\ &\quad (s + 4.5813)(s + 2.2875) \\ d_{21}(s) &= 1.0653(s + 180)(s - 1.1398e1 + 1.8453e1 i)(s + 1.1398e1 - 1.8453e1 i) \\ &\quad (s + 4.4779)(s + 2.2405) \end{aligned}$$

and,

$$\begin{aligned} d_{22}(s) &= (s + 180)(s - 6.7915e-1 + 1.9678e1 i)(s - 6.7915e-1 - 1.9678e1 i)(s + 1.162e1) \\ &\quad (s + 4.4779)(s + 2.2405) \end{aligned}$$

where,

$$\begin{aligned} D_d(s) &= D(s) = (s + 1)(s + 2)(s + 3)(s + 4)(s + 5)(s + 6) \\ D_a(s) &= s(s + 1.154e-1 + 1.9195 i)(s + 1.154e-1 - 1.9195 i)(s + 180)^2(s + 6.77e-3)D(s) \\ D_b(s) &= 1.0066e10(s + 2.9583e-1)D(s) \end{aligned}$$

From the matrices $A^{-1}(s)$ and $B_1^{-1}(s)$, we get the following values of polynomials $\gamma_1(s)$, $\gamma_2(s)$, $\Omega_1(s)$, and $\Omega_2(s)$ using equations (4.25) and (4.26):

$$\gamma_1(s) = \gamma_2(s) = s \quad (4.92)$$

$$\Omega_1(s) = \Omega_2(s) = 1 \quad (4.93)$$

Hence, we get

$$m_1(s) = m_2(s) = s \quad (4.94)$$

and,

$$z_1(s) = z_2(s) = z(s) = s. \quad (4.95)$$

The first order closed loop transfer function of $\frac{20}{s+20}$ provides the desired time response. The closed loop transfer functions for both the roll rate and yaw rate channels are taken of 5th order, same as that of the plant, satisfying the inequality (2.18) for the poles and zeros of the closed loop and open loop systems. For the controller given by the equation (4.20), to be proper, the closed loop systems in both roll rate and yaw rate channels should have two zeros.

Here, we have $\Omega_1(s) = \Omega_2(s) = 1$. Therefore, to satisfy the conditions (ii) and (iii) of Lemma 2, the requirements of proper controller and causality of the closed loop system as given in equations (4.20) and (4.28), respectively, we choose $l_1(s)$, $l_2(s)$, $f_1(s)$ and $f_2(s)$ in the following forms:

$$l_1(s) = s^4 + a_3 s^3 + a_2 s^2 + a_1 s + a_0 \quad (4.96)$$

$$l_2(s) = s^4 + a'_3 s^3 + a'_2 s^2 + a'_1 s + a'_0 \quad (4.97)$$

$$f_1(s) = b_2 s^2 + b_1 s + b_0 \quad (4.98)$$

and

$$f_2(s) = b'_2 s^2 + b'_1 s + b'_0 \quad (4.99)$$

The closed loop poles for both roll rate and yaw rate channels are chosen to be five simple poles. Then $g_1(s)$ and $g_2(s)$ are of the following forms:

$$\begin{aligned} g_1(s) &= (s+p_1)(s+p_2)(s+p_3)(s+p_4)(s+p_5) \\ &= s^5 + g_4 s^4 + g_3 s^3 + g_2 s^2 + g_1 s + g_0 \end{aligned} \quad (4.100)$$

$$g_2(s) = (s+p'_1)(s+p'_2)(s+p'_3)(s+p'_4)(s+p'_5)$$

$$= s^5 + g'_{4s} s^4 + g'_{3s} s^3 + g'_{2s} s^2 + g'_{1s} s + g'_0 \quad (4.101)$$

The $g_1(s)$, $g_2(s)$, $l_1(s)$, $l_2(s)$, $f_1(s)$ and $f_2(s)$ are related by the equality given in equation (4.30). In this example one zero which appears in the denominator of $P^{-1}(s)$ at $-2.9583e-1$ has been taken in the polynomials $f_1(s)$ and $f_2(s)$. Remaining one zero of $f_i(s)$'s and five simple poles of $g_i(s)$'s have been taken as design variables. To avoid the introduction of additional constraints in the optimization problem due to equation (4.30), $l_1(s)$ and $l_2(s)$ have been calculated from the $g_1(s)$, $g_2(s)$, $f_1(s)$ and $f_2(s)$. The restriction has been imposed to have the roots of $l_1(s)$ and $l_2(s)$ in the L.H.P.

Therefore, the solution vector, R , of the optimization problem is given by,

$$R = [p_i, p'_i, z_i, z'_i]^T, \quad \forall i = 1, \dots, 5 \quad (4.102)$$

Here, z_i and z'_i are the zero locations in the polynomials $f_1(s)$ and $f_2(s)$, respectively. M_{\min} of 0.7 guarantees desirable gain and phase margins, as discussed in Example 1.

The initial values of bounds and scalar weight factors were taken same as in Example 1. Initially, the design was aimed at achieving $\omega_c = 25$ rad/s and $\omega_b = 45$ rad/s.

The same set of SA parameters, as in Example 1, were taken. With initial temperature of $1.0e6$, the optimal solution was obtained which gave satisfactory performance.

The scalar weight factors $\lambda_1, \lambda_2, \lambda_3, \lambda_4, \lambda_5, \lambda_6, \lambda_7, \lambda_8, \lambda_9, \lambda_{10}, \lambda_{11}$ and λ_{12} with the respective values of 1, 5, 500, 500, 70, 100, 100, 50, 30, 50, 42 and 20 gave satisfactory performance for both the body axis roll rate and yaw rate channels. Finally, the solution converged with the bounds :

$$U_{10} = 1.0 \text{ deg}$$

$$U_{20} = 2.0 \text{ deg}$$

$$b_s = 2.0$$

$$b_{f1} = 0.25$$

$$b_{f2} = 1.4$$

$$p_1 = 0.4, \text{ for } \omega_0 = 10 \text{ rad/s}$$

$$p_2 = 1.0$$

$$p_t = 1.4$$

and,

$$c_f = 0.7 .$$

The values of the ω_b and ω_c were to be adjusted to 40 and 25 rad/s for both the roll rate and yaw rate channels .

The following polynomials were obtained with the solution vector R:

$$l_1(s) = s^4 + 7.4009e2 s^3 + 2.0545e5 s^2 + 2.5354e7 s + 6.3211e7 \quad (4.103)$$

$$l_2(s) = s^4 + 2.6574e5 s^3 + 2.3496e10 s^2 + 6.516e14 s + 1.8468e14 \quad (4.104)$$

$$f_1(s) = 1.0759e4 s^2 + 1.114e9 s + 3.2956e8 \quad (4.105)$$

$$f_2(s) = 3.9826e13 s^2 + 1.3501e1 s + 3.9904e15 \quad (4.106)$$

$$g_1(s) = s^5 + 7.4009e2 s^4 + 2.0545e5 s^3 + 2.5364e7 s^2 + 1.1772e9 s + 3.2956e8 \quad (4.107)$$

and,

$$g_2(s) = s^5 + 2.6574e5 s^4 + 2.3496e10 s^3 + 6.9143e14 s^2 + 1.3685e16 s + 3.9904e15 \quad (4.108)$$

The corresponding controller, $C(s)$, as in equation (4.81), is obtained with the following polynomials:

$$C_{11}(s) = 5.0963e9 s^6 + 5.286e14 s^5 + 9.5297e16 s^4 + 5.9141e16 s^3 + 4.5903e17 s^2 \\ + 1.3308e17 s - 8.4553e-1$$

$$C_{12}(s) = 3.0582e16 s^6 + 1.5881e19 s^5 + 1.8582e21 s^4 - 7.0598e21 s^3 - 9.6327e23 s^2 \\ - 3.5078e23 s - 1.9668e22$$

$$C_{21}(s) = -9.4212e8 s^6 - 9.7718e13 s^5 - 1.766e16 s^4 - 6.7039e16 s^3 - 8.8125e18 s^2 \\ - 2.6016e18 s + 8.7086$$

$$C_{22}(s) = 8.4073e17 s^6 + 4.3658e20 s^5 + 5.182e22 s^4 + 1.8997e23 s^3 + 1.8838e25 s^2 \\ + 6.8574e24 s + 3.844e23$$

$$D_{c1}(s) = 1.0066e10 s^6 + 7.4527e12 s^5 + 2.07e15 s^4 + 2.5582e17 s^3 + 7.1178e17 s^2 + 1.88e17 s$$

$$D_{c2}(s) = 1.0066e10 s^6 + 2.675e15 s^5 + 2.3652e20 s^4 + 6.559e24 s^3 + 3.7994e24 s^2 + 5.5e23 s$$

The stability axis roll rate response due to roll rate command of 90 deg/s, between 2.0 and 4.0 secs, is shown in Fig.4.9. Fig.4.10 shows the yaw rate response.

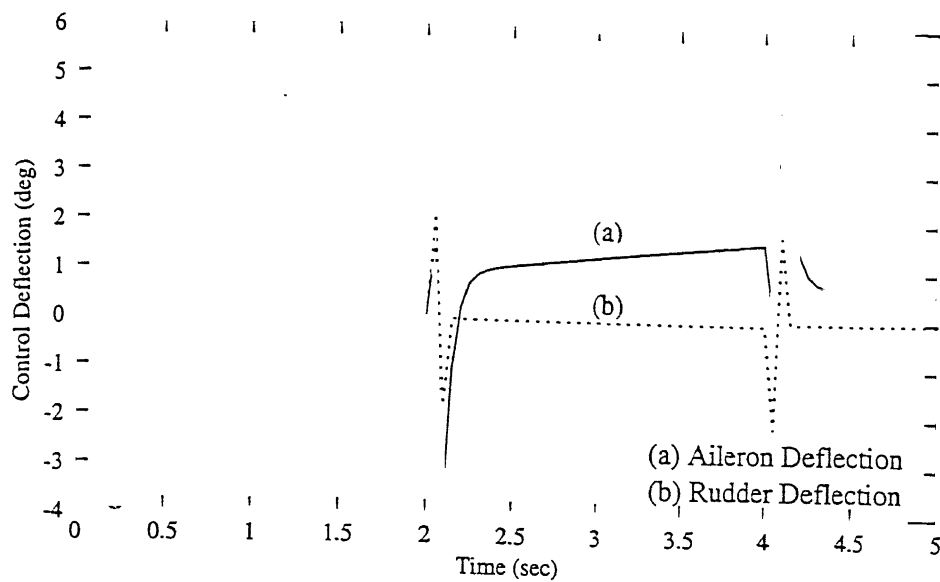


Figure 4.11 : Aileron and Rudder Deflections

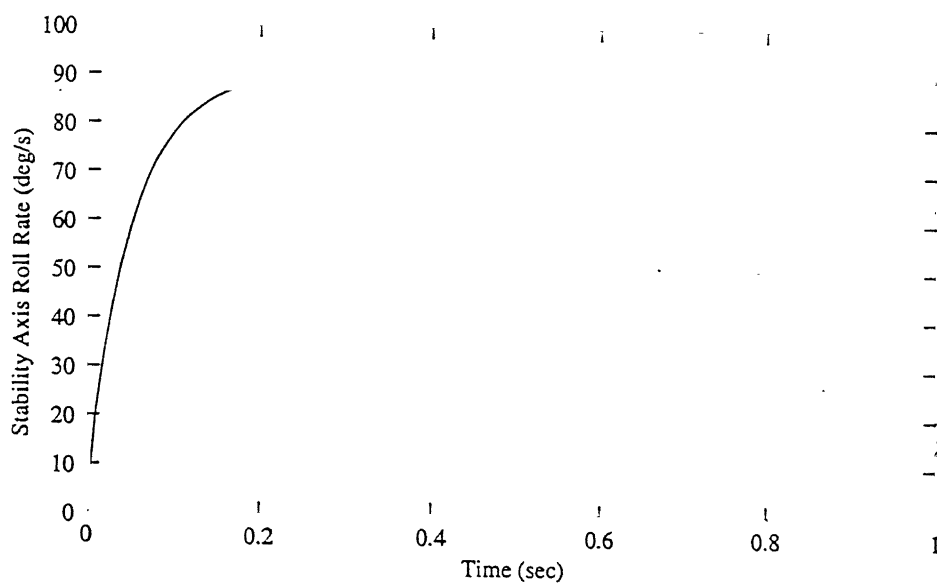


Figure 4.12 : Step Response for Stability Axis Roll Rate

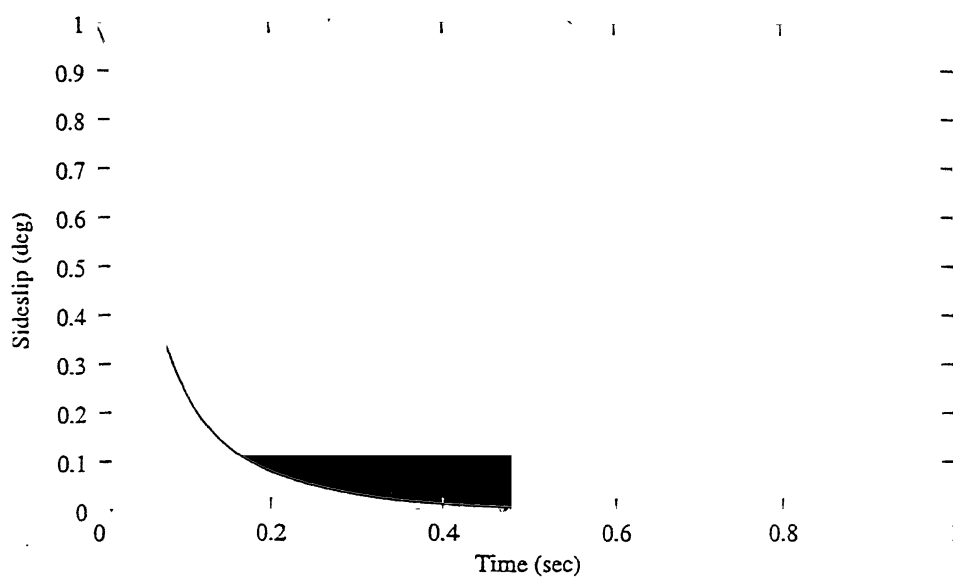


Figure 4.13 : Sideslip Response

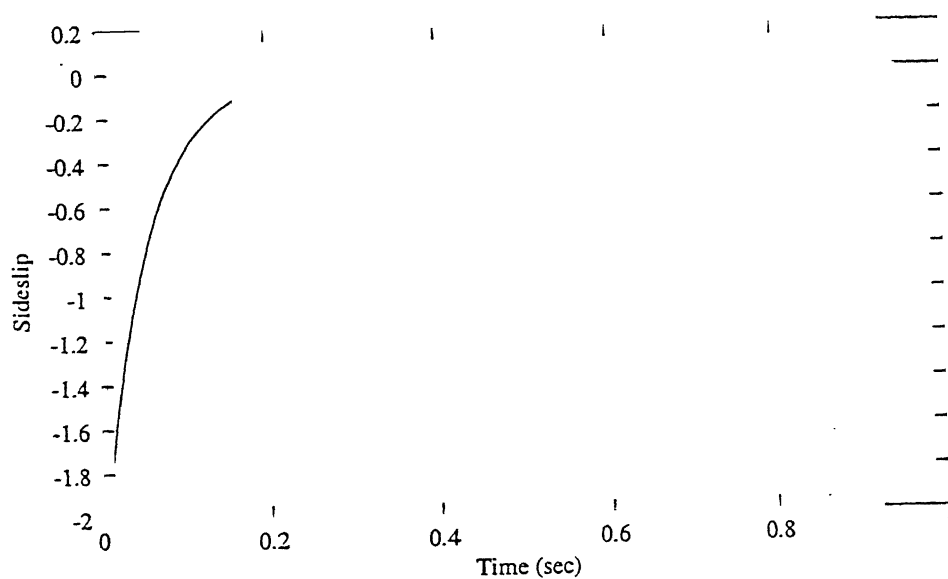


Fig.4.14 : Sideslip due to Step Stability Axis Roll Rate

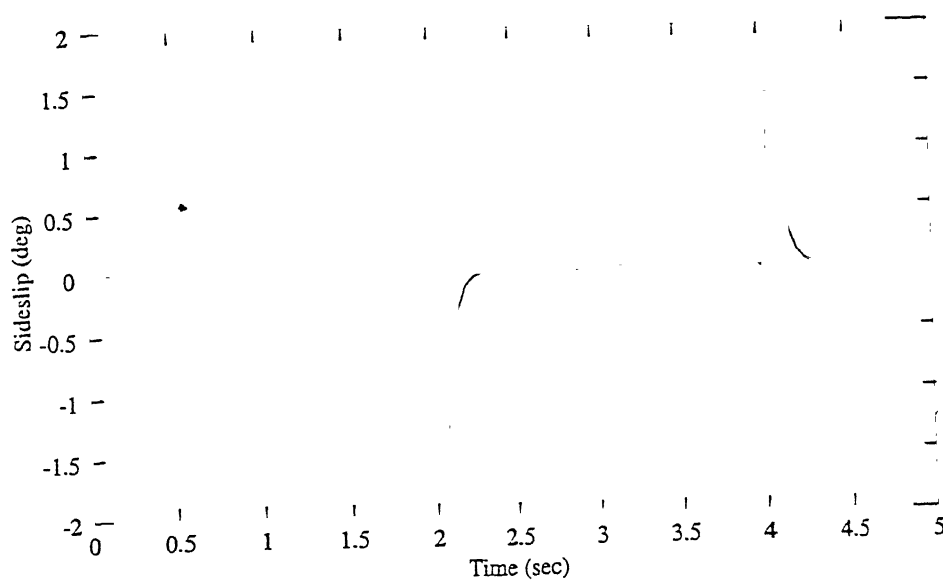


Figure 4.15 : Sideslip

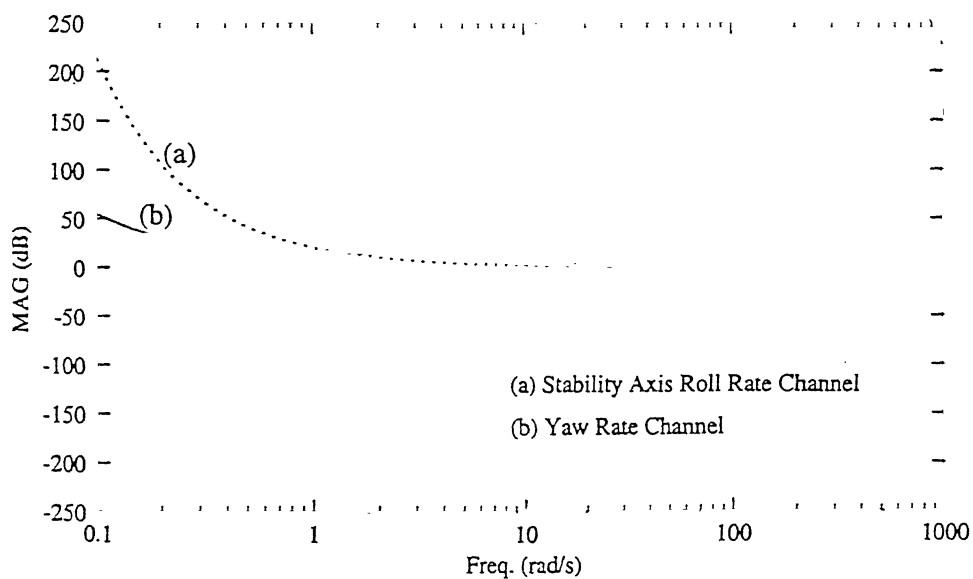


Figure 4.16(a) : Magnitude Plots for Stability Axis Roll Rate and Yaw Rate Channels

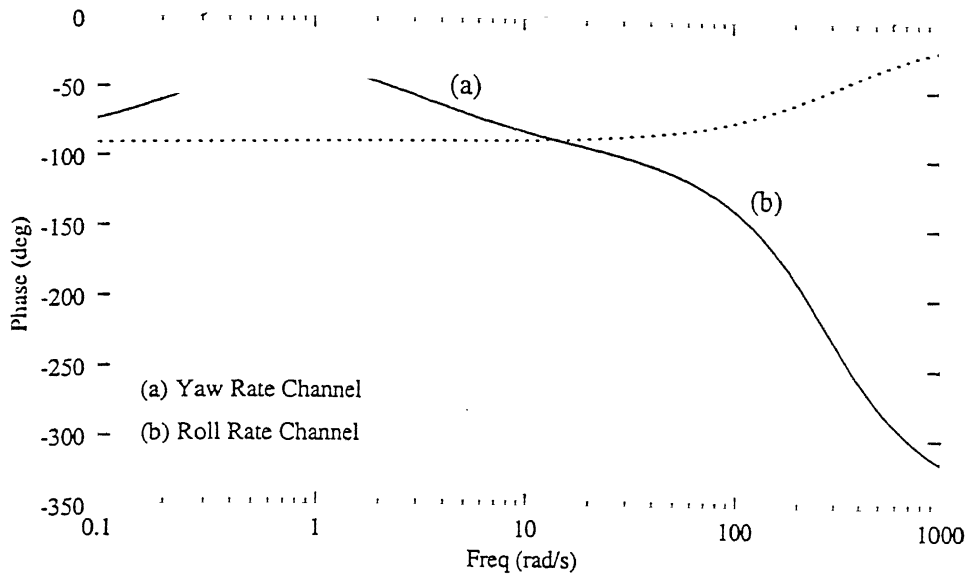


Figure 4.16(b) : Phase plots for Stability Axis Roll Rate Channel and Yaw Rate Channel

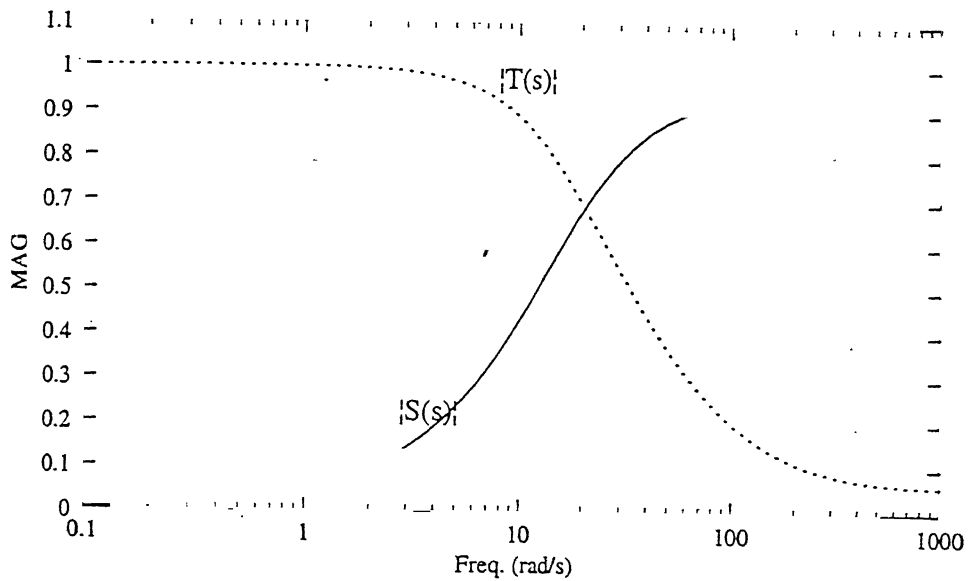


Figure 4.17 : Sensitivity and Complementary Sensitivity Functions for Roll Rate Channel at the Plant Output

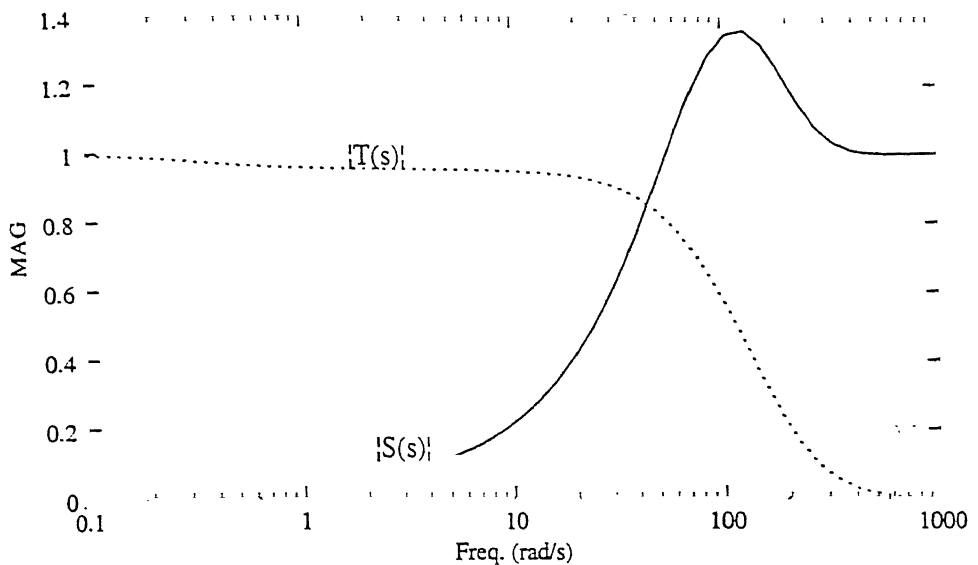


Figure 4.18 : Sensitivity and Complementary Sensitivity Functions for the Yaw Rate Channel at the Output of the Plant

stability axis roll rate due to 90 deg/s is shown in Fig.4.12. The sideslip response due to the initial condition is shown in the Fig.4.13. The Fig.4.14 shows the sideslip due to stability axis roll rate command of 90 deg/s. Fig.4.15 shows the sideslip due to roll rate command of 90 deg/s between 2.0 and 4.0 secs. The maximum sideslip is 1.9 deg.

Figs.4.16(a) and 4.16(b) show the Bode magnitude and phase plots for the stability axis roll rate and yaw rate channels with the loop broken at the output of the missile plant. Figs.4.17 and 4.18 show the gain characteristics of the sensitivity and complementary sensitivity functions for the roll rate and yaw rate channels, respectively, at the output of the plant.

The time domain and frequency domain performance specifications achieved with the designed autopilot are shown in Table 4.2. The maximum sideslip is 1.9 degrees.

4.8.3 Results and Discussion

Time domain and frequency domain performances for both the designs in Examples 1 and 2 are shown in the Tables 4.1 and 4.2, respectively. In Example 1, the design specifications have been reasonably achieved except overshoot, which is on higher side. High overshoot results due to limitation imposed by the RHP pole at 12.164 on time response and bandwidth. As pointed out by Middleton [76], the

Table 4.2
Time Domain and Frequency Domain Performance for the Body Axis Roll Rate and Yaw Rate (Example 2)

Channel	Rise Time (s)	Overshoot (%)	Settling Time (s)	Fin Deflection (deg)	Fin Rate (deg/s)	Gain Margin (dB)	Phase Margin (deg)	Gain Crossover Freq. (Hz)
Stability Axis Roll Rate	0.08	0.0	0.16	4.0	20.2	-6,+ ∞	± 93.442	3.3
Yaw Rate	0.08	0.0	0.16	2.5	10.6	-12.5,+14.3	± 71.884	7.1

Table 4.3
Tradeoff Among Rise Time, Overshoot and Bandwidth

t_r , sec	overshoot (%)	B.W. (rad/s)
0.02	14.37	115.0
0.03	23.43	76.67
0.04	34.0	57.5
0.06	60.43	38.33

overshoot, bandwidth, rise time and RHP pole location are restricted by the following two relations:

$$\text{overshoot} \geq \frac{1}{p \cdot t_r} [(p \cdot t_r - 1) e^{(p \cdot t_r)} + 1]$$

and,

$$t_r \omega_b = 2.3.$$

The second one is the empirical relation. The variation of the rise time, percentage overshoot and bandwidth are shown in the Table 4.3. At $p=12.164$, to have the rise time of 0.04 sec, the overshoot and bandwidth will be of the order of 34% and 57.5 rad/s, respectively. If the rise time is reduced, the lesser overshoot will be obtained but at the same time, the bandwidth will increase and vice versa. To reduce the overshoot at the cost of increased bandwidth is disadvantageous as it may excite high frequency modes of the missile dynamics and hence the robustness of the closed loop system against the neglected and mismodeled dynamics will reduce. On the other hand, since other time response specifications are good, the higher overshoot will not have significant effect.

As can be seen from the Table 4.2, the achieved performances in time and frequency domain in Example 2 are excellent. In this case, the overshoot does not occur. This is due to the fact that the design was attempted with real simple poles in LHP, and it worked out giving excellent results. The tracking response for stability axis roll rate is fast with the rise time of 0.08 sec and settling time of 0.16 sec.. Yaw rate response is also very fast which is required for turn coordination. Both the roll rate and yaw rate tracking responses have been independently achieved. The maximum sideslip is 1.9 degrees. With different sets of bounds and scalar weight factors, the wide variety of specifications can be achieved.

4.9 Conclusions

The design methodology developed in this Chapter, presents a systematic procedure of the autopilot design for the coupled roll-yaw dynamics for the stability axis roll rate command tracking, while keeping the sideslip small. The input-output decoupling has been achieved which facilitates stability axis roll rate command tracking

design with independent design of body axis roll rate and yaw rate channels. In other words, the stability axis roll rate command design can be achieved with varied capabilities in yaw maneuver. The design tradeoff has been achieved by varying the bounds on the performance functions and scalar weight factors during the design process. Therefore, the wide variety of design specifications can be achieved by suitably choosing the performance bounds and scalar weight factors. The SA algorithm proved to be very effective for optimization. Only one run of the algorithm was required to get the converged solutions.

Chapter 5

Robustness Analysis

5.1 Introduction

Primarily singular value and structured singular value analysis techniques [62,64-66] are the recent tools to evaluate the robustness of the feedback control systems.

Doyle [65] and Lehtomaki [66] developed singular value based robustness tests modeling uncertainties as a full single block matrix structure. If uncertainties are really unstructured and in this form, then these tests are not conservative. If the uncertainties occur in the system in a structured way, then the robustness tests produce conservative estimates of stability robustness.

In this Chapter the singular value based analysis techniques have been used to estimate the robustness of the autopilot designs in the Chapters 2, 3 and 4. The uncertainties modeled for the analysis include neglected actuator dynamics, mismodeled actuator dynamics and neglected sensor dynamics. These uncertainties are modeled as unstructured uncertainties.

5.2 Robustness Theory for Singular Value Based Analysis

The singular value based analysis for the unstructured uncertainty is based on the robustness theorems which are derived from an application of the multivariable Nyquist theorem [68]. The robustness problem using the multivariable Nyquist technique is to determine to what extent the parameters in the loop transfer matrix (LTM) can

•

vary without compromising the stability of the closed loop system. It is shown in [68] that

$$\det [I + L(s)] = \phi_{cl}(s) / \phi_{ol}(s) , \quad (5.1)$$

where $\phi_{cl}(s)$ and $\phi_{ol}(s)$ are open loop and closed loop characteristic polynomials, respectively.

The fundamental theorem of the robustness [62,66] is given below :

Theorem 1 [62,66]

The polynomial $\phi'_{cl}(s)$ has no closed right half plane zeros, and the perturbed feedback system is stable if the following holds :

(a) $\phi_{ol}(s)$ and $\phi'_{ol}(s)$ have the same number of closed right half plane zeros; $\phi_{cl}(s)$ has no closed right half plane zeros.

(b) $\det [I + L(s, \epsilon)] = 0, \forall (s, \epsilon) \text{ in } D_R \times [0, 1] \text{ and } \forall R \text{ sufficiently large,}$

where $\phi'_{ol}(s)$ and $\phi'_{cl}(s)$ are the polynomials $\phi_{ol}(s)$ and $\phi_{cl}(s)$ with uncertainties. $L(s, \epsilon)$ is the loop transfer function matrix with real coefficients which are continuous in ϵ for all ϵ such that $0 \leq \epsilon \leq 1$. D_R is Nyquist contour which encloses all closed right half plane zeros of $\phi_{ol}(s)$. $L(s, \epsilon)$ which satisfies

$$L(s, 0) = L(s) \quad (5.2)$$

and,

$$L(s, 1) = L'(s) \quad (5.3).$$

This theorem is used to develop the test for different types of model characterizations. The most common model error characterizations are additive errors and multiplicative errors.

Let $E(s)$ denote the modeling error under consideration. The additive model error is given by

$$E_a(s) = L'(s) - L(s) \quad (5.4)$$

and, the multiplicative model error is given by

$$E_m(s) = [L'(s) - L(s)] L^{-1}(s) \quad (5.5)$$

The perturbed LTM for additive errors is given by

$$L(s, \epsilon) = L(s) + \epsilon E_a(s) \quad (5.6)$$

and, the multiplicative error is given by

$$L(s, \epsilon) = [I + \epsilon E_m(s)] L(s) \quad (5.7)$$

The following are the stability robustness theorems for robustness analysis due to Lehtomaki [62,66]

Theorem 2 (for additive uncertainty model)

The polynomial $\phi'_{cl}(s)$ has no closed right half plane zeros and the perturbed feedback system is stable if the following holds:

- (i) $\phi_{cl}(s)$ has no closed right half plane zeros.
- (ii) $\underline{\sigma}[I + L(s)] \geq \overline{\sigma}[E_a(s)]$, $\forall s \in D_R$ and $\forall R$ sufficiently large, with $E_a(s)$ given by equation (5.4). $\underline{\sigma}(\cdot)$ and $\overline{\sigma}(\cdot)$ are smallest and largest singular values, respectively.

Theorem 3 (for multiplicative uncertainty model)

The polynomial $\phi'_{cl}(s)$ has no closed right half plane zeros, and the perturbed feedback system is stable if the following holds:

- (i) $\phi_{cl}(s)$ has no closed right half plane zeros.
- (ii) $\underline{\sigma}[I + L^{-1}(s)] > \overline{\sigma}[E_m(s)]$, $\forall s \in D_R$ and $\forall R$ sufficiently large, with $E_m(s)$ given by equation (5.5).

The proofs of the theorems 1 and 2 are available in [62,66]. These theorems provide sufficient tests of stability. As long as the singular value frequency responses do not overlap, the stability is guaranteed.

5.3 Autopilot Robustness Analysis

In this Section, the singular value based robustness theory is applied to the uncertainties due to neglected and mismodeled actuator dynamics, and neglected sensor dynamics. These uncertainties are modeled as unstructured multiplicative uncertainties. The autopilot sensitivity is analysed for the designs in Chapters 2, 3 and 4.

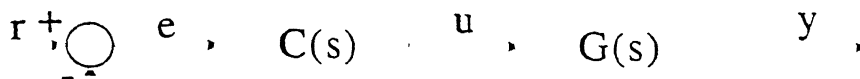


Figure 5.1 : Feedback Control System

5.3.1 Actuator Uncertainty Analysis

Here, the autopilot sensitivity is analysed for the neglected actuator dynamics and mismodeled actuator dynamics in respect of the designs in Chapters 2, 3 and 4.

5.3.1.1 Neglected Actuator Dynamics

Fig.5.1 shows the autopilot transfer function $C(s)$ and the uncertain missile dynamics $G(s)$. For the multiplicative plant uncertainty at the plant input, we have

$$G(s) = G_0(s) [I + E_m(s)] , \quad (5.8)$$

where $G_0(s)$ is the open loop transfer function matrix of the missile and $E_m(s)$ is the multiplicative uncertainty due to neglected actuator dynamics at the plant input. The loop transfer function at the plant input, for the true missile model is

$$L'(s) = C(s) G(s) [I + E_m(s)] , \quad (5.9)$$

and for the nominal design model is

$$L(s) = C(s) G(s). \quad (5.10)$$

Our aim is to study the robustness of the pitch and roll-yaw designs to neglected actuator dynamics. For this, the Theorem 3 of the Section 5.2 is applied. That is, the following relationship should hold for the stability robustness :

$$\underline{\sigma} [I + L^{-1}(s)] > \overline{\sigma} [E_m(s)], \quad (5.11)$$

with $L(s)$ given by the equation (5.10). This singular value based test is only sufficient condition for stability. As long as the singular value frequency responses of $\underline{\sigma} [I + L^{-1}(s)]$ and $\overline{\sigma} [E_m(s)]$ do not overlap, the stability is

guaranteed. The robustness test is applied here to find out the lowest actuator natural frequency of the actuator dynamics that guarantees stability.

Now the robustness test is applied to the longitudinal autopilot designs in Chapters 2 and 3, and the lateral autopilot design in Chapter 4.

5.3.1.1.1 Longitudinal Autopilot Design (Chapter 2)

The actuator in pitch dynamics is the elevator which is modeled as the second order transfer function. The multiplicative uncertainty created by neglecting the actuator dynamics is given by,

$$E_m(s) = \frac{\delta_e(s)}{\delta_{ec}(s)} - 1 = \frac{-s(s + 2\xi\omega_a)}{s^2 + 2\xi\omega_a s + \omega_a^2} \quad (5.12)$$

where $\xi = 0.6$ and ω_a is taken as the unknown actuator natural frequency. δ_e and δ_{ec} are elevator fin deflection and commanded elevator fin deflection, respectively. Here, $C(s) = [C_1(s) \ C_2(s) \ C_2(s)]$, where $C_1(s)$ and $C_2(s)$ are given by equations (2.26) and, (2.33), and $G(s)$ is given by equation (2.20), respectively, of the Chapter 2. The application of the equation (5.11) is shown in Fig.5.2. Three natural frequencies of actuator dynamics at $\omega_a = 2, 3.2$ and 5 rad/s are taken for the plots of $\bar{\sigma}[E_m(s)]$. The intersection of frequency response curves of $\underline{\sigma}[I + L^{-1}(s)]$ and $\bar{\sigma}[E_m(s)]$ violates the condition given by equation (5.11). It is evident from the Fig.5.2 that for $\omega_a = 3.2$ rad/s, $\bar{\sigma}[E_m(s)]$ curve is just touching $\underline{\sigma}[I + L^{-1}(s)]$ curve and for $\omega_a < 3.2$ rad/s the robustness condition is violated. This shows that the stability of the missile pitch control system is not guaranteed for the actuator natural frequencies below 3.2 rad/s.

5.3.1.1.2 Longitudinal Autopilot Design (Chapter 3)

The application of the robustness test for the neglected actuator dynamics, given by equation (5.11) is shown in Fig.5.3. $G(s)$ and $C(s)$ used here for the robustness analysis are the same as shown in Fig.3.2 of Chapter 3. $\bar{\sigma}[E_m(s)]$ is plotted for the four natural frequencies of actuator dynamics at $\omega_a = 2, 3.2, 5.0$ and 10 rad/s. For $\omega_a = 10$ rad/s, the stability of the missile control system is not guaranteed.

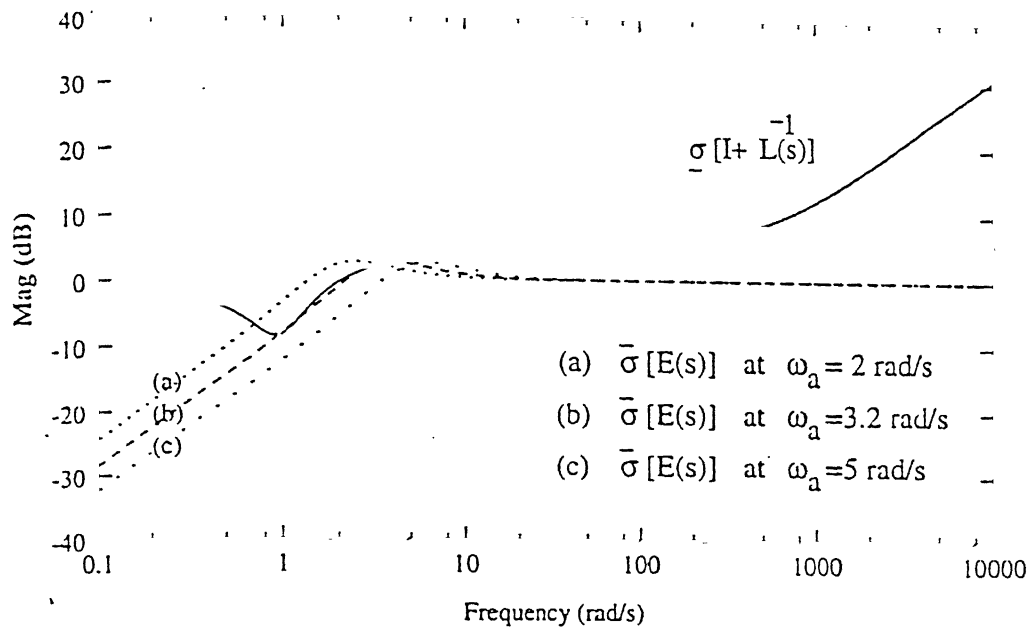


Figure 5.2 : Pitch Robustness to Neglected Actuator Dynamics in Chapter 2

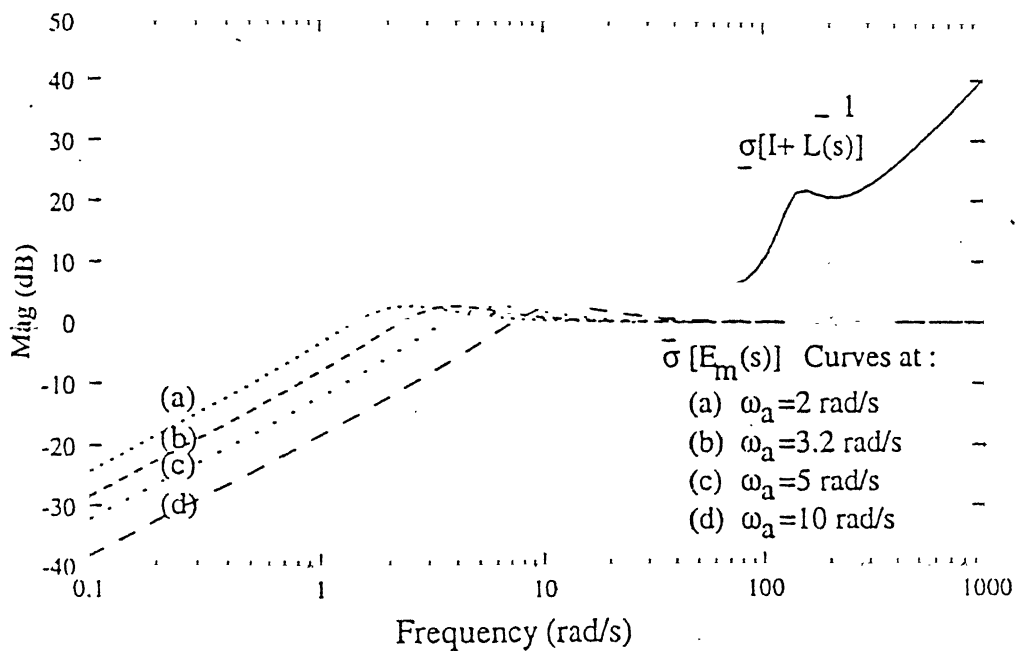


Figure 5.3 : Pitch Robustness to Neglected Actuator Dynamics in Chapter 3

5.3.1.1.3 Lateral Autopilot Design (Chapter 4)

The actuators in the lateral missile dynamics are aileron and rudder. The dynamics of the aileron and rudder is taken same as the elevator dynamics. Therefore, here the $E_m(s)$ is a 2×2 matrix with diagonal elements given by equation (5.12). Now, the robustness of the lateral autopilot designs in Examples 1 and 2 of Sections 4.8.1 and 4.8.2 is evaluated.

(a) Example 1

The application of the equation (5.11) for the neglected actuator dynamics is shown in Fig.5.4(a). $\bar{\sigma}[E_m(s)]$ is plotted for three natural frequencies of actuator dynamics at $\omega_a = 20, 60$ and 120 rad/s. It is clear from the Fig.5.4(a) that the missile control system in roll-yaw does not guarantee stability for the actuator natural frequencies below 20 rad/s.

(b) Example 2

Fig.5.4(b) shows the application of the equation (5.11) for the neglected actuator dynamics. It is clear from the Fig.5.4(b) that the missile control system in roll-yaw does not guarantee stability for the actuator natural frequencies below 60 rad/s. The missile model taken in this example has first order actuator with the natural frequency of 180 rad/s. Therefore, the robustness against the neglected actuator dynamics is good.

5.3.1.2 Mismodeled Actuator Dynamics

5.3.1.2.1 Longitudinal Autopilot Design (Chapter 2)

The natural frequency of the actuator dynamics is mismodeled by the relation $\omega_{true} = \varepsilon \omega_a$ [62]. Here, ω_a is the nominal actuator frequency and is assumed to

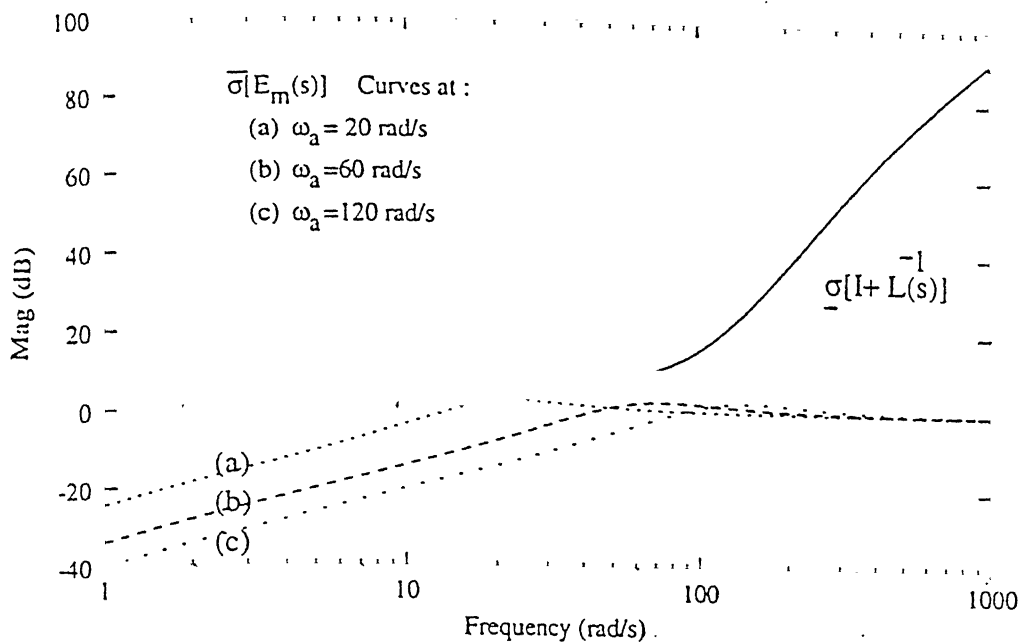


Figure 5.4(a) Roll-Yaw Robustness to Neglected Actuator Dynamics.

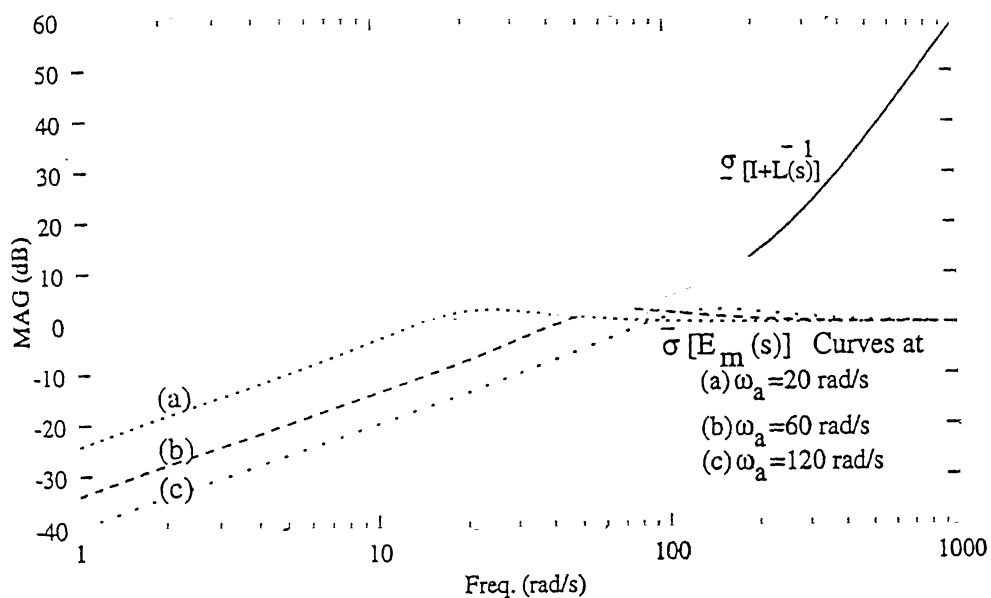


Figure 5.4(b) : Roll-Yaw Robustness to Neglected Actuator Dynamics
(Example 2)

be 67.8 rad/s. The multiplicative uncertainty model for the mismodeled dynamics is given by,

$$E_m(s) = \frac{-s[(1-\epsilon^2)s + 2\xi\omega_a\epsilon(1-\epsilon)]}{s^2 + 2\xi\omega_a\epsilon s + \omega_a^2\epsilon^2} \quad (5.13)$$

The Fig.5.5 shows the application of the robustness test given by equation (5.11). $\bar{\sigma}[E_m(s)]$ is plotted for four actuator frequencies at $\omega_{true} = 3.14, 12.56, 31.4$ and 62.8 rad/s. The stability robustness condition given by equation (5.11) is violated for $\omega_{true} < 3.14$ rad/s.

5.3.1.2.2 Longitudinal Autopilot Design (Chapter 3)

Fig.5.6 depicts the application of the condition given by equation (5.11). $\bar{\sigma}[E_m(s)]$ is plotted for the four actuator frequencies at $\omega_{true} = 6.28, 12.56, 31.4$ and 62.8 rad/s. The missile control system in the pitch does not guarantee stability against mismodeled actuator dynamics for the actuator natural frequencies below 6.28 rad/s.

5.3.1.2.3 Lateral Autopilot Design (Chapter 4)

(a) Example 1

Here, the $E_m(s)$ is a 2×2 matrix with the diagonal entries given by equation (5.13). Fig.5.7(a) displays the application of the stability robustness condition given by equation (5.11). $\bar{\sigma}[E_m(s)]$ is plotted for four frequencies at $\omega_{true} = 10, 20, 60$ and 120 rad/s. The stability robustness condition is violated for $\omega_{true} < 14$ rad/s.

(b) Example 2

Fig.5.7(b) shows the application of the stability robustness condition given by equation (5.11). $\bar{\sigma}[E_m(s)]$ is plotted for the four frequencies at $\omega_{true} = 10, 20, 60$

and 120 rad/s. The stability robustness condition is violated for $\omega_{true} < 55.2$ rad/s.

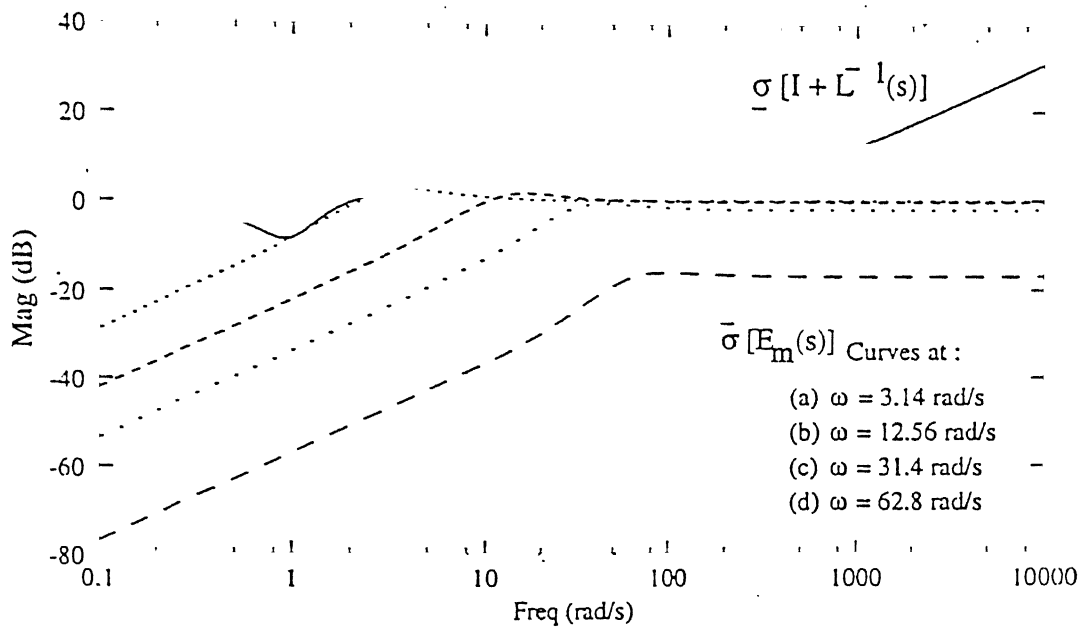


Figure 5.5 : Pitch Robustness to Mismatched Actuator Dynamics in Chapter 2

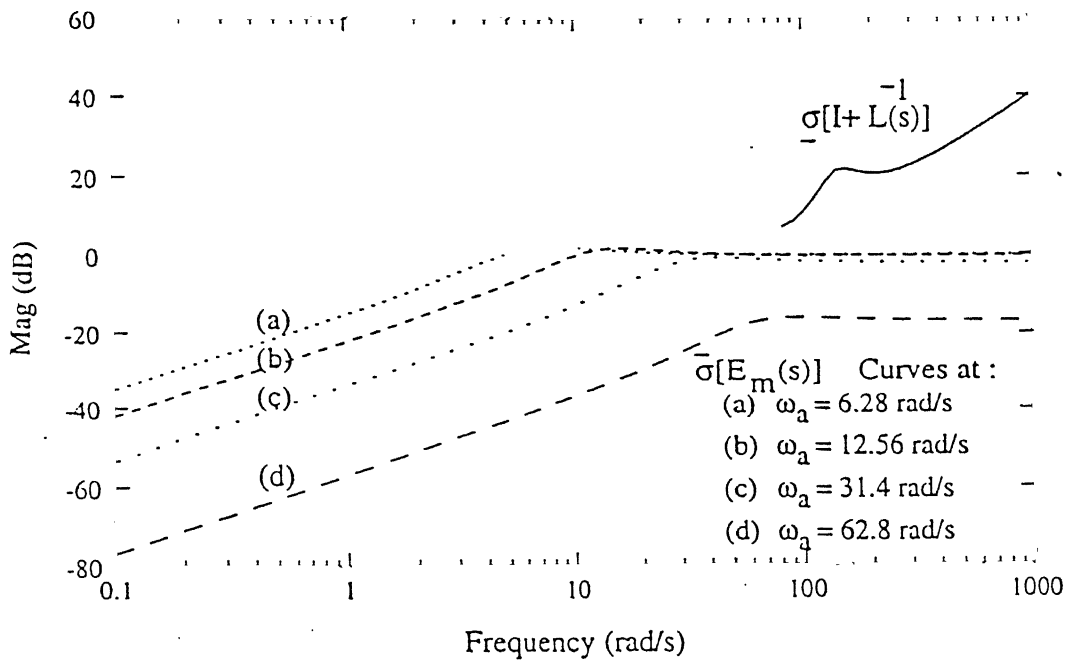


Figure 5.6 : Pitch Robustness to Mismatched Actuator Dynamics in Chapter 3

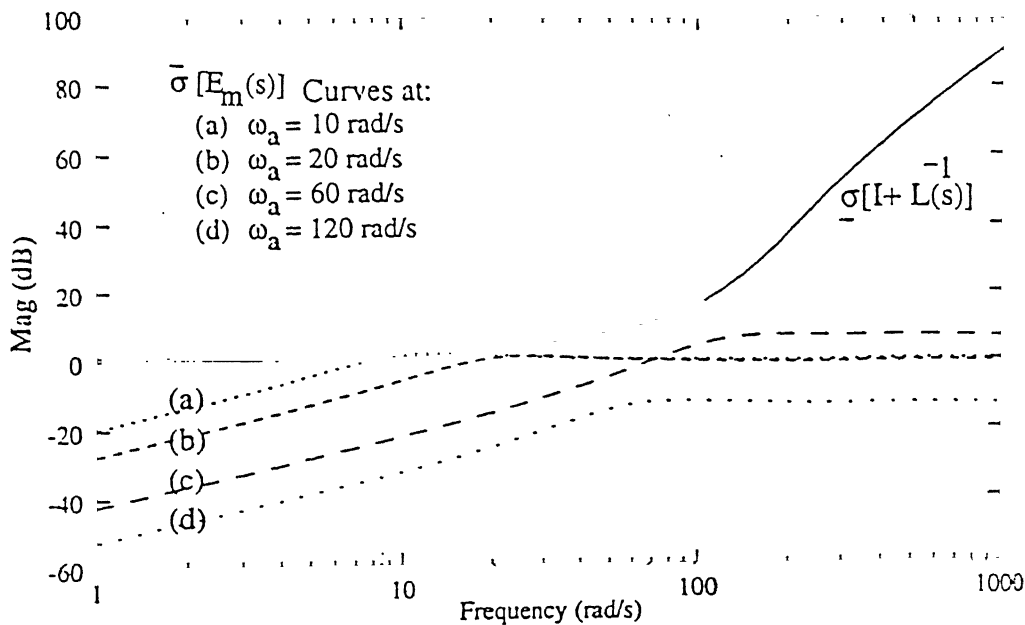
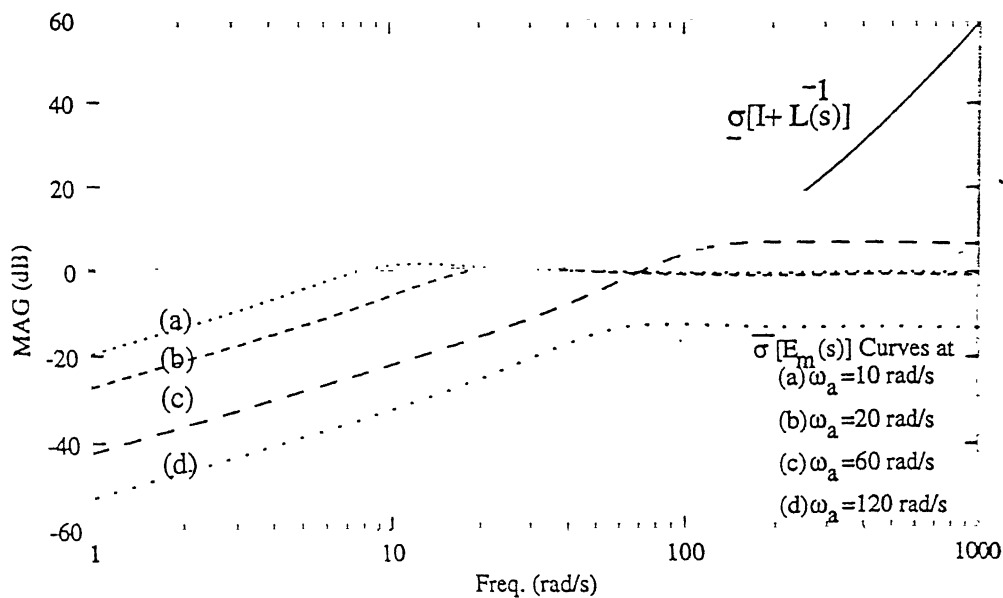


Figure 5.7(a) Roll-Yaw Robustness to Mismatched Actuator Dynamics


 Figure 5.7(b) : Roll-Yaw Robustness to Mismatched Actuator Dynamics
(Example 2)

This is good robustness against the mismodeled actuator, in this example, as the actuator model taken in the missile dynamics is of the first order with the natural frequency of 180 rad/s.

5.3.2 Sensor Uncertainty Analysis

The uncertainty due to neglected sensor dynamics is modeled as multiplicative uncertainty at the output of the plant.

5.3.2.1 Longitudinal Autopilot Design (Chapter 2)

The sensor dynamics has been neglected in the autopilot design. The accelerometer and the rate gyro are used for measuring the normal acceleration and pitch rate respectively. For the robustness analysis purpose, we model both the accelerometer and rate gyro dynamics using second order transfer function given by

$$\frac{\delta_s}{\delta_{sc}} = \frac{\omega_s^2}{s^2 + 2\xi_s \omega_s s + \omega_s^2}, \quad (5.14)$$

where δ_s and δ_{sc} are sensor (accelerometer, rate gyro) deflection and commanded deflection respectively. ω_s and ξ_s are the sensor natural frequency and damping ratio respectively. $\xi_s = 0.5$ and ω_s is taken as unknown sensor frequency. The sensitivity of the autopilot design is analysed by finding out the minimum natural frequency of the sensor dynamics violating robustness condition given by equation (5.11). In equation (5.11), the $L(s)$ becomes the loop transfer function with the loop broken at the output of the plant.

Here, the error due to the neglected sensor dynamics, both for accelerometer and rate gyro, is given by

$$E_{ms}(s) = \frac{-s(s + 2\xi_s \omega_s)}{s^2 + 2\xi_s \omega_s s + \omega_s^2} \quad (5.15)$$

The $E_{m1}(s)$ in equation (5.11) becomes a 2×2 matrix with the diagonal entries given by equation (5.15).

Fig.5.8 shows the application of the equation (5.11) for the robustness analysis due to the neglected sensor dynamics. $\overline{\sigma}[E_m(s)]$ is plotted for three sensor natural frequencies at $\omega_s = 40, 80$ and 200 rad/s.

As can be seen from the plots, the plots of $\overline{\sigma}[E_m(s)]$ for $\omega_s = 40$ and 80 rad/s intersect with $\underline{\sigma}[I+L^{-1}(s)]$ plot where as $\overline{\sigma}[E_m(s)]$ plot for $\omega_s = 200$ rad/s does not intersect. It has been found that below $\omega_s = 107.5$ rad/s, the plots of $\underline{\sigma}[I+L^{-1}(s)]$ and $\overline{\sigma}[E_m(s)]$ always intersect with each other and hence the missile control system in pitch does not guarantee stability against neglected sensor dynamics below sensor natural frequencies of 107.5 rad/s. The $\underline{\sigma}[I+L^{-1}(s)]$ curve does not look smooth. It is due to the fact that in the computation of $\underline{\sigma}[I+L^{-1}(s)]$, the poor condition number estimate was indicated.

5.3.2.2 Longitudinal Autopilot Design (Chapter 3)

Fig.5.9 depicts application of the equation (5.11) for the robustness analysis against neglected sensor dynamics. $\overline{\sigma}[E_m(s)]$ is plotted for three sensor natural frequencies at $\omega_s = 40, 80$ and 200 rad/s. The plot of $\overline{\sigma}[E_m(s)]$ for $\omega_s = 40$ and 80 rad/s intersect with the $\underline{\sigma}[I+L^{-1}(s)]$ plot whereas $\overline{\sigma}[E_m(s)]$ plot for $\omega_s = 200$ rad/s does not intersect. It has been found that intersection always takes place between $\overline{\sigma}[E_m(s)]$ and $\underline{\sigma}[I+L^{-1}(s)]$ below $\omega_s = 102.6$ rad/s. Hence, the robustness condition given by equation (5.11) is violated for $\omega_s = 102.6$ rad/s. Again, here also, in the computation of the $\underline{\sigma}[I+L^{-1}(s)]$, the poor condition number estimate was indicated.

5.3.2.3 Lateral Autopilot Design (Chapter 4)

The roll-yaw autopilot design in Chapter 4 uses body axis roll rate and yaw rate for the feedback. The sensors employed are rate gyros for both the roll and yaw channels. The dynamics of the roll rate gyro and yaw rate gyro are taken same as given in equation (5.14). Now, the robustness against the neglected sensor dynamics

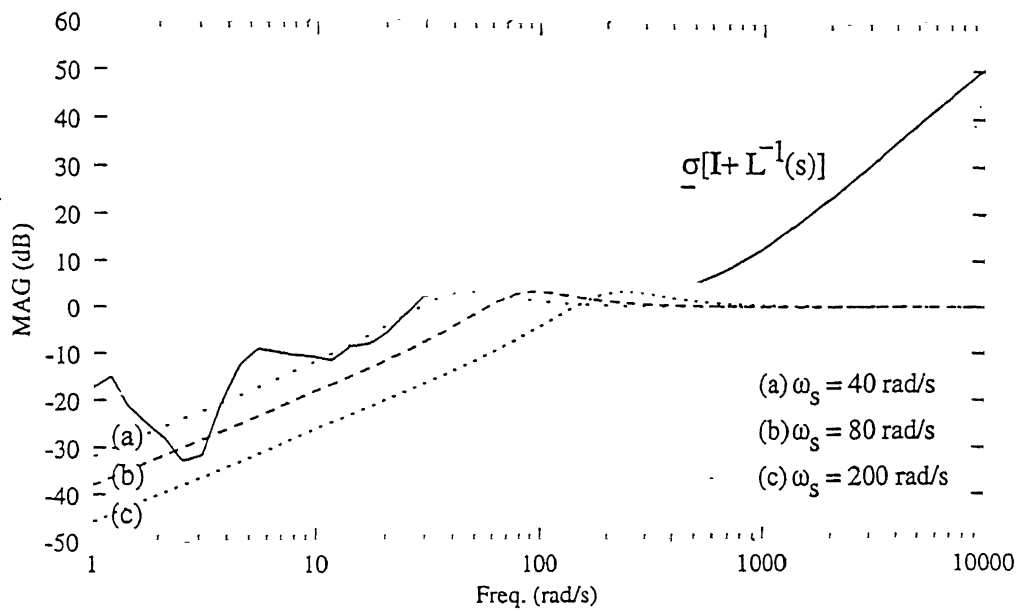


Figure 5.8 : Pitch Robustness to Neglected Sensor Dynamics in Chapter 2.

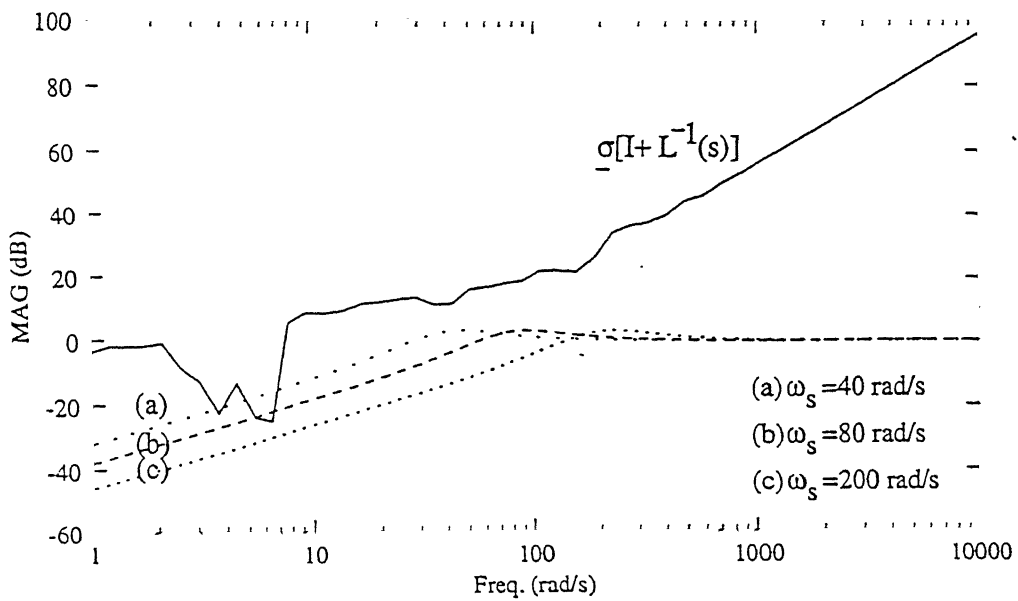


Figure 5.9 : Pitch Robustness to Neglected Sensor Dynamics in Chapter 3

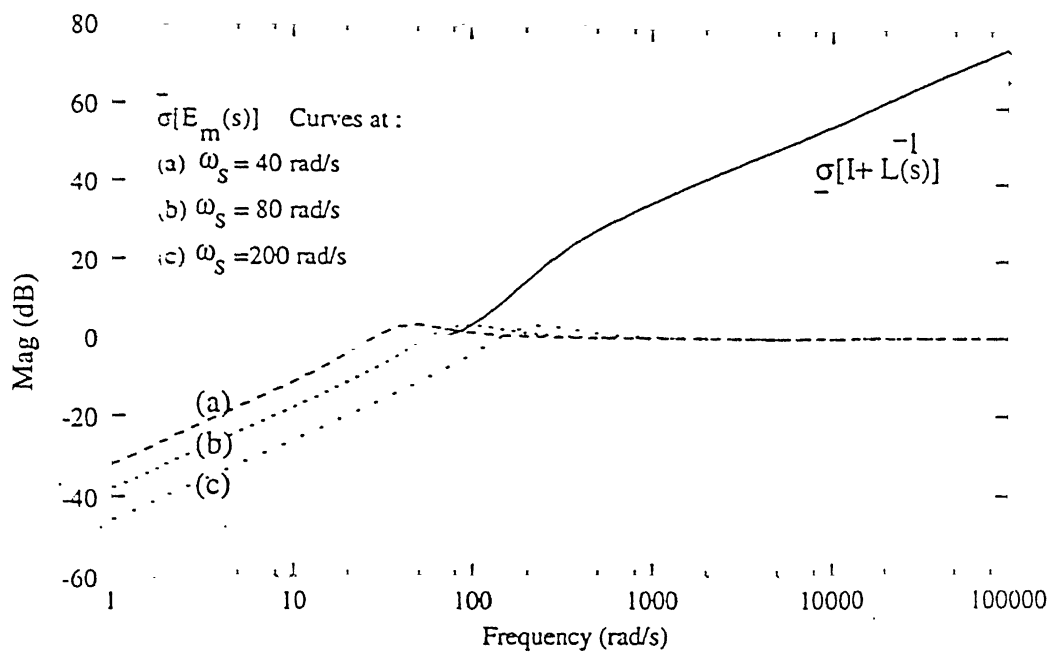


Figure 5.10 : Roll-Yaw Robustness to Neglected Sensor Dynamics for Example 1

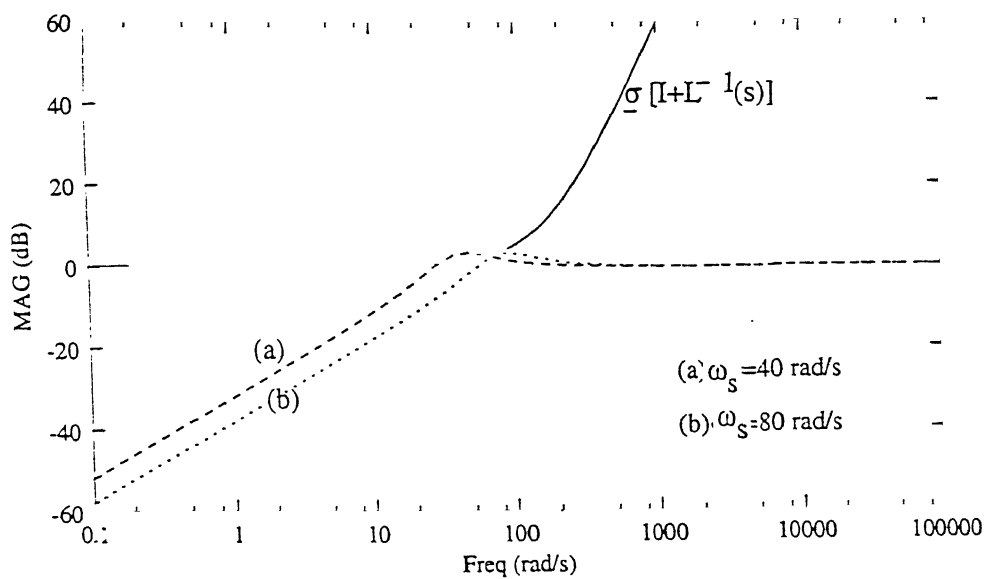


Figure 5.11 : Roll-Yaw Robustness to Neglected Sensor Dynamics for Example 2

is evaluated for the Examples 1 and 2 of the Sections 4.8.1 and 4.8.2.

(a) Example 1

The application of the stability robustness condition given by equation (5.11) is shown in Fig.5.10. $\bar{\sigma}[E_m(s)]$ is plotted for $\omega_s = 40, 80$ and 200 rad/s.

As is seen from the Fig.5.10, the $\bar{\sigma}[E_m(s)]$ and $\underline{\sigma}[I+L^{-1}(s)]$ plots intersect for $\omega_s=40$ and 80 rad/s while they do not overlap for $\omega_s=200$ rad/s. It has been found that intersection always occurs for $\omega_s = 95$ rad/s. Hence the lateral missile control system does not guarantee stability for the sensor frequencies below 95 rad/s.

(b) Example 2

The plots for $\underline{\sigma}[I+L^{-1}(s)]$ and $\bar{\sigma}[E_m(s)]$ are shown in Fig.5.11. $\bar{\sigma}[E_m(s)]$ is plotted for $\omega_s = 40$ and 80 rad/s. It is seen from the Fig.5.11 that $\bar{\sigma}[E_m(s)]$ curve at $\omega_s = 80$ rad/s intersects the $\underline{\sigma}[I+L^{-1}(s)]$ curve whereas $\bar{\sigma}[E_m(s)]$ curve at $\omega_s=40$ rad/s just touches. Therefore, the stability robustness condition is violated for the sensor frequencies below 40 rad/s.

5.3.3 Results and Discussions

The results for the singular value based robustness analysis are given in Table 5.1. It can be seen from the Table 5.1 that all the autopilot designs provide reasonably good stability robustness against neglected actuator dynamics and mismodeled actuator dynamics. The frequencies below which the robust stability is not guaranteed against the neglected actuator dynamics and mismodeled actuator dynamics for closed loop system in roll-yaw dynamics, for the Example 2 in the Section 4.8.2 of Chapter 4, are 60.0 and 55.2 , respectively. Though frequencies look higher in comparison with the corresponding frequencies in other designs but the natural frequency of the actuator used here is 180 rad/s. Thus, these are also the good results for robust stability against neglected and mismodeled actuator dynamics.

Table 5.1
Robustness Analysis Results

	Minimum Actuator Natural Frequency for Stability Against Neglected Actuator Dynamics (rad/s)	Minimum Actuator Natural Frequency for Stability Against Mismodeled Actuator Dynamics (rad/s)	Minimum Sensor Natural Frequency for Stability Against Neglected Sensor Dynamics (rad/s)
Longitudinal Autopilot Design (Chapter 2)	3.2	3.14	107.5
Longitudinal Autopilot Design (Chapter 3)	10.0	6.28	102.6
Lateral Autopilot Design (Chapter 4, Example 1)	20.0	14.0	94.8
Lateral Autopilot Design (Chapter 4, Example 2)	60.0	55.2	40.0

The results against neglected sensor dynamics are relatively poor. For the longitudinal autopilot designs in Chapters 2 and 3, for keeping the closed loop system stable in pitch, the minimum sensor natural frequencies should be more than 107.5 and 102.6 rad/s, respectively. In practice, the sensors are chosen with the natural frequencies higher than these values. For example, rate gyros selected for high performance missiles have natural frequencies of the order of 200 rad/s. But, still the margin available here is lesser than that for actuator natural frequencies. For the roll-yaw autopilot design, the minimum frequency for the sensor dynamics to guarantee stability are 95 rad/s and 40 rad/s for the Examples 1 and 2, respectively, which are reasonable.

5.4 Conclusions

The singular value based robustness analysis has been carried out to analyse the autopilot sensitivity to neglected and mismodeled actuator dynamics, and neglected sensor dynamics. These results, given in Table 5.1, show that all the autopilot

designs provide reasonably good stability robustness against neglected and mismodeled actuator dynamics. The results against neglected sensor dynamics are relatively poor for longitudinal autopilot designs in Chapters 2 and 3.

The reason for the poor results for the stability robustness against the neglected sensor dynamics for the longitudinal autopilot designs can be attributed to the fact that frequency loop shaping in the longitudinal autopilot designs has been carried out at the input of the plant. For improving the stability robustness against neglected sensor dynamics, the frequency loop shaping should be carried out at the output of the missile plant also.

Chapter 6

Conclusions

6.1 General

The bank-to-turn missiles are high performance missiles employed for air to air and air to ground applications. The BTT configuration taken for autopilot design in this thesis work is meant for air to ground applications. These missiles have to perform under changing and uncertain environments. This poses a challenging task for the autopilot design. The objective of the work reported in this thesis has been the parametric synthesis of the autopilot for BTT missile.

In this Chapter, the results obtained in the work reported in this thesis are reviewed and the contributions made are summarised. Suggestions for further scope of the work in this area are also indicated.

6.2 Review of The Work Done

In Chapter 2, the parametrized longitudinal autopilot has been designed using pole-zero assignment. The systematic design methodology and algorithms have been developed. The pitch dynamics form a SIMO system with one input and two measured outputs, namely normal acceleration and pitch rate. In the design methodology developed here, one loop has been designed at a time. The inner pitch rate loop has been designed for stabilization, damping and minimum control input whereas the outer acceleration loop has been designed for acceleration command tracking with specified gain and phase margins at the input of the missile plant. The control law

is based on the Youla parametrization of stabilizing controllers which facilitates incorporation of poles and zeros through the proper choice of the polynomials. The poles and zeros are selected solving a nonlinear optimization problem. The objective function includes the terms corresponding to command tracking error, overshoot, undershoot, gain and phase margins. The objective function is non-differentiable and has been solved using the direct search methods of Simplex search, Powell's conjugate direction and the Pattern search. The methodology developed, provides systematic synthesis procedure for the autopilot design in which the subjective judgement is minimized but the drawbacks are : (i) the order of the controller is high, and (ii) the conventional search methods used here, do not guarantee global optimum solution but only local optimum.

In Chapter 3, the longitudinal autopilot has been designed using parametrization of stabilizing controllers in two degrees of freedom configuration. The possible classes of stabilizing controllers and the desired characteristics are provided by the choice of two free parameters. The tracking performance depends on one parameter whereas the feedback properties depend on the other parameter. The parameter appearing in the tracking performance has been selected using closed loop model matching concept for the desired time domain performance. The parameter appearing in the feedback properties has been selected for the desired frequency loop shaping. The frequency loop shaping has been done at the input of the plant. The frequency domain loop shaping requirements for the autopilot have been expressed as the performance functions with hard bound constraints. These performance functions are related with the disturbance rejection over the bandwidth of the feedback system, stability robustness to plant uncertainty and the shapings of the sensitivity and complementary sensitivity functions. These performance functions with constraints have been used to pose the frequency loop shaping problem as constrained optimization problem which has been solved using the Simulated Annealing (SA) technique. For getting the desired frequency loop shaping, the bounds on the performance functions are tuned during optimization process. The SA technique has been found suitable for achieving optimal solutions. The design methodology and algorithm developed here provide systematic synthesis procedure but the order of the autopilot turns out to be high.

In Chapter 4, the lateral (roll-yaw) autopilot has been synthesized. The autopilot has been designed for the system to track the stability axis roll rate while keeping the sideslip minimum. The design methodology and algorithm are based on the control law which provides input-output decoupling and thus facilitates independent designs for roll rate and yaw rate channels. The design methodology developed here, facilitates the stability axis roll rate command tracking with varying capabilities in yaw. The control law also facilitates the assignment of poles and zeros through the selection of polynomials. The polynomials have been selected for the desired time domain and frequency domain responses. The time domain and frequency domain specifications have been defined as hard bound constraints on the time domain and frequency domain performance functions. The time domain performance functions are related with the tracking error, overshoot, control input and sideslip whereas the frequency domain performance functions are related with the disturbance rejection, robust stability and, sensitivity and complementary sensitivity functions. The frequency domain performance functions have been defined at the output channels of the roll-yaw missile plant. These performance functions have been used to pose the design problem as the weighted sum constrained optimization problem which has been solved using the Simulated Annealing technique. The order of the autopilot is high in this design methodology also.

In Chapter 5, the robustness analysis has been carried out using singular values for the designs in Chapters 2, 3 and 4. The uncertainty models considered are the neglected actuator dynamics, mismodeled actuator dynamics and the neglected sensor dynamics. These uncertainties have been modeled as multiplicative uncertainties. In the robustness analysis, the autopilot sensitivity due to the neglected actuator dynamics, mismodeled actuator dynamics and neglected sensor dynamics has been evaluated. The minimum actuator and sensor natural frequencies have been found out to guarantee the stability of the closed loop system.

In summary, the contributions of this thesis are as follows :

- (1) A systematic design methodology and algorithm have been developed for the parametric synthesis of longitudinal autopilot for a BTT missile using direct

search methods of nonlinear optimization. The autopilot has been designed taking one channel at a time.

(2) A two degrees of freedom longitudinal autopilot has been designed in which normal acceleration command tracking and feedback properties have been independently achieved. A systematic design algorithm has been developed to achieve the desired command tracking using closed loop model matching concept, and to achieve the desired frequency domain specifications using constrained optimization. The constrained optimization problem for the frequency response shaping has been solved using Simulated Annealing technique.

(3) A systematic design methodology and algorithm have been developed for the synthesis of input-output decoupled lateral (roll-yaw) autopilot for a BTT missile to track the stability axis roll rate command with minimum sideslip. The design methodology proposed, facilitates independent designs for the roll and yaw channels. In the design methodology proposed, various time domain and frequency domain specifications have been achieved by formulating the design problem as constrained optimization problem which has been solved using Simulated Annealing technique.

(4) Singular value based analysis has been used to investigate the stability robustness against the neglected actuator dynamics, mismodeled actuator dynamics and the neglected sensor dynamics. The minimum actuator and sensor natural frequencies have been found out to guarantee stability of the closed loop system.

6.3 Suggestions for Further Work

In continuation of the research work carried out and reported in this thesis, the following problems need further investigations.

(i) In all the three designs in Chapters 2, 3 and 4, the controller orders have come out to be high. The controller order reduction techniques may be applied to get the reduced order controllers.

(ii) In Chapters 2 and 3, the loop shaping has been carried out at the input of the plant whereas in Chapter 4, the loop shaping has been carried out at the output of the plant. The design algorithms may be modified to incorporate the loop

shaping at both the input and output channels of the plant to improve the time domain and frequency domain responses.

(iii) All the designs in the thesis have been carried out at one operating point. The feasibility of gain scheduling methods can be studied in the reported framework of the design.

Bibliography

- [1] J.R.Cloutier, J.H. Evers, and J.J. Feeley, "*Assessment of Air-to-Air Missile Guidance and control Technology*", IEEE Control Systems Magazine, Vol.9, No.6, pp. 27-34, October 1989.
- [2] P. Garnell, *Guided Weapon Control Systems*, 2nd Ed., Pergamon Press, 1980.
- [3] M.J. Kovach, T.R. Stevens, and A. Arrow, " *A Bank to Turn Autopilot Design for an Advanced Air-to-Air Interceptor*", Proc. AIAA GNC Conference, Monterey, C.A., pp.1346-1353, August 1987.
- [4] K.A. Wise, "*Maximising Performance and Stability Robustness in a Conventional Bank-to-Turn Missile Autopilot Design*", presented at AIAA Missile System, Missile Sc. Conf. Monterey, CA., November 1988.
- [5] F.W. Nesline, B.H. Wells and P. Zarchan, "*Combined Optimal/Classical Approach to Robust Missile Autopilot Design*", Journal of Guidance, Control and Dynamics, Vol.4, No.3, pp.316-323, May-June 1981.
- [6] D.E. Williams, B. Friedland and A.N. Madiwale, "*Modern Control Theory for Design of Autopilots for Bank-to-Turn Missiles*", Journal of Guidance, Control and Dynamics, Vol.10, No.4, pp.378-386, July-August 1987.
- [7] K.A. Wise, "*Bank to Turn Missile Autopilot Design using Loop Transfer Recovery*", Journal of Guidance, Control and Dynamics, Vol.13, No.1, pp. 145-152, January-February 1990.

- [8] C.L. Shephard and L.Valavani, " *Autopilot design for Bank to Turn Flight vehicles*", Proceedings of American Control Conference, Atlanta, G.A., June 1988.
- [9] J.A. Bossi, D.A. Hoskins and M.A. Langehough, " *Multivariable Autopilot Designs for a Bank to Turn Missile*", Proceedings of American Control Conference, Atlanta, GA, pp.567-572, June 1988.
- [10] C.F. Lin and S.P. Lee, " *Robust Missile Autopilot Design Using a Generalized singular Optimal Control Technique*", Journal of Guidance, Control and Dynamics, Vol.8, No.4, pp.498-507, July-August 1985.
- [11] R.E. Reichert, " *Dynamic Scheduling of Modern Robust Control Autopilot designs for Missiles*", IEEE Control Systems Magazine, Vol. 12, No.5, pp. 35-42, October 1992.
- [12] K.A. Wise, B.C. Mears, and K. Poola, " *Missile Autopilot Design Using H-infinity Optimal Control with mu-synthesis*", Proceedings of American Control Conference, San Diego, CA, pp. 2362-2367, May 1990.
- [13] K.A. Wise and T. Nguyen, " *Optimal Disturbance Rejection in Missile Autopilot Design Using Projective Controls*", IEEE Control Systems Magazine, Vol.12, No.5, pp. 43-49, October 1992.
- [14] K. Sobel and J.R. Cloutier, " *Eigen structure Assignment for the Extended Medium Range Air to Air Missile*", Journal of Guidance, Control and Dynamics, Vol. 15, No. 2, pp. 529-531, March-April 1992.
- [15] J.S. Shamma and J.R. Cloutier, " *Gain Scheduled Missile Autopilot Design Using Linear Parameter Varying Transformations*", Journal of Guidance, Control and Dynamics, Vol.16, No.2, pp.256-263, March-April 1993.

- [16] D.G. Benshabat and Y. Chait, "*Application of Quantitative Feedback Theory to a Class of Missiles*", Journal of Guidance, Control and Dynamics, Vol.16, No.1, pp.47-52, January-February 1993.
- [17] C.F. Lin, J.R. Cloutier and J.H. Evers, "*High Performance Robust Bank to Turn Missile Autopilot Design*", Journal of Guidance, Control and Dynamics, Vol. 18, No.1, pp. 46-53, January-February 1995.
- [18] J. Krause and G. Stein, "*General Adaptive Control Structures with Applications to Missiles*", Proceedings of American Control Conference, Atlanta, G.A. pp. 561-566, June 1988.
- [19] E.W. Kamen, T.E. Bullock, and C.H. Song, "*Adaptive Control Applied to Missile Autopilots*", Proceedings of American Control Conference, Atlanta, GA, June 1988.
- [20] W. A. Wolovich, *Linear Multivariable Systems*, Springer Verlag, New York, 1974.
- [21] T. Kailath, *Linear Systems*, Prentice Hall, Engle wood Cliffs, N.J, 1980.
- [22] C.T. Chen, *Linear System Theory and Design*, Holt, Rinehart and Wiston, New York, 1984.
- [23] K.J. Astrom, and B. Wittenmark, *Computer Controlled Systems*, Prentice Hall, Englewood Cliffs, NJ, 1990.
- [24] B. Bengtsson, "*Output Regulation and Internal Models: A Frequency Domain Approach*", Automatica, Vol.13, No.4, pp.333-345, 1977.
- [25] W.A. Wolovich, "*Multi purpose Controllers for Multivariable Systems*", IEEE Transactions on Automatic Control, Vol. AC-26, No.1, pp.162-170, 1981.
- [26] R. Saeks and J. Murray, "*Feedback System Design : the Tracking and Disturbance Rejection Problem*", IEEE Transactions on Automatic Control, Vol. AC-26, No.1, pp. 203-217, February 1981.

- [27] M.H. Tu and C.M. Lin, "*Synthesis of Pole-Zero Assignment Control Law with Minimum Control Input*", IEE Proceedings, Part D, Vol. 139, No. 3, pp. 291-295, May 1992.
- [28] B.D.O. Anderson and J.B. Moore, *Linear Optimal Control*, Prentice Hall, Englewood Cliffs, NJ, 1989.
- [29] D.C. Youla, J.J. Bongiorno and H.A. Jabr, "*Modern Wiener Hopf Design of Optimal Controllers, Part I : the Single Input-Output Case*", IEEE Transactions on Automatic Control, Vol. AC-21, No.1, pp. 3-13, February 1976.
- [30] C.A. Desoer, R.W. Liu, J. Murray and R. Sacks, "*Feedback System Design : The Fractional Representation Approach to Analysis and Synthesis*", IEEE Transactions on Automatic Control, Vol. AC-25, No. 3, pp. 399-412, June 1980.
- [31] J.S. Liu, K. Yuan and W.S. Lin, "*On Minimum Fuel Control of Affine Nonlinear Systems*", IEEE Transactions on Automatic Control, Vol. AC-34, No.7, pp.767-770, 1989.
- [32] J.M. Maciejowski, *Multivariable Feedback Design*, Addison Wesley, New York, 1990.
- [33] D. Graham and R.C. Lathrop, "*The Synthesis of Optimum Transient Response: Criteria and Standard Forms*", AIEE, Vol. 72, Part II, pp. 273-288, November 1953.
- [34] C.T. Chen, *Control System Design : Conventional, Algebraic and Optimal Methods*, Stony Brook, NY, Pond Woods Press, 1987.

- [35] A. Nassirharand and A. Patwardhan, "*Parametric Synthesis of SISO Automatic Control Systems*", Computer Aided Design, Vol. 22, No. 5, pp. 301-307, June 1990.
- [36] J.A. Nelder and R. Mead, "*A Simplex Method for Function Minimization*", Computer Journal, Vol.7, pp. 308-313, 1965.
- [37] W.H. Press, S.A. Teukolsky, W.T. Vetterling and B.P. Flannery, Numerical Recipes in FORTRAN, Second Edition, Cambridge University Press, 1993.
- [38] K. Deb, Optimization for Engineering Design: Algorithms and Examples, Prentice Hall of India Pvt.Ltd, New Delhi, 1995.
- [39] S.S.L. Chang, Synthesis of Optimum Control Systems, New York, PA, Maple Press, 1961.
- [40] I Horowitz, Synthesis of Feedback Systems, New York: Academic, 1963.
- [41] C.A. Desoer and C.L. Gustafson, "*Algebraic Theory of Linear Multivariable Feedback Systems*", IEEE Transactions on Automatic Control, Vol. AC-29, pp. 909-917, 1984.
- [42] S. Hara, "*Parametrization of Stabilizing Controllers for Multivariable Servo Systems with Two Degrees of Freedom*", International Journal of Control, Vol. 45, No.3, pp.779-790, 1987.
- [43] T. Yoshikawa, T. Sujie and H. Hanafusa, "*General Solution of Robust Tracking Problem in Two-Degree-of-Freedom Control System*", IEEE Transactions on Automatic Control, Vol.AC-31, No.6, pp.552-554, June 1986.
- [44] M. Vidyasagar, Control System Synthesis: A Factorization Approach, Cambridge, MA, M.I.T. Press, 1985.
- [45] L.R. Pujara, "*Computer Aided Control Systems Design Technique with Applications to Aircraft Flying Qualities*", Journal of Guidance, Control and Dynamics, Vol. 11, No. 5, pp. 250-255, May-June 1988.

- [46] A. Nassirharand, "*Factorization Approach to Control System Synthesis*", Journal of Guidance, Control and dynamics, Vol. 16, No.2, pp. 402 March-April 1993.
- [47] B.A. Francis and J.C. Doyle, "*Linear Control Theory with an H_∞ Optimality Criterion*", SIAM Journal of Control and Optimization, Vol. No. 4, pp.815-844, 1987.
- [48] H. Kwakernak, "*Minimax Frequency Domain Performance and Robust Optimization of Linear Feedback Systems*", IEEE Transactions on Automatic Control, Vol.AC-30, No.10, pp.994-1004, 1985.
- [49] E. Polak and S.E. Salcudean, "On the Design of Linear Multivariable Feedback Systems Via Constrained Nondifferentiable Optimization in H_∞ Spaces", IEEE Transactions on Automatic Control, Vol.34, No. 3, pp. 268-276, March 1989.
- [50] S.P. Boyd and C.H. Barrat, Linear Controller Design: Limits of Performance Prentice Hall, Englewood Cliffs, New Jersey, 1991.
- [51] S.P. Boyd, C.H. Barrat and S. Norman, "*Linear Controller Design : Limits of Performance Via Convex Optimization*", Proceedings of IEEE, Vol. 78, No. 3, pp. 529-573, March 1990.
- [52] A. Corana, M. Marchesi, C. Martini and S. Ridella, "*Minimizing Multimodal Functions of Continuous Variables with the 'Simulated Annealing' Algorithm*", ACM Transactions on Mathematical Software, Vol. 13, No. 3, pp. 262-280, September 1987.
- [53] J.S. Freudenberg and D.P. Looze, Frequency Domain Properties of Scalar and Multivariable Feedback Systems, Springer-Verlag, Berlin, 1987.

- [63] A.W. Goffe, N.R. Ferrier and D.J. Rogers, "*Global Optimization of Statistical Functions with Simulated Annealing*", Journal of Econometrics, Vol. 60, No. 1/2, pp. 65-100, January-February 1994.
- [64] B.D.O. Anderson and J.B. Moore, Optimal Control : Linear Quadratic Methods, Prentice-Hall of India Private Limited, New Delhi, 1991.
- [65] J.C. Doyle, "*Robustness of Multiloop Linear Feedback Systems*", Proceedings of the IEEE Conference on Decision and Control, Institution of Electrical and Electronics Engineers, Piscataway, NJ, pp. 12-18, 1978.
- [66] N.A. Lehtomaki, "*Practical Robustness Measures in Multivariable Control System Analysis*", Ph.D. Dissertation, M.I.T., Cambridge, M.A., 1981.
- [67] N.A. Lehtomaki, N.R. Sandel, Jr., and M. Athans, "*Robustness Results in Linear Quadratic Gaussian Based Multivariable Control Designs*", IEEE Transactions on Automatic Control, Vol. AC-26, No. 1, pp. 75-92, February 1981.
- [68] Postlethwaite and A.G.J. MacFarlane, A Complex Variable Approach to the Analysis of Linear Multivariable Feedback Systems, Springer-Verlag, New York, 1979.
- [69] P. Apkarian, J.M. Biannic and P. Gahinet, "*Self-scheduled H-infinity Control of Missile Via Linear Matrix Inequalities*", Journal of Guidance, Control and Dynamics, Vol. 18, No. 3, pp. 532-538, May-June 1995.
- [70] H.J. Gratt and W.L. Mc Cowan, "*Feedback Linearization Autopilot Design for Advanced Kinetic Energy Missile Boost Phase*", Journal of Guidance, Control and Dynamics, Vol. 18, No. 5, pp. 945-950, September-October 1995.

- [71] K.A. Wise and J.L. Sedwick, "*Nonlinear H-infinity Optimal Control for Agile Missiles*", Journal of Guidance, Control and Dynamics, Vol. 19, No. 1, January-February, 1996.
- [72] L.H. Carter and J.S. Shamma, "*Gain-Scheduled Bank to Turn Autopilot Design Using Linear Parameter Varying Transformations*", Journal of Guidance, Control and Dynamics, Vol. 19, No. 5, pp. 1056-1063, September-October 1996.
- [73] Li-Chen Fu, Wei-Der Chiang, Jung-Hua Yang and Te-son Kuo, "*Adaptive Robust Bank-to-Turn Missile Autopilot Design using Neural Networks*", Journal of Guidance, Control and Dynamics, Vol. 20, No.2, pp. 346-354, March-April 1997.
- [74] J. Jim Zhu and M. Christopher Mickle, "*Missile Autopilot Design using a New Linear Time Varying Control Technique*", Journal of Guidance, Control and Dynamics, Vol. 20, No. 1, pp. 150-157, January-February 1997.
- [75] Z.J. Geng and Clair L. Mc Cullough, "*Missile Control Using Fuzzy Cerebellar Model Arithmetic Computer Neural Networks*", Journal of Guidance, Control and Dynamics, Vol. 20, No. 3, pp. 557-565, May-June 1997.
- [76] R.H. Middleton, "*Tradeoffs in Linear Control System Design*", Automatica, Vol. 27, No. 2, pp. 281-292, 1991.

Appendix 1

Missile Dynamics

The dynamics of a missile is described by a set of three force equations along x, y and z directions and three moment equations about x, y and z axis. This forms a set of nonlinear coupled equations. For a BTT missile, as shown in Fig.1.1 of Chapter 1, the coupling is more prominent due to asymmetric nature of the airframe configuration. The nonlinear equations are linearized in order to form a linear time invariant (LTI) model. The linearized model so obtained is used for the design of LTI autopilot.

Linearized missile dynamics for a kind of BTT missile shown in Fig. 1.1 is taken from [7] and is described in the following.

Fig. 1.1 displays a highly asymmetric BTT missile configuration. Aerodynamic analysis of this airframe configuration shows that very strong roll-yaw coupling is present. Large roll rates are induced by sideslip angle created primarily by the asymmetry of the vehicle. For this reason, the linearized pitch dynamics are separated from linear coupled roll-yaw dynamics. The resulting autopilot design consists of a longitudinal pitch acceleration command autopilot and a lateral roll-yaw autopilot in which a roll rate about the velocity vector is commanded.

The important variables defined in the Fig.1.1 are (p, q, r) which are body axis roll, pitch and yaw angular rates, respectively; (ϕ, θ, ψ) are integrals of (p, q, r) ; α is the angle of attack; and β is the sideslip angle. The LTI flight control design equations

are formed by linearizing the nonlinear aerodynamic equations of the motion about a trim condition.

The pitch LTI flight control equations are :

$$\dot{\alpha} = Z_{\alpha} \cdot \alpha + Z_{\delta} \cdot \delta_e + q \quad (\text{A1.1})$$

$$\dot{q} = M_{\alpha} \cdot \alpha + M_{\delta} \cdot \delta_e \quad (\text{A1.2})$$

$$\dot{\delta}_e = -2 \xi \omega \dot{\delta}_e - \omega^2 \delta_e + \omega^2 \delta_{ec} \quad (\text{A1.3})$$

The measurements that are available from the inertial measurement unit are normal acceleration $A_z = VZ_{\alpha} \cdot \alpha + VZ_{\delta} \cdot \delta_e$ and pitch rate q (rad/s). The scalar control input $u = \delta_{ec}$ (rad) is the elevator fin angle command. V , ξ and ω are the missile velocity, actuator (elevator) damping and natural frequency respectively.

The variables Z_{α} , Z_{δ} , M_{α} and M_{δ} are the dimensional aerodynamic stability derivatives derived from aerodynamic measurements (wind tunnel) of lift and pitching moment.

The LTI roll-yaw flight control equations are

$$\dot{\beta} = p \sin(\alpha) - r \cos(\alpha) + Y_{\beta} \cdot \beta + Y_{\delta a} \cdot \delta_a + Y_{\delta r} \cdot \delta_r \quad (\text{A1.4})$$

$$\dot{p} = L_{\beta} \cdot \beta + L_{\delta a} \cdot \delta_a + L_{\delta r} \cdot \delta_r \quad (\text{A1.5})$$

$$\dot{r} = N_{\beta} \cdot \beta + N_{\delta a} \cdot \delta_a + N_{\delta r} \cdot \delta_r \quad (\text{A1.6})$$

$$\ddot{\delta}_a = -2 \xi \omega \cdot \dot{\delta}_a - \omega^2 \delta_a + \omega^2 \delta_{ac} \quad (\text{A1.7})$$

$$\ddot{\delta}_r = -2 \xi \omega \dot{\delta}_r - \omega^2 \delta_r + \omega^2 \delta_{rc} \quad (\text{A1.8})$$

The variables Y_{β} , $Y_{\delta a}$, $Y_{\delta r}$, L_{β} , $L_{\delta a}$, $L_{\delta r}$, N_{β} , $N_{\delta a}$ and $N_{\delta r}$ are dimensional aerodynamic stability derivatives derived from aerodynamic measurements of lateral side force and, roll and yaw moments. Equations (A1.7) and (A1.8) describe the actuator dynamics for aileron and rudder fins. δ_a and δ_r are aileron and rudder fin deflections respectively.

The stability axis coordinate system is defined as the transformation of body axes to the stability axes using angle of attack (α). Wind axis coordinate system is defined as the transformation of stability axes to wind axes using sideslip β . The missile velocity vector is pointed along the x -axis of the wind coordinate system, as shown in Fig. 1.1. In a BTT autopilot, induced sideslip is minimized by rolling the missile about the velocity vector. Assuming that β is very small, this is a rotation

about the x-axis in the stability axis coordinate system. Thus the commanded roll rate is the stability axis roll rate p_s , ie.

$$p_s = p \cos (\alpha) + r \sin (\alpha) \quad (\text{A1.9})$$

Appendix 2

Parametrization of Stabilizing Controllers with Two Degrees of Freedom

A2(a) Servo Problem And Solvability Condition

The system shown in Fig. 3.1 is said to be a servo system if the following two conditions are satisfied [42] :

- (i) Internal stability, meaning BIBO stability of the feedback system , ie.

$$H(G, C) \stackrel{d}{=} \begin{bmatrix} (I + GC)^{-1} & -G(I + CG)^{-1} \\ C(I + GC)^{-1} & (I + CG)^{-1} \end{bmatrix} \in R_- \quad (A2.1)$$

We say that the pair $H(G, C)$ is stable and that C stabilizes G if equation (A2.1) holds ie. all the transfer function matrices of matrix $H(G, C)$ are stable rational matrices.

- (ii) Output regulation, meaning BIBO stability of the system with input r_0 and output e , ie.

$$H_{ero}(s) \stackrel{d}{=} \begin{bmatrix} I + M(I + PC_2)^{-1} PC_1 \end{bmatrix}^{-1} R \in R_- \quad (A2.2)$$

The controller achieving these two properties is called the servo controller and the servo problem (P, M, R) is said to be solvable if such a controller exists.

Let

$$P = \begin{bmatrix} P_1 \\ P_2 \end{bmatrix} \begin{matrix} p \\ q-p \end{matrix} = ND^{-1} = \begin{bmatrix} N_1 \\ N_2 \end{bmatrix} D^{-1} \quad (A2.3)$$

$$= \tilde{D}^{-1} \tilde{N} = \begin{bmatrix} \tilde{D}_1 & \tilde{D}_2 \\ p & q-p \end{bmatrix} \tilde{N} \quad (\text{A2.4})$$

be a right coprime factorization (r.c.f) and a left coprime factorization (l.c.f.) respectively, of the plant and let $R = \alpha I = \psi \phi^{-1} I$ be a coprime factorization with $\phi(s) \neq 0$ for $s \in C^- \stackrel{d}{=} \{s : \text{Re } s < 0\}$. The condition for solvability of the servo problem (P, M, R) given in [42] as theorem 1 is reproduced below as Lemma without proof :

Lemma A2.1

The servo problem (P, M, R) is solvable if and only if

$$N_1 \text{ and } \phi I_p \text{ are left coprime} \quad (\text{A2.5})$$

or equivalently.

$$[\tilde{N} \ \tilde{D}_2] \text{ and } \phi I_q \text{ are left coprime} \quad (\text{A2.6})$$

A 2(b) The Class of Stabilizing Controllers

This section gives two lemmas drawn from [42] for the servo system shown in Fig. 3.2 which contains the internal model $I/\phi(s)$ for the reference command at error channel. These two lemmas stated below without proof give the coprime factorization of $G_e(s)$ and

$$P_\phi(s) \stackrel{d}{=} \begin{bmatrix} P_1(s) / \phi(s) \\ P_2(s) \end{bmatrix} \quad (\text{A2.7})$$

Lemma A2.2

Suppose that l.c.f. of $P(s)$ is represented by equation (A2.4) and that the condition (A2.5) or (A2.6) holds, then

$$G_e = \tilde{D}_e^{-1} \tilde{N}_e = \begin{bmatrix} \phi I - M^{-1} & 0 \\ 0 & \tilde{D} \end{bmatrix} \begin{bmatrix} \tilde{N} \end{bmatrix} \quad (\text{A2.8})$$

and

$$P_\phi = \tilde{D}_\phi^{-1} \tilde{N}_\phi = \begin{bmatrix} \phi \tilde{D}_1 & \tilde{D}_2 \end{bmatrix}^{-1} \tilde{N} \quad \text{are l.c.f.} \quad (\text{A2.9})$$

Lemma A2.3

Suppose that an r.c.f of $P(s)$ is represented by (A 2.3) and that $N_1(s)/\phi(s)$ has an r.c.f. of

$$N_1/\phi = \hat{N} \hat{D}^{-1} \quad (\text{A2.10})$$

then

$$G_e = N_e D_e^{-1} = \begin{bmatrix} \hat{N} \\ N_2 \hat{D} \end{bmatrix} (\phi \hat{N} \quad (D \hat{D})^{-1})^{-1} \quad (\text{A2.11})$$

and

$$P_\phi = N_\phi D_\phi^{-1} = \begin{bmatrix} \hat{N} \\ N_2 \hat{D} \end{bmatrix} (\phi \hat{N} \quad (D \hat{D})^{-1})^{-1} \quad (\text{A2.12})$$

are r.c.f of G_e and P_ϕ under the assumption of (A2.5) or (A2.6).

The above two lemmas A2.2 and A2.3 give the possible classes of servo controllers and attainable characteristics stated in Lemma 3.1 of Chapter 3. The proofs of all above stated lemmas are available in [42].

Appendix 3

Fundamental Relations of Sensitivity And Complementary Sensitivity Functions

Fig.3.3, which is redrawn from Fig.3.1 in the standard form [32], including disturbance signal vector $d(s)$ and measurement noise vector $m(s)$. Other notations are defined in Section 3.2.2 with reference to Fig.3.1 of Chapter 3.

From the Fig.3.3 we see that

$$y(s) = d(s) + G(s) C(s) [r(s) - m(s) - y(s)] \quad (\text{A3.1})$$

Hence,

$$[I + G(s) C(s)] y(s) = d(s) + G(s) C(s) [r(s) - m(s)] \quad (\text{A3.2})$$

or

$$y(s) = [I + G(s) C(s)]^{-1} \{d(s) + G(s) C(s) [r(s) - m(s)]\} \quad (\text{A3.3})$$

Output sensitivity and complementary sensitivity functions are defined as

$$S_0(s) = [I + G(s) C(s)]^{-1} \quad (\text{A3.4})$$

and

$$T_0(s) = [I + G(s) C(s)]^{-1} G(s) C(s) \quad , \quad (\text{A3.5})$$

respectively. (

Then equation (A3.3) can be written as

$$y(s) = S_0(s) d(s) + T_0(s) [r(s) - m(s)] \quad (\text{A3.6})$$

From the Fig.3.3 we see that

$$u(s) = C(s) [r(s) - m(s) - d(s) - G(s) u(s)] \quad . \quad (\text{A3.7})$$

Hence,

$$[I + C(s) G(s)] u(s) = C(s) [r(s) - m(s) - d(s)] . \quad (\text{A3.8})$$

The input sensitivity function, $S_i(s)$, and input complementary sensitivity function $T_i(s)$, are defined as

$$S_i(s) = [I + C(s) G(s)]^{-1} \quad (\text{A3.9})$$

and

$$T_i(s) = C(s) G(s) [I + C(s) G(s)]^{-1} \quad (\text{A3.10})$$

Then equation (A 3.8) can be written as

$$u(s) = S_i(s) C(s) [r(s) - m(s) - d(s)] \quad (\text{A3.11})$$

From equations (A3.4), (A3.5), (A3.9) and (A3.10), the following two relations are obtained :

$$T_i(s) + S_i(s) = I \quad (\text{A3.12})$$

$$T_0(s) + S_0(s) = I \quad (\text{A3.13})$$

Dropping the suffix, in general, we can write

$$T(s) + S(s) = I \quad (\text{A3.14})$$

From the equations (A3.3) and (A3.11) we see that for disturbance attenuation and for the output to be insensitive to the measurement noises, it is needed that both $S(s)$ and $T(s)$ should be small in some sense. However, equation (A3.14) implies that both $S(s)$ and $T(s)$ cannot be made small simultaneously, if $T(s)$ is made nearly zero, then $S(s)$ becomes nearly identity. On the other hand, if $S(s)$ is made nearly zero, then $T(s)$ becomes almost identity. Thus we have an unavoidable trade off between the attenuating disturbances and filtering out the measurement noises. This trade off is one of the factors which make the feedback design difficult. The equation (A3.14) is called fundamental relation between sensitivity and complementary sensitivity functions in feedback control.

Appendix 4

Simulated Annealing

A4(a) Introduction

The SA optimization algorithm can be considered analogous to the physical process by which a material changes state while minimising its energy [52]. A slow careful cooling brings the material to a highly ordered crystalline state of lowest energy. A rapid cooling instead yields defects and glass like intrusions inside the material.

From optimization point of view, an iterative search accepting only new points with lower function values is like rapidly quenching a physical system at zero temperature. It is very likely to get stuck in a metastable local minimum. On the contrary, SA permits uphill moves under the control of a temperature parameter. At higher temperature only the gross behaviour of the cost function is relevant to the search. As temperature decreases finer details can be developed to get a good final point.

The SA method is based on the random evaluations in such a way that transitions out of a local minimum are possible. This method is able to discriminate between "gross behaviour" of the function and finer "wrinkles". First, it reaches an area in the function domain where a global minimum should be present, following the gross behaviour irrespectively of small local minima found on the way. It then develops

finer details, finding a good, near optimal local minima, if not the global minimum itself. The details of SA algorithm in the following sections are drawn from [52].

A4(b) Method

Let \bar{X} be a vector in R^n and (x_1, x_2, \dots, x_n) its components. Let $f(\bar{X})$ be the function to minimize and let $a_1 < x_1 < b_1, \dots, a_n < x_n < b_n$ be its n variables each ranging in a finite continuous interval. The function f does not need to be bounded

The SA algorithm is schematically shown in Fig. A4.1. It proceeds iteratively : Starting from a given point \bar{X}_0 it generates a succession of points : $\bar{X}_0, \bar{X}_1, \dots, \bar{X}_i, \dots$ tending to the global minimum of the cost function. New candidate points are generated around the current point \bar{X}_i applying random moves along each coordinate direction, in turn. The new coordinate values are uniformly distributed in intervals centered round the corresponding coordinate of \bar{X}_i . Half the size of these intervals along each coordinate is recorded in the step vector \bar{V} . If the point falls outside the definition domain of f , a new point is randomly generated until a point belonging to the definition domain is found. A candidate point \bar{X} is accepted or rejected according to Metropolis Criterion [58] :

If $\Delta f \leq 0$, then accept the new point : $\bar{X}_{i+1} = \bar{X}'$ else accept the new point with probability:

$$p(\Delta f) = \exp(-\Delta f/T),$$

where $\Delta f = f(\bar{X}') - f(\bar{X}_i)$ and T is a parameter called temperature.

At a fixed value of T the succession of points $\bar{X}_0, \bar{X}_1, \dots, \bar{X}_i, \dots$ is not downhill, except when $T=0$. For values of T large compared to the mean value of $|f(\bar{X}_h) - f(\bar{X}_k)|$ (\bar{X}_h and \bar{X}_k are points randomly chosen inside the definition domain of f) almost all new points are accepted and the succession is a random sampling of f .

The SA algorithm starts at some "high" temperature T_0 given by the user. A sequence of points is then generated until a sort of "equilibrium" is approached ; that is a sequence of points \bar{X}_i whose average value of f reaches a stable value as

Initialize parameters

Perform a cycle of random moves, each along one co-ordinate direction. Accept or reject each point according to the Metropolis criterion. Record the optimum point reached so far.

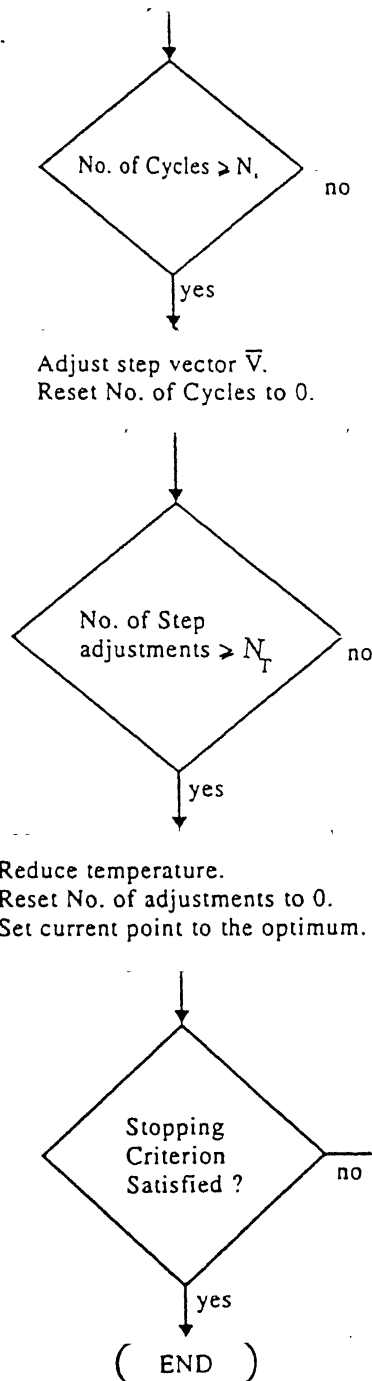


Figure A4.1 - The SA algorithm

i increases. During this phase the step vector \bar{V}_m is periodically adjusted to better follow the function behaviour. The best point reached is recorded as \bar{X}_{opt} .

After thermal equilibration, the temperature T is reduced and a new sequence of moves is made starting from \bar{X}_{opt} , until the thermal equilibrium is reached again, and so on. The process is stopped at a temperature low enough that no more useful improvement can be expected, according to a stopping criterion that will be described later.

The detailed description of the algorithm is given below :

Step 0 (Initialization)

Choose

A starting point \bar{X}_0 .

A starting step vector \bar{V}_0 .

A starting temperature T_0 .

A termination criterion ε and a number of successive temperature reductions to test for termination N_ε .A test for step variation N_s and a varying criterion \bar{c} .

A test for temperature reduction N_T and a reduction coefficient r_T .

Set i, j, m and k to 0, i is the index denoting successive points, j denotes successive cycles along every direction, m describes successive step adjustments, and k covers successive temperature reductions.

Set h to 1. h is the index denoting the direction along which the trial point is generated, starting from the last accepted point.

Compute $f_0 = f(\bar{X}_0)$

Set $\bar{X}_{opt} = \bar{X}_0$, $f_{opt} = f_0$.

Set $n_u = 0$, $u = 1, \dots, n$.

Set $f_u^* = f_0$, $u = 0, -1, \dots, -N_\varepsilon + 1$.

Step 1

Starting from the point \bar{X}_i , generate a random point \bar{X}' along the direction h as

$$\bar{X}' = \bar{X}_i + r_{vmh} \bar{e}_h$$

where r is a random number generated in the range $[-1,1]$ by a pseudo random number generator; \bar{e}_h is the vector of the h_{th} co-ordinate direction; and V_{mh} is the component of the step vector \bar{V}_m along the same direction.

Step 2

If the h th coordinate of \bar{X}' lies outside the definition domain of f , that is, if $X_h' < a_h$ or $X_h' > b_h$, then return to Step 1.

Step 3

Compute $f' = f(\bar{X}')$.

If $f' \leq f_i$, then accept the new point :

set $\bar{X}_{i+1} = \bar{X}'$,

set $f_{i+1} = f'$,

add 1 to i ,

add 1 to n_h ;

If $f' < f_{opt}$, then set

$$\bar{X}_{opt} = \bar{X}'$$

$$f_{opt} = f'.$$

endif;

else ($f' > f_i$) accept or reject the point with acceptance probability p (Metropolis move).

$$p = \exp \left(\frac{f_i - f'}{T_k} \right).$$

In practice, a pseudorandom number p' is generated in the range $[0,1]$ and is compared with p . If $p' < p$, the point is accepted, otherwise it is rejected.

In the case of acceptance

set $\bar{X}_{i+1} = \bar{X}'$,

set $f_{i+1} = f'$,

add 1 to i ,

add 1 to n_h .

Step 4

Add 1 to h .

If $h \leq n$, then go to Step 1 ;
 else set h to 1 and add 1 to j .

Step 5

If $j < N_s$ then go to step 1 ;
 else update the step vector \bar{V}_m ;

for each direction u the new step vector component V_u' is

$$V_u' = V_{mu} \begin{pmatrix} 1 + C_u \frac{n_u/N_s - 0.6}{0.4} \end{pmatrix} \quad \text{if } n_u > 0.6 N_s ,$$

$$V_u' = \frac{V_{mu}}{1 + C_u \frac{0.4 - n_u/N_s}{0.4}} \quad \text{if } n_u < 0.4 N_s ,$$

$$v_u' = v_{mu} \quad \text{otherwise}$$

Set $\bar{V}_{m+1} = \bar{V}'$,

set j to 0,

set n_u to 0, $u = 1, \dots, n$,

add 1 to m .

The aim of these variations in step length is to maintain the average percentage of accepted moves at about one-half of the total number of moves. The C_u parameter controls the step variation along each u th direction.

Step 6

If $m < N_T$, then go to step 1;

else, it is time to reduce the temperature T_k :

set $T_{k+1} = r_T \cdot T_k$,

set $f_k^* = f_i$,

add 1 to k ,

set m to 0.

It is worth noting that a temperature reduction occurs every $N_s \cdot N_T$ cycles of moves along every direction and after N_T step adjustments.

Step 7 (termination criterion)

If :

$$\left| f_k^* - f_{k-u}^* \right| \leq \varepsilon, \quad u = 1, \dots, N$$

and

$$f_k^* - f_{opt} \leq \varepsilon$$

then stop the search;

else :

add 1 to i ,

Set $\bar{X}_i = \bar{X}_{opt}$,

set $f_i = f_{opt}$.

Go to Step 1.